Universidad de Concepción
Faculty of Engineering
Master of Engineering Sciences mentioned in Electrical Engineering

Análisis longitudinal de cambios anatómicos y de difusión mediante resonancia magnética en pacientes con esclerosis múltiple.

"Longitudinal analysis of anatomical and diffusion changes by magnetic resonance imaging in patients with multiple sclerosis"

The thesis report was presented to the Faculty of Engineering of the Universidad de Concepción to qualify for the academic degree of Master of Engineering Sciences mentioned in Electrical Engineering

Víctor Ignacio Leiva Ormeño
CONCEPCIÓN-CHILE
2023

Supervising Professor: **Pamela B. Guevara A Ph.D**.
Co-Advisor Professor: **Korhan Buyukturkoglu Ph.D**.
Co-Advisor Professor: **Carlos Guevara O. PhD**.
Electrical Engineering Department, Faculty of Engineering
Universidad de Concepción

Abstract

Multiple Sclerosis (MS) is a neurodegenerative disease whose main affected area is the central nervous system. The regions most affected by this disease are usually the motor and sensory regions. The study of the effects of MS has become increasingly relevant given that the prevalence of this pathology has been increasing in recent decades. Based on this, this work aimed to search for a relationship between cortical anatomical changes and changes in brain structural connectivity in subjects with MS.

During this research, the study of changes was divided into two aspects: cortical anatomical changes and changes in brain structural connectivity. First, the anatomical study was applied over two databases. The first had only anatomical images, where each subject has 3 time points, separately by 12 month each one. The second has anatomical and diffusion data, where each subject has 2 time points, separated by 3 years. The software for the longitudinal analysis was FreeSurfer. Then, to determine the anatomical changes, we used the generalized linear model (GLM). On the other hand, diffusion magnetic resonance imaging (dMRI) was used to study changes in brain structural connectivity. This study was carried out by analyzing the dMRI metrics of the brain fibers tracts. These metrics were obtained from the generalized q-sampling imaging (GQI) model. To examine the changes in the diffusion metrics obtained we employed a generalized equation model (GEE). Finally, we determined the relationship between the regions presenting significant changes at the cortical level and the brain fibers showing substantial differences across time.

The regions that suffered significant anatomical changes at the cortical level are the pre and post-central regions and the superior temporal region, among others. In addition, there were changes in the parietal and occipital region, but these were much smaller compared to the previous ones. Concerning brain structural connectivity, the brain fibers that presented the significant changes are associated with the cortical regions highlighted in the anatomical analysis. From these results, the short brain fiber connecting the superior frontal and the pre-central region of the left hemisphere stands out since it was the only one that showed significant differences in all dMRI metrics.

The values of the dMRI metrics did not match with the literature, our interpretation was that the treatments given to the subjects might be effective. We arrived at this conclusion by analyzing the relationship between the change in the Expanded Disability Status Scale (EDSS) value and the dMRI metrics. The analysis revealed there was an improvement in the EDSS value. However, due to the size of the database, it’s recommended that other kind of analyses be conducted to further support this conclusion.

Table of Contents

List of tables

List of Figures

Abbreviations

Alphabetic order

AD	Axial diffusivity
ADC	Apparent Diffusion Coefficient
CI	Cognitively Impaired
CNS	Central nervous system
CP	Cognitively Preserved
DB1	Database 1
DB2	Database 2
DTI	Diffusion Tensor Imaging
DWM	Deep White Matter
EDSS	Expanded Disability Status Scale
FA	Fractional Anisotropy
FC	Cross Section Fiber bundle
FLAIR	Fluid-Attenuated Inversion Recovery
FSGD	FreeSurfer Group Descriptor
FWHM	Full width at half maximum
GEE	Generalized Estimated Equations
GLM	Generalized linear model
GM	Gray Matter
GQI	Generalized q-sampling
GUI	Graphical user interface
LME	Lineal mixed-effects
MANCOVA	Multivariate analysis of covariance
MD	Mean Diffusivity
MRI	Magnetic Resonance Imaging
MS	Multiple Sclerosis
QA	Quantitative Anisotropy
RD	Radial Diffusivity
RRMS	Relapsing-Remitting Multiple Sclerosis
ROIs	Region of Interests
SDMT	Symbol Digit Modalities Test
SSIM	Structural similarity index
SPSS	Statistical Package for the Social Sciences
SUSAN	Smallest Univalued Segment Assimilation Kernel
SWM	Superficial White Matter
TBSS	Tract-Based Spatial Statistics
VBM	Voxel-Based Morphometry
WM	White Matter

Capítulo 1. Introduction

1.1. General Introduction

Multiple Sclerosis (MS) is a neurological inflammatory disease that is more common in young adults by demyelination of neurons and axonal damage [1]. It generates a deterioration at motor, sensory, and cognitive levels in the Central Nervous System (CNS) [2]. MS is the second leading cause of disability in young people in Latin America. The most affected part of the CNS by this disease is the brain.

MS can manifest in three different ways: relapsing-remitting MS (RRMS), secondary progressive MS (SPMS), and primary progressive MS (PPMS). RRMS is the most common type, characterized by subjects experiencing relapses that persist for a short period of time and then disappear. Around 80 to 85% of MS patients are initially diagnosed with this form of the disease. SPMS has similar characteristics to RRMS, but instead of the subject experiencing relapses, this type of MS has a steady progression without periods of no symptoms. Finally, PPMS is the least common type, accounting for less than 10% of initial diagnoses. PPMS is characterized by presenting all the symptoms of MS at the beginning of the illness, with no relapses [3]. All the subjects of this research were diagnosed with RRMS.

To carry out an MS study, the pathology's temporal evolution is a highly relevant variable for its analysis. For this reason, a longitudinal analysis provides a better overview of the impact of the pathology on the patients. Therefore, the application of this type of study is fundamental since it has the potential to guide the application of more appropriate treatments depending on the characteristics of each patient. This approach benefits the patient by receiving better treatment and the doctors who can carry out a better and more efficient follow-up of their patients [4].

Magnetic Resonance Imaging (MRI) is undoubtedly one of the most widely used tools for studying MS. Various imaging studies about MS have focused on multiple morphological or qualitative aspects and many others on the quantitative properties of MRI. The T1-weighted and Fluid-Attenuated Inversion Recovery (FLAIR) images are the most widely used. T1-weighted images are a sequence of pulses that detect differences in longitudinal T1 relaxation times of tissues [5]. FLAIR images use a special inversion recovery sequence with a long inversion time, which removes the signal from the cerebrospinal fluid in the resulting images [6]. Another vital image used to analyze the impact of the MS is diffusion MRI (dMRI). The basic principles of dMRI are related to the movement of

water molecules in tissues. Water molecules in an anisotropic medium take a trajectory according to the shape of the bodies that restrict them [7].

Work related to MS usually focuses on the changes that the disease generates at the cortical level or in the WM. In the latter case, most studies focus on changes in the lesions developed in the WM. However, a common point between most of these research is using metrics that determine the levels of disability and the cognitive damage generated by the disease. The most used indices for this are the Expanded Disability Status Scale (EDSS) index, which measures the levels of disability of the patients, and the Symbol Digit Modalities Test (SDMT) index, which measures cognitive deterioration by measuring the response speed of the subjects.

Works focusing on anatomical changes highlight regions that present significant changes, such as the precentral and superior frontal regions, and sensory areas, such as the superior temporal region. On the other hand, most works associated with the study of changes in WM focus on changes in lesions; few seek to see the changes that MS has on brain connectivity. Those who focus on changes in connectivity highlight the corpus callosum and the thalamus as connectivity centers.

Finally, very few works seek the conjunction between anatomical changes and changes in the white matter, particularly studying brain connectivity through short brain fibers.

This study aims to establish a relationship between the changes in cortical anatomical structures and the progression of the disease. We will use statistical methods and a longitudinal analysis to determine this relationship. Also, we will perform an analysis of the diffusion MRI metrics in a set of white matter bundles. This analysis allows us to associate the diffusion MRI changes with the anatomical changes to generate a better understanding of structural brain connectivity and its impact on the subjects with MS.

In this thesis, we will work with two databases, DB1 and DB2. DB1 is integrated by 39 subjects, each with three T1 MRI anatomical images separated for one year of difference. In addition, DB2 is integrated by 24 subjects, each with two T1 images, two FLAIR images, and two dMRI images separated for three years of difference. Both databases are local. DB1 acquired at the Hospital Clinico of the University of Chile, Santiago, Chile and DB2 acquired at the Columbia University Irving Medical Center, New York, USA. These databases will be described in greater detail in section 1.5.

1.2. Hypothesis

Significant changes ($p<0.05$) can be found in cortical regions and be related to changes in white matter fiber bundles from T1, FLAIR, and diffusion magnetic resonance images of patients with Multiple Sclerosis in a longitudinal study of 2-time points.

1.3. Goals

1.3.1 General Goal.

Study anatomical changes correlated with clinical metrics in individuals with Multiple Sclerosis by utilizing two longitudinal MRI databases, employing longitudinal pipelines and statistical analyses. Additionally, establish associations between these changes and statistically significant alterations in diffusion MRI metrics, with the aim to enhance our understanding of the progressive structural modifications in the brain caused by the disease over time.

1.3.2 Specific Goals.

- Determine anatomical variations in Multiple Sclerosis patients through a longitudinal analysis of T1 magnetic resonance images using FreeSurfer software on the DB1 and DB2 databases.
- Evaluate disease progression associated with clinical metrics using statistical models, such as generalized linear models (GLM) and linear mixed-effects models (LME), on the DB1 database, and the GLM model on the DB2 database.
- Explore alterations in the microstructure of white matter fibers through statistical analysis in the DB2 database using generalized estimating equations (GEE) and their relation with anatomical changes.

1.4. Scope and limitations

A database of T1-w images provided by Professor Dr. Carlos Guevara, called DB1, will be used first. In addition, we will use a database of T1-w and dMRI images provided by Professor Dr. Victoria M Leavitt from Columbia University called DB2. We used different software tools to make all the analyses during this research. First, we used FreeSurfer (version 7.1.0, Athinoula A. Martinos Center for Biomedical Imaging, Charlestown, Massachusetts, USA) [8], which provides tools for analyzing MR images. It has visualization tools, atlases, and statistical methods that could be applied to the images. Also, during this thesis, we used DSI Studio. This software provides tools for diffusion

MRI analysis and brain connectivity and correlates findings with neuropsychological diseases [9]. In addition, to perform some of the statistical analysis, we used the Statistical Package for the Social Sciences (SPSS) software. This software supports executing different statistical models and ways to visualize statistical data [10].

The longitudinal analysis will be applied to 39 MS subjects of DB1 and 24 MS subjects of DB2, and the diffusion MRI analysis will be applied only to the DB2 subjects.

1.5. Materials

There are two MRI databases available. DB1 comprises 39 subjects suffering from RRMS. The database was acquired on a Siemens 1.5 T MRI scanner. The acquisition protocol includes standard T1 anatomical images using 3D inversion-recovery prepared spoiled gradient-echo (IR SPGR). The parameters used for the volumetric sequence were the following: FOV of 250x234 [mm], matrix of 256x240 [mm], repetition time (TR) of 12 [ms], echo time (TE) of 5.68 [ms], angle excitation spin of 15°, isotropic voxel size of 0.98x0.98x0.98 [mm]. The patients underwent a second and third brain MRI within two years of follow-up. In addition, this database has two clinical metrics that will be used during this research work, the EDSS value and the SDMT test. Both clinical metrics were taken in person for all subjects at the moment of the acquisition of every time point. Every subject has both clinical metrics for every time point. Both clinical metrices that will be used in this research work are without corrections of any kind, so we used the raw value of the EDSS and SDMT test.

DB2 is made up of 26 patients with RRMS. The database was acquired on a Siemens-Skyra 3T MRI scanner using a 16-channel carbon head. The acquisition protocol for standard T1 anatomical images was 3D inversion-recovery prepared spoiled gradient-echo (IR SPGR), repetition time (RT) of 2400 [ms], echo time (TE), and repetition time (TR) of 2 [ms], rotation angle of 8°, voxel size of 1x1x1 [mm], FOV = 256x256 [mm], 176 slices. Diffusion tensor images: TE, TR = 91 [ms], 4100 [ms]; twist angle = 85°, FOV = 92x110 [mm], voxel size = 2.0x2.0x2.0 [mm], 75 slices, multiband acceleration factor = 3.0, 60 broadcast encoding directions with b = 1200 seconds/mm2 and a b = 0 seconds/mm2. The patients underwent a second brain MRI within three years of follow-up.

Both databases were acquired with the patient's consent and approved for research by local ethics committees. DB1 was approved by the ethics committee of Hospital Clinico of the University of Chile, Santiago, Chile, and DB2 was approved by the ethics committee of the Columbia University Irving Medical Center, New York, USA.

1.6. Methodology

In this thesis, we carried out a bibliographical review of the works on Multiple Sclerosis disease and its longitudinal impact on different subjects. After that, a detailed study was conducted on the processing methods and the other types of longitudinal analysis of anatomical data. Then, based on the results of those studies, the statistical model, GLM model, was applied to our data to determine significant changes in the cortical thickness. Additionally, diffusion MRI data was processed and the dMRI metrics were analyzed using the GEE model to determine the level of significance of the fiber bundle alterations. Finally, we correlated the anatomical and diffusion changes.

1.6.1 Analysis over DB1

For DB1 database only T1-w images were available, which we used for testing concepts and methods during anatomical analysis. The results of this analysis were used later to compare them with the results of the DB2 analysis. This analysis was conducted in a local computer cluster available in the laboratory.

A. Preprocessing and Longitudinal Analysis

The DB1 database was pre-processed using a non-linear filtering tool to reduce the noise of the images and preserve their structure, called “Smallest Univalued Segment Assimilation Kernel” (SUSAN) [11], which is available in the FSL FMRIB Library software [12].

After the pre-processing step, we applied the longitudinal processing. This step was performed using the FreeSurfer software [8], divided into three stages: cross-sectional (CROSS), creation of the template (BASE), and longitudinal analysis (LONG).

In CROSS, each image was processed independently. From this, a segmentation and a reconstruction of the cortical surface of each time point were generated, which were used in the following stages.

In BASE, a template was built based on the three different time points of the database. For this, each image was resampled in the voxel space of the template using a cubic B-splice interpolation [13].

In LONG, the actual longitudinal processing was performed. Here, a brain mask was created by joining the previous results of all the time points of the same subject to compare each time point to the template.

B. Statistical Analysis.

The longitudinal analysis was performed using two statistical models: the GLM and the LME model. The GLM model was applied using the toolbox available in FreeSurfer, and the LME model was applied using mass univariate analysis through a script using MATLAB R2020b software.

In this statistical analysis, we looked for a correlation between the cortical thickness and the cortical volume with the EDSS and the SDMT parameters.

1.6.2 Analysis over DB2.

The analysis of the DB2 database was divided into two stages: the anatomical and diffusion MRI stages. The first stage was executed in the computer cluster provided by Professor Dr. Victoria M Leavitt from Columbia University. The second stage was conducted in a local computer cluster available in the laboratory.

A. Anatomical Analysis.

The DB2 data was preprocessed within the anatomical stage with a lesion inpainting process performed using the LST lesion segmentation tool [14], available in the SPM8 software.

After this, DB2 was processed using the same longitudinal analysis applied to DB1, using FreeSurfer software.

Statistical analysis was performed using a GLM statistical model, applied using the toolbox available in the FreeSurfer software.

The application of this model requires several previous steps. The first stage was to move the time points to a common space (fsaverage). To do that, we used the command *long_mris_slopes* [8]. First, a table was generated, including each subject's features and some variables relevant to the analysis, such the hemisphere, the Full width at half maximum (FWHM) value, and the measure to be calculated, described in detail in a posterior section.

Subsequently, the analysis was performed through the graphical user interface (GUI). In this GUI, we had to specify some parameters. First, we had to upload the previously created table, and we selected the comparison parameters. In this case, the comparison variables were the EDSS and SDMT. Finally, the type of analysis to be performed was initialized. Then, the graphical and statistical results are extracted through the command *long_stats_slopes* [8]. This command allowed us to visualize the results using the FreeSurfer visualizer.

B. Diffusion MRI Analysis.

Finally, we applied a diffusion MRI processing pipeline. The diffusion MRI data was analyzed using DSI Studio software to extract the white matter bundles from DB2. This analysis was carried out in previous work by Buyukturkoglu et al. [15] using the same database.

DSI Studio software was used for dMRI pre-processing, tractography calculation, and computing of the diffusion metrics, such as fractional anisotropy (FA), axial diffusivity (AD), radial diffusivity (RD), mean diffusivity (MD) and quantitative anisotropy (QA). In addition, Python and C++ codes were used to segment the WM bundles and calculate different tract-based diffusion metrics.

Our analysis was divided into two steps to identify the most significant fiber bundle features. We began by applying a student t-test as an initial filter to the 168 bundles from our atlas. Next, we conducted a longitudinal statistical analysis. In this case, we used the generalized estimated equations (GEE) model to assess the significance level of each fiber bundle. This model uses diffusion metrics as factors and EDSS and SDMT values as covariates.

Finally, a relation was computed between the anatomical and diffusion MRI results.

1.7. Available resources

A computer capable of working with existing databases was available, with an Intel i7-9700 processor, 24 GB of RAM, and a Radeon RX570 video card financed by FONDECYT Project 1221665.

.

Capítulo 2. Bibliographic Review

2.1. Brain Anatomy

The brain is the main structure of the nervous system and corresponds to 80% of the encephalic mass. It performs the so-called higher functions, for example, motor functions, sensitivity, and control of body functions. It is constituted by two hemispheres connected by a structure of fiber tracts called the corpus callosum [16]. The cerebral cortex mainly comprises gray matter (GM) and white matter (WM). The GM are regions of high-density neuronal bodies or somas, neuroglia, and demyelinated axons. In contrast, WM are regions where the myelinated axons of the neurons are located [17].

In the encephalon, two structures have the largest cortices, corresponding to the brain and the cerebellum. However, the highest concentration of neuronal cell bodies is found in the brain, given the multiple folds in the cerebral cortex, as shown in Figure 2.1.

The primary function of the neuronal bodies is to process the information they receive from the different areas of the body, highlighting the control of movements, memory, sensations, and emotions, among others.

The anatomical division of the cerebral cortex is into five lobes: frontal, parietal, temporal, occipital, and insula, each with different but associated functions. Also, there is the functional division of the cortex. The three central regions are the sensory, motor, and association.

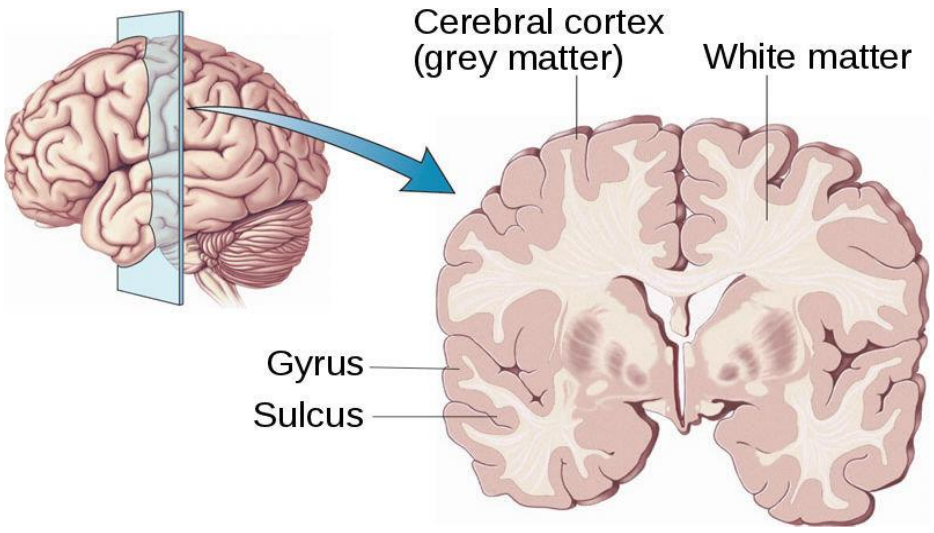

Figure 2.1 Cerebral cortex's location and white matter [18].

On the other hand, there are the neuronal axons, whose primary function is to transmit the information generated in the neuronal bodies to different sections of the WM. These axons are grouped, forming the so-called brain fiber tracts composed of fibers similar in trajectory, position, and size. These brain fibers can be classified as short fibers (~35 - 80 mm) that mainly connect close areas of the cortex and long fibers (~80 - 150 mm) that are present in the deep regions of the WM.

These fiber tracts are traditionally grouped into three groups: association fibers are those that connect areas of the same cerebral hemisphere; projection fibers are those that connect areas of the cortex with deep nuclei of the brain, such as the basal nuclei; and finally, the commissural fibers are those that connect similar areas with their counterpart in the opposite hemisphere[19]. These classifications can be seen in Figure 2.2.

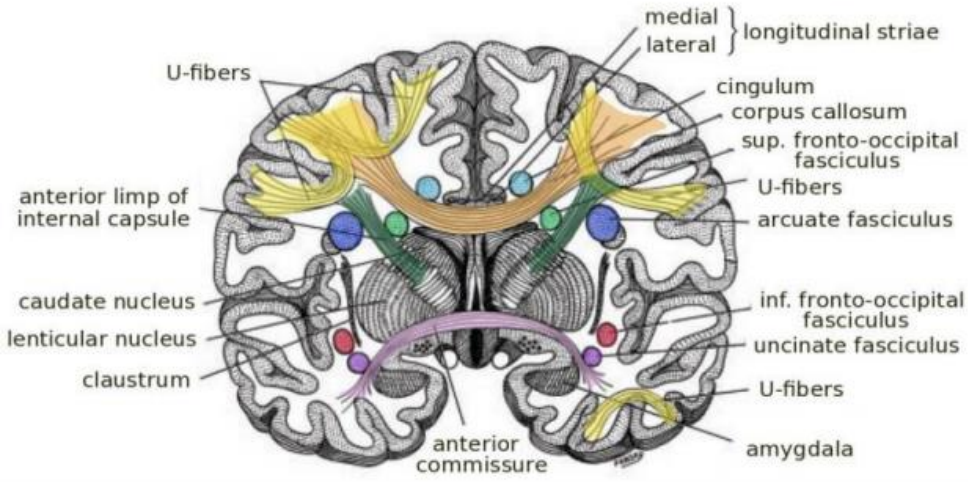

Figure 2.2 Illustration shows the types of fibers in white matter [20].

2.2. State of the Art

This section discusses the works related to MRI analysis in Multiple Sclerosis (MS). Firstly, we focus on works studying changes in the cortical surface using a longitudinal approach. Secondly, we highlights works related to alterations structural connectivity and its effects on the cortical surface of MS patients. Then, we present works similar to this thesis's objective, which is to search for a relationship between structural connectivity and changes in the cortical surface. Finally, the methods applied to the data will be described, such as the methods for the anatomical analysis and those used for the diffusion MRI analysis.

2.2.1 Study of Multiple Sclerosis using Magnetic Resonance Imaging

A. T1-weighted MRI image, FLAIR image, and dMRI

The principle of Magnetic Resonance Images is generally based on the atomic properties of water nuclei. In a simplified way, an external magnetic field aligns the hydrogen atoms within the tissue's water nuclei. This alignment is then perturbed by a radio frequency pulse (RF). During the image acquisition process, two times are defined. One is the repetition time (TR), the time between successive pulses applied to the same slice. The echo time (TE) is the time between the RF pulse and the reception of the echo signal.

The sequences used in this work will be T1, FLAIR, and dMRI images. A short TR and TE characterize T1 images. In this image, the brightness and contrast depend on the T1 properties of the tissue [5]. On the other hand, in FLAIR images, the fluid signal is suppressed using an adequate long TE and a long inversion time (IT). The function of the inversion time is to flip the initial magnetization of all tissues in the image to a point opposite the main magnetic field. An inversion recovery sequence with a long IT of 2000-2500 [ms] is used for fluid suppression [6]. Finally, the dMRI images are based on measuring the random Brownian motion of water molecules within a tissue voxel. This image aims to attenuate TR based on how easily water molecules can diffuse in a specific region. The more easily water can diffuse, the less initial TR will remain [21].

B. Longitudinal and cortical approach to Multiple Sclerosis

A longitudinal study is carried out based on multiple measurements of individuals for a prolonged time [22]. In the case of Multiple Sclerosis (MS), some longitudinal studies with anatomical and radiological correlation have enabled the measurement of this disease's impact at the cortical level or finding patterns that could help researchers prevent any relapse in their patients. Within this line, Rocca et al. [23] reviewed multiple longitudinal studies focused on the impact of MS on GM and its correlation with cognitive damage. Among the works mentioned by Rocca et al. is the one carried out by Camp et al. [24], considered a fundamental work when starting any longitudinal work associated with MS. This study established that there was a relationship between cognitive impairment and its impact on the GM at the cortical level.

Among the works that follow this line is one from Hidalgo de la Cruz et al. [25], whose main objective was to find a regional pattern of alteration of the cortical thickness and its evolution in one year in patients with several types of MS. For the cross-sectional processing they used the software

FreeSurfer [8], that determined the cortical thickness of every image. As shown in Figure 2.3, the authors were able to decide that when comparing the baseline image and a later image, there was a decrease in the cortical thickness in MS patients, especially in three regions of the cortex: orbitofrontal lobe, precuneus, and frontal lobe lower-left parietal. In addition, they related the loss of cortical thickness in these areas to a high EDSS index value [26]. However, the researchers mention that the patients with long disease duration did not have high EDSS values, which could create some bias in the results. Finally, they did not perform any cognitive tests for the neurological evaluation of the patients.

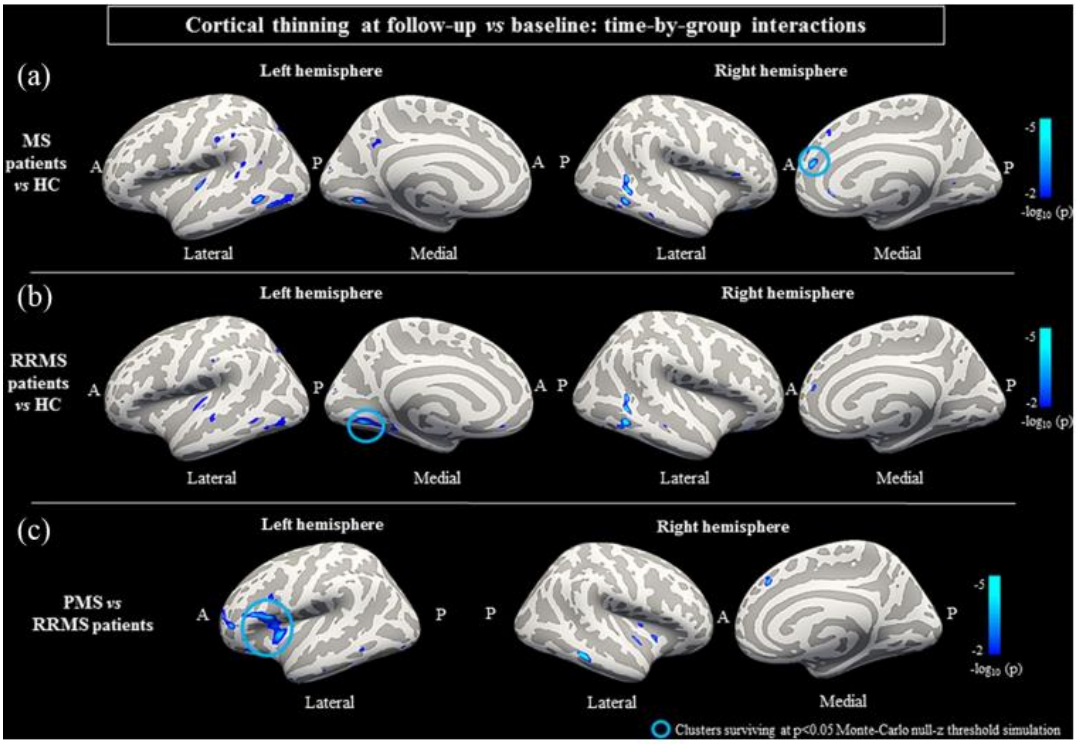

Figure 2.3 Cortical Regions Showing Significant Interaction of Cortical Thinning in (a) MS Patients vs. Control, (b) RRMS vs. Control, and (c) SPMS vs. RRMS. SPMS: Secondary Progressive Multiple Sclerosis, RRMS: Relapsing-Remitting Multiple Sclerosis [25].

In the work carried out by Pravata et al. [27] the aim was to investigate the association of the change in the cerebral cortex and other GM regions with depression and cognitive impairments associated with MS. FreeSurfer [8] was used to obtain the volumes of the cerebral cortex. Various neurological tests were used to determine the subjects' cognitive impairment levels. One of the tests they used was the SDMT [28]. To detect the brain areas with the most significant alteration, they used a multivariate covariance (MANCOVA) analysis to compare groups (control and subjects with MS). In general terms, they were looking for changes in the cortex and other brain areas. As shown in Figure

2.4, the most significant alterations were for the front-parietal-temporal lobe and the entorhinal cortex. A relationship was also found between cognitive impairment and depression, where the right temporal pole and the inferior frontal gyrus are affected. On the other hand, this research did not consider the dysfunction of cognitive domains and the decrease in the cortex thickness, which can generate alterations in the final results. In addition, the absence of longitudinal data made it difficult to determine whether MS or another pathology causes the degeneration of the cortex.

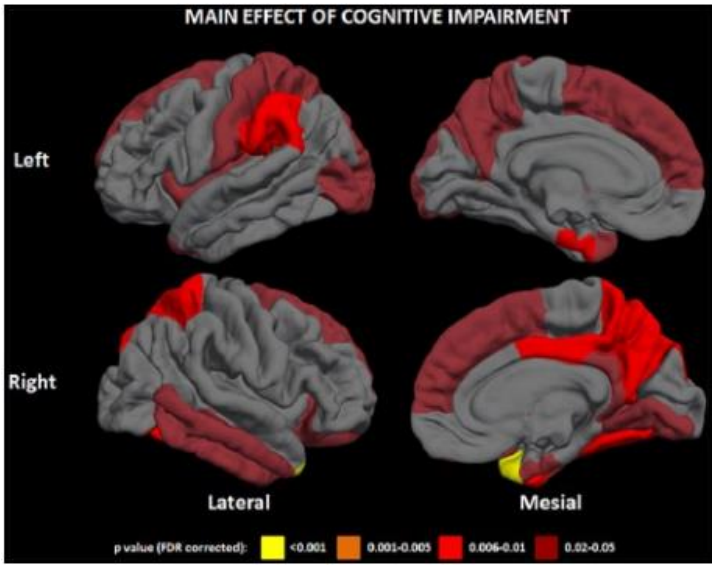

Figure 2.4 Significant regions in the cerebral cortex according to the impact on cognitive impairment in patients with MS. The areas of light red and yellow colors present the highest levels of significance versus the darkest ones, the lowest level of significance [27]**.**

In work by Fleischer et al. [29], the main interest was to evaluate the change of the GM at the cortical level and determine the brain atrophy through neuronal dynamics using atrophy parameters. The researchers used four metrics: modularity, clustering coefficient, local efficiency, and transitivity. In general terms, modularity measures the relationship between the connections of the regions of the brain, the clustering coefficient is a measure of the local organization through the number of relations between the areas of the brain, the local efficiency is a metric that tries to reflect how the information is exchanged between the regions of the brain, and finally, the transitivity is the probability of how close two areas are to each other. As shown in Figure 2.5, the four metrics increased in the first twelve months. The increased modularity was related to cortical reorganization and strengthening intra-modular connections. The local efficiency and transitivity increases were associated with reinforcing communication between nearby regions. Finally, an increase in the clustering coefficient can be interpreted as an increase in the affected area by the MS in regions close to each other. The change in all these metrics was construed as a change in the neuronal dynamics of the MS subjects. No

significant differences were found in the cortex volume when considering the patients' inflammatory activity. However, the heterogeneity of the patients made it difficult to make comparisons. They did not analyze the relationship of the cognitive and the neural dynamics.

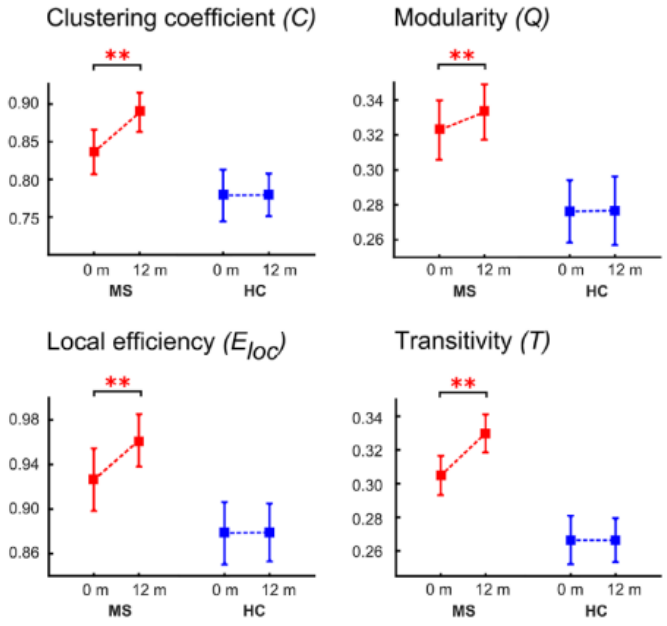

Figure 2.5 Longitudinal Neural Connection Measures of MS Patients Versus Control Patients. (**p < 0.001). [29].

C. Structural Connectivity and its Alterations in Multiple Sclerosis

The use of dMRI for the study of MS allows us to detect the effects of the disease on the WM connections.

Mustafi et al. [30] was the first approach that analyzed brain fibers to detect alterations in WM in patients with MS. To see such alterations, the researchers used four metrics extracted from Diffusion Tensor Imaging (DTI). These metrics are AD, RD, MD, and FA. These metrics were described in detail in [31]. In addition, they selected regions of interest (ROIs) based on the number of lesions on the WM. For each subject, the researcher determines three types of ROIs: lesion, perilesion (regions surrounding the lesion), and normal-appear white matter. The authors used these ROIs to calculate the mean and standard deviations of the MRI measures. Figure 2.6 shows the relationships between the three ROIs and the different metrics. Finally, the researchers detected significant alterations in some of the DTI metrics of the ROIs classified as normal-appear white matter and those classified as perilesion. They concluded that using DTI metrics was a relevant source of information to detect alteration in the WM of subjects with MS.

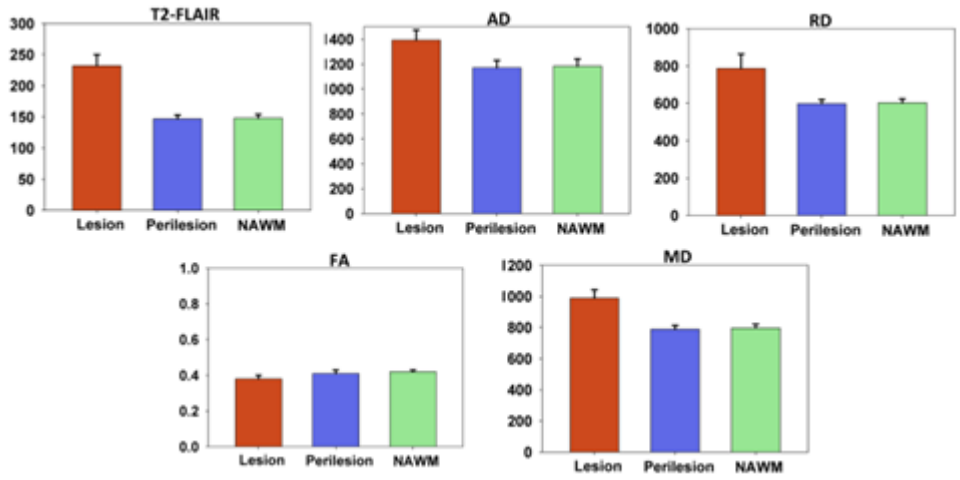

Figure 2.6 Bar plots of T2-FLAIR and diffusion metrics in the three ROIs [30].

The lesion, perilesional, and NAWM ROIs are color-coded in red, blue, and green. Error bars denote the standard deviation across 36 ROI sets. The overhead arrows indicate significant differences in measurements between pairs of ROIs at a Bonferroni-corrected P threshold of 0.017. Note that T2-FLAIR intensity is not a quantitative measure; thus, it was not tested for statistical significance at the group level. FLAIR: Fluid attenuated inversion recovery; NAWM: normal-appearing white matter; ROIs: regions of interest [30].

Another work related to the use of DTI was carried out by Klistorner et al. [32], whose main objective was determining the progression of WM alterations in patients with MS. For this, they used the same metrics that were used in [30]. The main difference between these two works was that [32] is longitudinal. They used two-time point images per subject (one as a baseline and another taken approximately two years later). The researchers used Jim 7 software for lesion inpainting. The authors detected two changes. The first was the significant change in the MD, which indicates the progression of brain atrophy. The second is the RD and AD correlation, as shown in Figure 2.7. This correlation led the researchers to conclude that the longitudinal alterations of diffusion metrics in subjects with MS were significant.

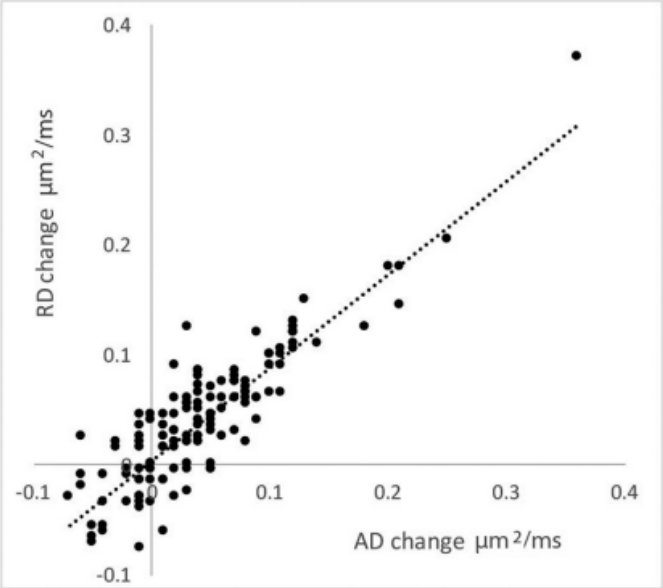

Figure 2.7 Correlation between AD and RD changes in individual lesions [32]**.**

Another work by Kolasa et al. [33] aimed to study normal WM areas in MS patients using DTI metrics. The authors used T2 images to select ROIs where no lesions were detected. The researchers determined significant changes between the DTI metrics from the healthy control and the MS subjects, particularly in the corpus callosum, which presents the most important variations. Table 2.1 shows part of the original table where such variations are presented. The researchers observed diffusion MRI changes associated with MS patients but clarified that these changes had a different dynamic change for anatomical location. In another related work by Pokryszko-Dragan et al. [34] the aim was to assess both GM and WM damage in brain regions associated with disability using DTI metrics, such as FA and the apparent diffusion coefficient (ADC). The researchers found a decrease in FA and an increase in ADC in the thalamic connections and corpus callosum. In addition, the researchers determined that the changes in the DTI metrics are associated with alterations in tissue integrity. Also, the authors recommend using other metrics, such as brain region volume, and changing some methodological issues, like image acquisition.

Table 2.1 Part of the table showing the relationship of baseline DTI metrics with disability progression in the MS measured by EDSS increase over the 4-year follow-up [33].

	Stable group *n* = 24			Progression group *n* = 22						
DTI metrics	Median	Min	Max	Median	Min	Max	*p*-Value[a]	Odds ratio	95% CI	
Corpus callosum genu										
FA	0.81	0.52	0.88	0.74	0.48	0.88	**0.04**	0.00	0.00	0.61
MD	0.80	0.62	1.21	0.83	0.67	1.31	0.06	1.05	1.00	1.10
AD	1.70	1.47	2.07	1.76	1.55	2.25	0.36	1.02	0.98	1.06
RD	0.28	0.17	0.80	0.37	0.17	0.84	**0.04**	1.05	1.00	1.09
Corpus callosum body right										
FA	0.67	0.40	0.87	0.52	0.30	0.77	**0.01**	0.00	0.00	0.24
MD	0.80	0.58	1.07	0.87	0.69	1.08	**0.04**	1.08	1.00	1.15
AD	1.51	1.07	1.79	1.39	1.18	1.84	0.25	0.98	0.95	1.01
RD	0.46	0.20	0.73	0.62	0.30	0.92	**0.01**	1.07	1.02	1.12
Corpus callosum body left										
FA	0.66	0.38	0.85	0.53	0.29	0.82	0.07	0.02	0.00	1.37
MD	0.81	0.67	1.32	0.84	0.70	1.39	0.12	1.03	0.99	1.08
AD	1.50	1.19	2.08	1.42	1.06	2.04	0.53	0.99	0.97	1.02
RD	0.46	0.23	0.93	0.58	0.30	1.14	**0.04**	1.04	1.00	1.08
Corpus callosum splenium										
FA	0.82	0.63	0.89	0.76	0.52	0.94	**0.04**	0.00	0.00	0.76
MD	0.71	0.56	0.95	0.79	0.68	1.28	**0.01**	1.13	1.03	1.23
AD	1.62	1.23	1.87	1.80	1.50	2.13	**0.01**	1.08	1.02	1.14
RD	0.25	0.16	0.50	0.35	0.11	0.86	**0.02**	1.07	1.01	1.14

In the previous works, the focus was to identify the alterations in the WM and its relation to the disability of the patients. In the following works, the focus will be on its association with the cognitive level.

The first work was proposed by Manca et al. [35], where the main objective was to establish a pattern between macrostructure and microstructure with the WM and cognitive performance. To find this pattern, researchers used two techniques: voxel-based morphometry (VBM) to T1 images [36] and tract-based spatial statistics (TBSS) to dMRI data [37]. The VBM was applied using SPM8, and TBSS was applied using FSL. Through a battery of cognitive tests, the researchers calculate the mental processing speed of the subjects. They use this metric to classify them according to their cognitive state. Both techniques generated different but related results. In the case of VBM, as shown in Figure 2.8, the main changes were detected in the semantic fluency area, where it is correlated with changes in cortical and subcortical regions of the GM, such as the occipital and temporal areas. On the other hand, TBSS results highlight the frontal associative and commissural areas as the regions that present the most significant changes. These areas are related to the cognitive state of the subjects.

Finally, the researchers said that preserving the WM fiber bundles is crucial to maintaining the integration of information regarding the cognitive condition of the subjects.

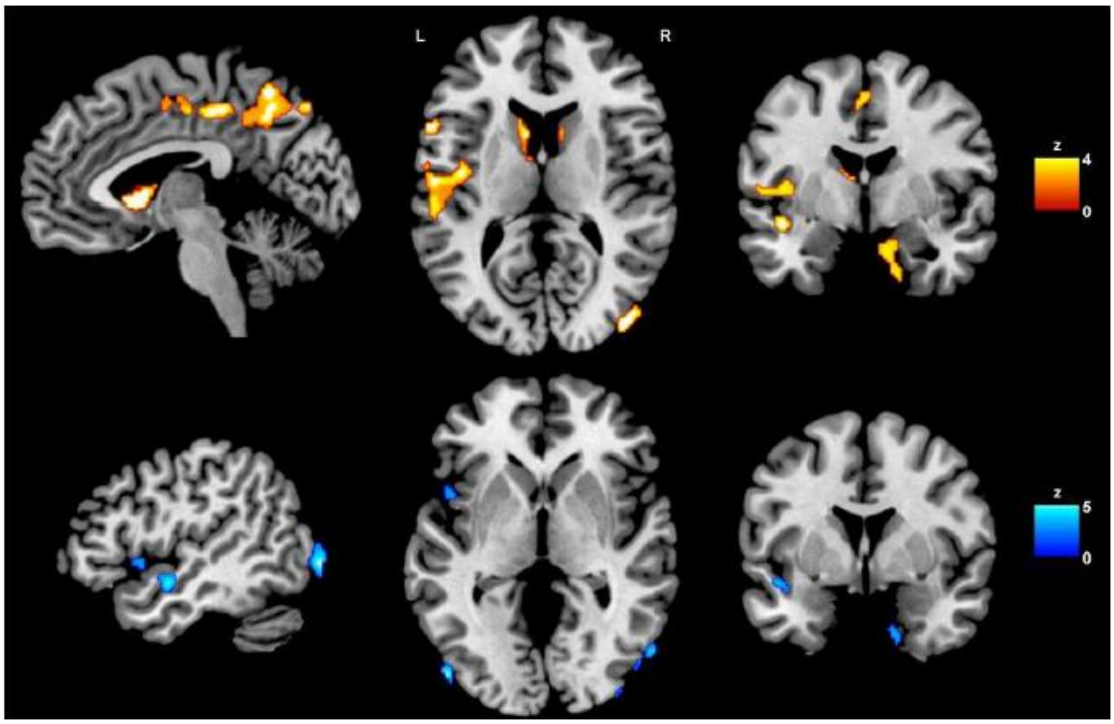

Figure 2.8 GM regions correlated with scores on the semantic fluency task before (red) and after (blue) its execution, correcting for processing speed abilities at $p < 0.05$. The analysis here was made using VBM [35].

Also, the work proposed by Zhao et al. [38] had an objective similar to that of Manca et al. The difference was that instead of calculating the mental processing speed, the researchers divided the participants into two groups: cognitively impaired (CI) and cognitively preserved (CP). Both works employed TBSS as a correlation method. Additionally, this work used the FA to determine the changes between the groups. As shown in Figure 2.9, comparing the results between both groups, the right inferior longitudinal fasciculus, the right inferior frontal-occipital fasciculus, and the right corona radiata were the most affected among CI patients compared to CP patients. When diffusion metrics and cognitive performance were correlated, the connection with the most significant connection was the corpus callosum. Finally, the researchers highlight the importance of the white matter's microstructures and the use of FA as a metric for measuring these changes and the cognitive changes in the subjects.

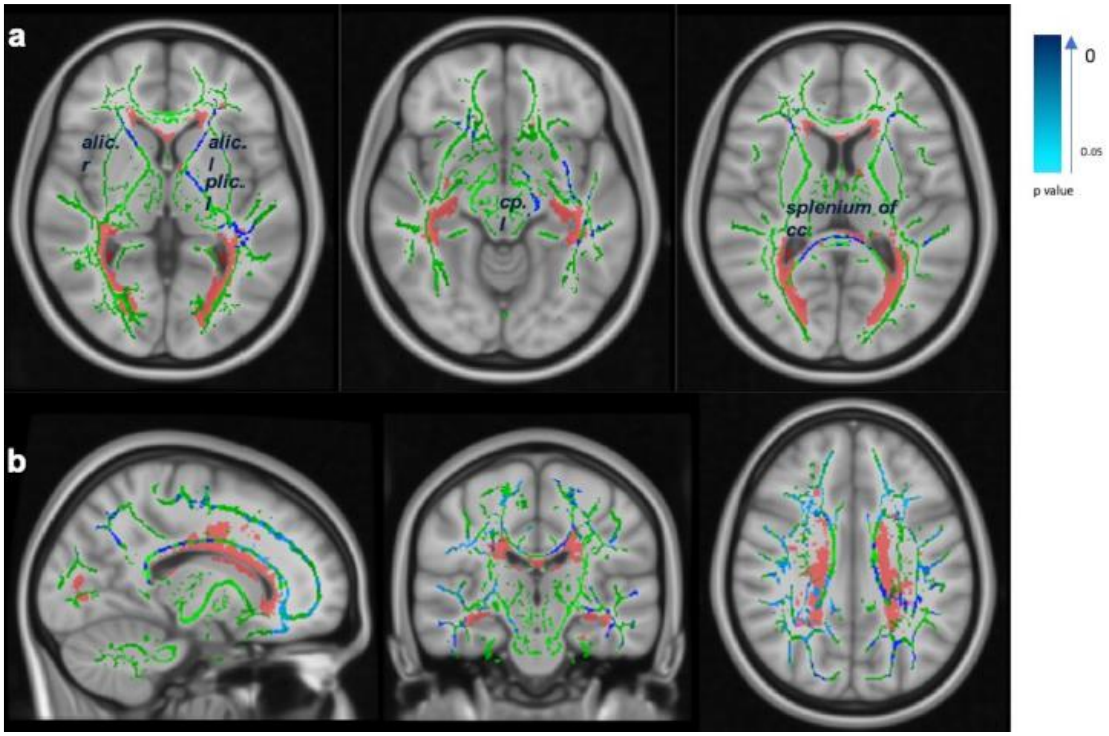

Figure 2.9 TBSS results are in blue on mean FA (green) and MNI 1mm standard space, overlaid by lesion probability map (red). Tracts in deep blue displayed a smaller p-value or more meaningful results. (a) Reduced mean FA value on splenium of the corpus callosum, left anterior and posterior limb of the internal capsule and left cerebellar peduncle in CI patients compared to CP patients (b) Widespread areas of increased mean skeleton MD in CI patients compared with CP patients [38].

The following work focuses on the change of brain fibers and how such changes are related to MS subjects' clinical symptoms. This work was carried out by Storelli et al. [39] focus was on evaluating the capacity of the cross-section fiber bundle (FC) [40] for detecting atrophy in specific fiber bundles. They used the constrained spherical deconvolution (CSD) model, which employs a density function to obtain the orientation of the fibers [41]. They used a fixed-based morphometry analysis to assess differences in fiber bundles between the MS and control subjects. Also, they used a voxel-based analysis to determine the regions with the most significant changes in FA. The researchers found a generalized reduction in FC in patients with MS compared to healthy controls, as shown in Figure 2.80. A, where the most significant changes are presented in the right anterior cingulate, bilateral cerebellum, and several mesencephalic and diencephalic. They also found a reduction in FA in various connections. Figure 2.10.B shows the bundles with the most significant changes, such as the periventricular zone and the corpus callosum.

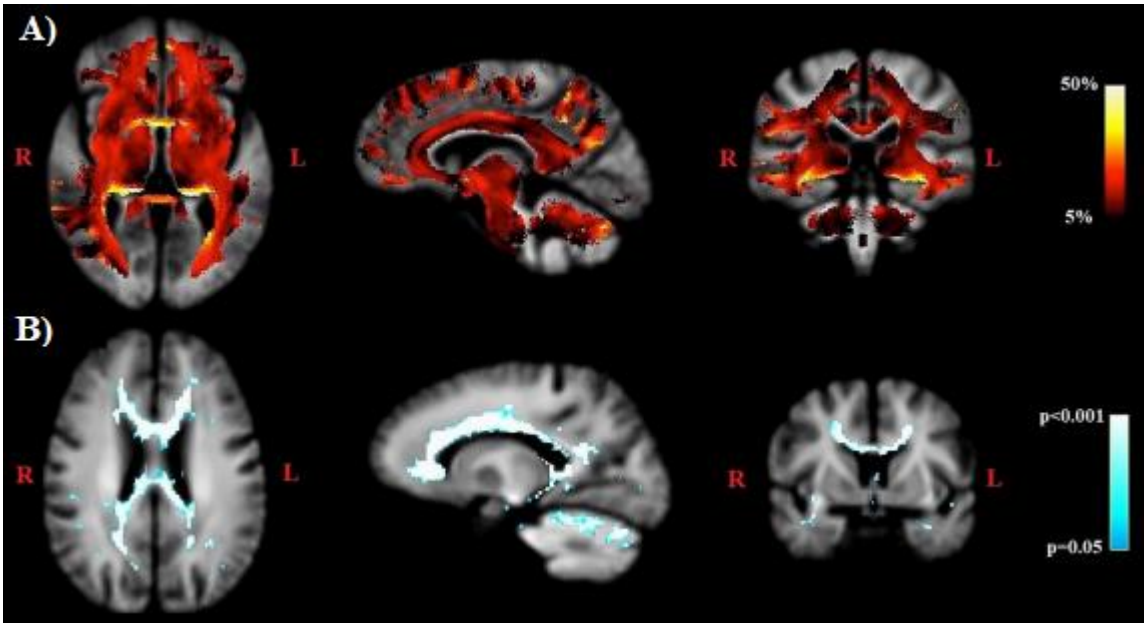

Figure 2.80. In (A), streamline segments were cropped from the template tractogram so that only streamline points that correspond to significant pixels (p value<0.05) were shown. Streamlines are colored by the percentage of decreased FC value in MS patients compared to Healthy Controls. (B) Voxels exhibited a significant (p value<0.05) reduction in FA in MS patients compared to Healthy Controls in axial, sagittal, and coronal views [39]**.**

D. Relationship between cortex, fibers, and Multiple Sclerosis

In the previous sections, we exposed the works performing anatomical and diffusion analysis of MS from a general point of view. Here, we will present various works that relate to these two analyses.

First, Cooper et al. [42] established a relationship between normal white matter (NAWM) lesions and cortical thickness. In previous works, such as those proposed by Steenwijk et al. [43] and Dayan et al. [44], the primary way to measure damage in NAWM was by DTI. In this case, the researchers used the T1/T2-weighted ratio to measure the myelin in the WM. This is described in detail in [45]. Methodologically, the images were processed in the MNI space. Then, the images were co-registered based on the FLAIR images. Then, the lesions were extracted using the LST toolbox, and the masks were generated using the CAT12 toolbox, both available in the SPM12 software. The main results they found were that cortical thickness decreased significantly with increasing lesion volume. Also, they associated NAWM diffusivity changes with a decrease in the cortical thickness, which correlates with the first result obtained. Ultimately, they concluded that using the T1/T2 weight ratio was an effective metric for determining the effects of the NAWM in the cortex. Still, they suggest continuing the work for its validation in other regions. The disadvantage of this technique is the lower sensitivity compared to other methods. Even though this work is not directly related to what was done

in this thesis, it can be noted that it shows a relationship between changes in cortical thickness and alterations in white matter.

On the other hand, Zhang et al. [46] evaluated the alterations in the GM and the microstructure of the WM. They used source-based morphometry (SBM), described in detail in [47]. Looking for these alterations was essential to establishing relationships between change in GM and WM. The first difference between previous studies was that the authors in this study used two databases. The first database was used to make all the measurements. The second database applied reliability tests to support the results from the first database. The researchers started by detecting and inpainting the lesions using proton density (PD) images through the Jim 6.0 tool. For the generation of masks, they used the FSL toolbox. Also, using FSL, they processed DTI data to calculate the FA metric, which will be used to detect changes in WM, and then used the SPM12 software through the VBM tool to generate segmentation and volume extraction of the brain GM. To facilitate the analysis, the GM was divided into the deep GM (caudate and thalamus), the sensorimotor GM, the inferior frontal gyrus and pars opercularis, the posterior GM, the occipital GM, and the cerebellar cortex. One of the main conclusions was that there was a pattern of change in cortex regions associated with the motor area, and they found the same way of change in subcortical regions. Also, significant differences were found in brain fibers related to the cognitive area, memory area, and processing speed. Finally, they concluded that they could not detect a significant connection between changes in cortical GM and WM. Still, they determined that the differences were clinically relevant and suggested continuing with studies associated with this topic.

Unlike the previously mentioned work, Pagani et al. [48] assess how changes in connectivity affect the motor and cognitive areas of MS patients focused on the impact of the WM lesions. First, they segmented and inpainted the WM lesions using the Jim 6.0 tool. Using DTI images, they calculated the FA. Then, they constructed a structural connectivity atlas, described in detail in [48]. Subsequently, this atlas was applied to each subject to calculate the connectome. Five properties to evaluate the results: the mean strength, the assortativity, the transitivity, the global efficiency, and the characteristic path length [49]. The results shown in Figure 2.91 indicate significant changes between groups in all the properties except in assortativity—the results of the disconnection analysis are shown in Figure 2.102. The connections are shown as nodes classified into centers from the control patients based on the strength and betweenness of the centers. The assortativity parameter was the one that presented the highest values in MS patients. The researchers found that the precuneus was identified as a hub of brain fibers altered for RRMS patients, suggesting that this region was critical when

disruptions in brain GM connectivity occur. Finally, the researchers determined that connectivity does not show significant changes based on their disconnection model, suggesting that the brain was resistant to damage from MS lesions. However, they recommend continuing with studies given the limitations they presented during the work.

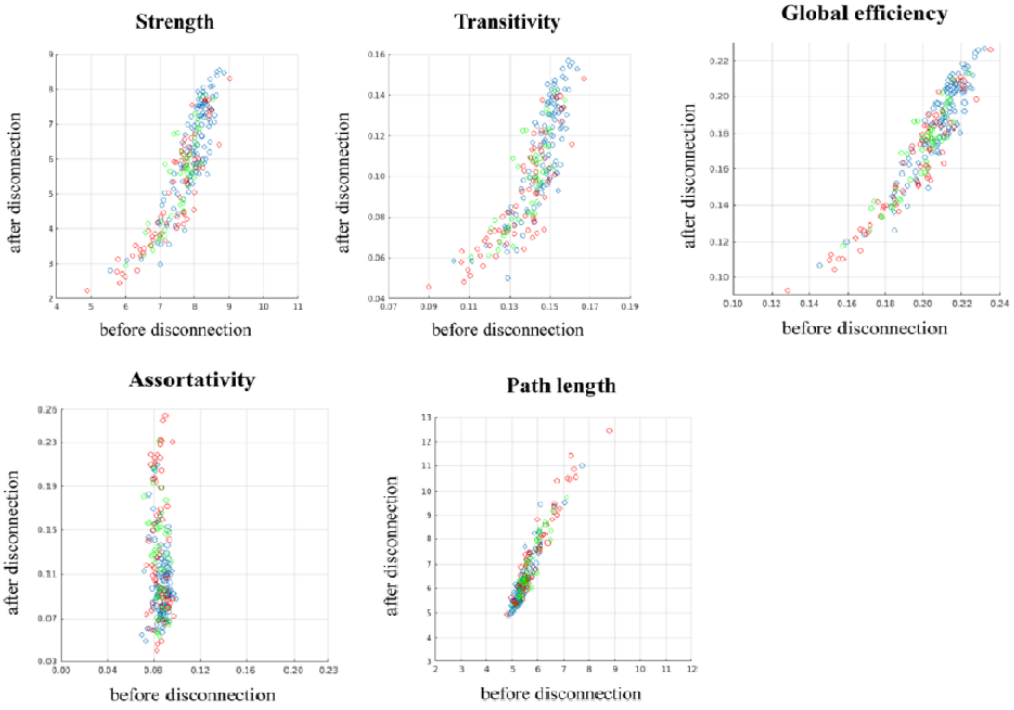

Figure 2.91 Results that show the linear dependence before and after disconnection. Scatter plots of global metrics before (x-axis) and after (y-axis) modeling of disconnection. Relapsing-remitting Multiple sclerosis (RRMS) patients are shown in blue, secondary progressive MS (SPMS) in red, and benign MS in green [48]**.**

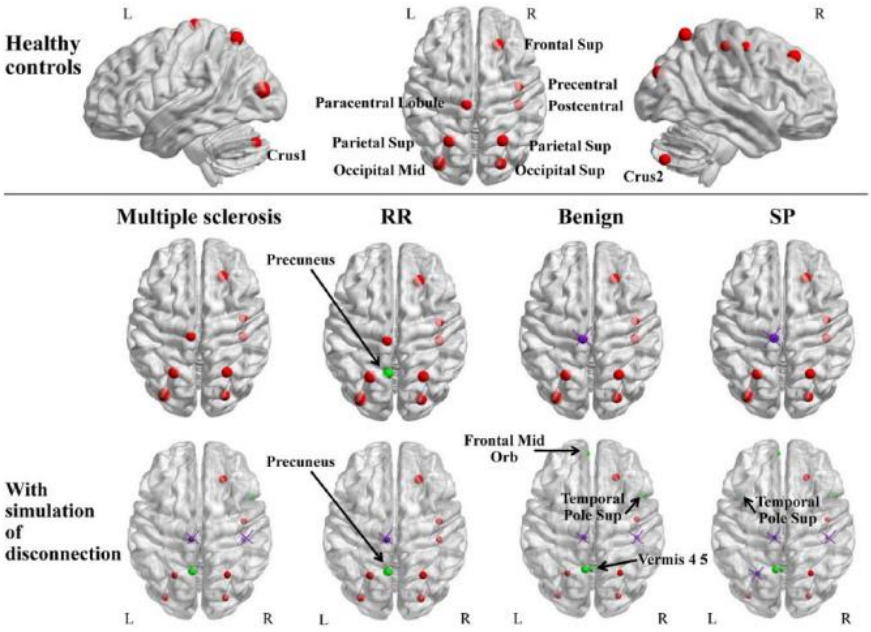

Figure 2.102 Standard brain surface with hubs of the network. Hubs were found in healthy controls (first row), Multiple Sclerosis (MS) patients, and according to clinical phenotypes (second row), and the same after modeling of disconnection (third row). New hubs are colored green. Lost hubs are identified in violet. RR: Relapsing-Remitting MS; SP: Secondary Progressive MS [48]**.**

The following work corresponds to the closest research to the work performed in this thesis. Bussas et al. [50] assessed whether WM fiber connectivity alterations in MS subjects could explain GM atrophy throughout the brain. As mentioned in previous works, WM lesions and cortical atrophy are fundamental when evaluating the severity of MS [51]. In this work, the preprocessing stages were like those of previous works: the lesion inpainting and the creation of gray and white-matter masks, using the LST and CAT12 tools, respectively. For the connectivity assessment, the researchers used the connectome rendered from the Human Connectome Project [52] to create a disconnectome map. The creation of this map is described in [50]. They performed two kinds of analysis: cross-sectional and longitudinal. For the cross-sectional study, they used the first image they took from the patients, and for the longitudinal, they used the first and the last image. They conducted the same study for every time point, considering each time point as an individual image. In contrast, they performed the difference between both time points for the longitudinal analysis and then determined the significant changes between them. They found a strong correlation between changes in subcortical structures and disconnection in the cross-sectional study. In addition, as shown in Figure 2.113.A, they found a correlation between disconnection and atrophy regions of the cerebral cortex. In the latter case, the areas with the most significant correlation were the precentral, middle frontal, and lingual regions.

Furthermore, the longitudinal results showed a strong correlation between atrophy in subcortical structures and disconnection. At the cortical level, as shown in Figure 2.113.B, they found a significance similar to the cross-sectional analysis, but it covers a larger area in this case. In conclusion, the authors determined an interesting correlation between the changes produced in the GM and WM at cortical and subcortical levels.

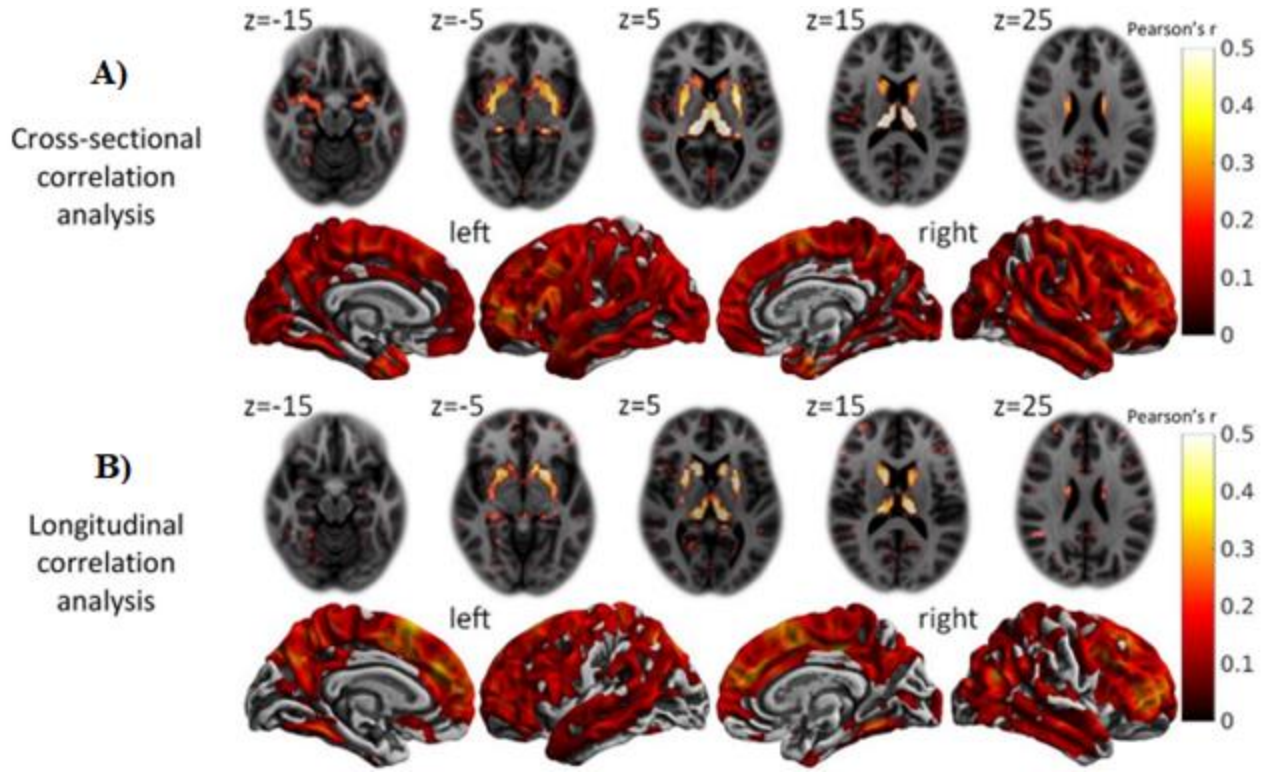

Figure 2.113 Correlation of disconnection with gray matter atrophy. (a) Cross-sectional correlations between disconnectome maps and gray matter atrophy maps. (b) Longitudinal correlations between maps of disconnection increase and maps of atrophy increase. (a)–(b) Each panel contains axial slices of the voxel-wise correlations (top) as well as medial and lateral views of the surface-based correlations (bottom). The colors indicate the strength of the correlation according to the bars on the right (Pearson's r). Only voxels or vertices that were significant levels are colored [50]**.**

E. Discussion

Based on state of the art, we can observe the clinical importance of knowing how cortical GM changes are related to the WM alterations produced in MS disease. The T1 images provide helpful information regarding the anatomical effects of MS on GM. At the same time, diffusion MRI images enable the identification of the WM brain fiber alterations. Studies in which both images are used establish a more complete understanding of the impact of MS on the subjects.

Many studies have been carried out on this topic, proposing several methods to identify the effects of MS on GM and WM. Such work has allowed us to increase our understanding of the effects of the disease on the brain. A main approach is the longitudinal analysis. Although the implementation of this analysis varies across the authors.

Several works studied the impact of MS at the cortical level, some longitudinally, and others analyzed the relation of these changes with the degree of physical and psychological disability. This allows us to determine the regions where this pathology is most affected, highlighting the motor and sensory regions. In the case of the motor regions, the precentral and the superior frontal were the most mentioned by the researchers. The reason for that may be because this disease is characterized by having a significant effect on the mobility of the subjects. On the other hand, the highlighted sensorial regions were the superior parietal and superior temporal. These two regions are strongly related to the visual and auditive processing. Also, the superior parietal region is associated with the sensory input of one of the hands of the subjects. All these effects, motor and sensory, are well-known and associated with MS.

Other works establish the relationship between the WM changes, and MS. Some works studied the WM lesions, while others explored the changes in the brain fibers. From those works, it has been possible to conclude that the alterations in the WM are significant and that these could be related to the changes in the GM. The DTI was the primary technique to determine these changes. Specifically, using the DTI metrics, FA changes as one of the most essential and significant indicators of change in the WM brain fibers. The bundles most mentioned by the researchers that present substantial changes were the corpus callosum and the thalamic variations. The corpus callosum is highlighted because it is an important inter-hemispheric brain fiber hub connecting different motor and sensitive regions. The thalamus is well-known to be one of the most affected subcortical structures by MS.

On the other hand, only a few studies have tried to establish the relationship between the three aspects: GM, WM, and MS clinical effects. Some associations have been observed between these three data types, some associated with subcortical areas, while others focused on cortical surface

regions. In these few studies, the anatomical cortical regions identified were those highlighted by previous purely anatomical studies, such as the precentral and the superior parietal regions. Likewise, the WM fibers identified in these few studies were also mentioned in previous studies: the corpus callosum and the thalamic variations.

Finally, the lower number of this kind of works gives us optimism during this thesis work because it will allow us to contribute to the study of Multiple Sclerosis.

2.2.2 Modeling of Longitudinal Data for Multiple Sclerosis

A. Longitudinal Study in FreeSurfer

Longitudinal analysis of medical images has become increasingly relevant in the clinical area due to its ability to provide a better perspective of changes that patients experience throughout their illness. Physicians can use these studies to track treatment progress and make the necessary modifications. A software extensively used to perform such analysis is FreeSurfer [7], which benefits from technical capabilities and specialization.

FreeSurfer analysis consists of three stages: cross-sectional processing (CROSS), creation of a within-subject template (BASE), and longitudinal processing (LONG). First, in the CROSS stage, each image undergoes a cross-sectional analysis, which includes a full cortical reconstruction. Second, in the BASE stage, a template is generated for each subject using all the images from every time point. Finally, in the LONG stage, the longitudinal analysis is performed.

B..1 CROSS Stage

All images are processed independently using the recon-all function, which performs a cortical reconstruction of the images. This function executes 31 steps, described in Table A.1 in Annex A. On average, this stage can take five to six hours per image on a high-performance computer. Once completed, several directories are created containing all the new images and statistics. Sometimes, errors affect the reconstruction of the surface and subsequent analysis. However, manual editing is not recommended as it can add bias to the image and affect the quality of subsequent studies [7]. In such cases, it is recommended first to check the image for any errors during acquisition and then re-run the stage. If the error persists, it is recommended to discard the image.

B..2 BASE Stage

In this stage, a template is made for each subject using the data obtained in the previous stage. The aim is to establish the average anatomy of each subject. Like the CROSS stage, this process takes four to five hours for each subject.

When creating the template, the software makes several adjustments. Firstly, it treats all images equally to prevent any asymmetry. Additionally, it avoids using higher-order warps to prevent any temporal contrast smoothing.

This stage is divided into five steps:

- Initialization of the template: It is determined by calculating the mean or median of each one of the images, then each input image is registered and resampled, and finally, this process is repeated. In the end, the file *norm_template.mgz* is obtained, which will be used in the following steps.
- Normalization: Creation of control points and variation fields
- Skull removal: the brain mask is resampled and averaged.
- Registry: Uses *norm_template.mgz* for the Talairach registry.
- Normalization: Uses *norm_template.mgz* for normalization. This ensures that *norm_template* is correctly normalized.

B..3 LONG Stage

The algorithm is initialized during the final processing stage using the information generated in the previous stages. Some data is copied directly, while others are used as inputs later. Similar procedures were done in this stage, that in the CROSS stage, which are explained in detail in Table A.1 in Annex A. The time taken for this stage is approximately two to three hours for each image, which is about half the time taken for the last two stages. A summary of the entire longitudinal processing carried out with FreeSurfer can be seen in Figure 2.14.

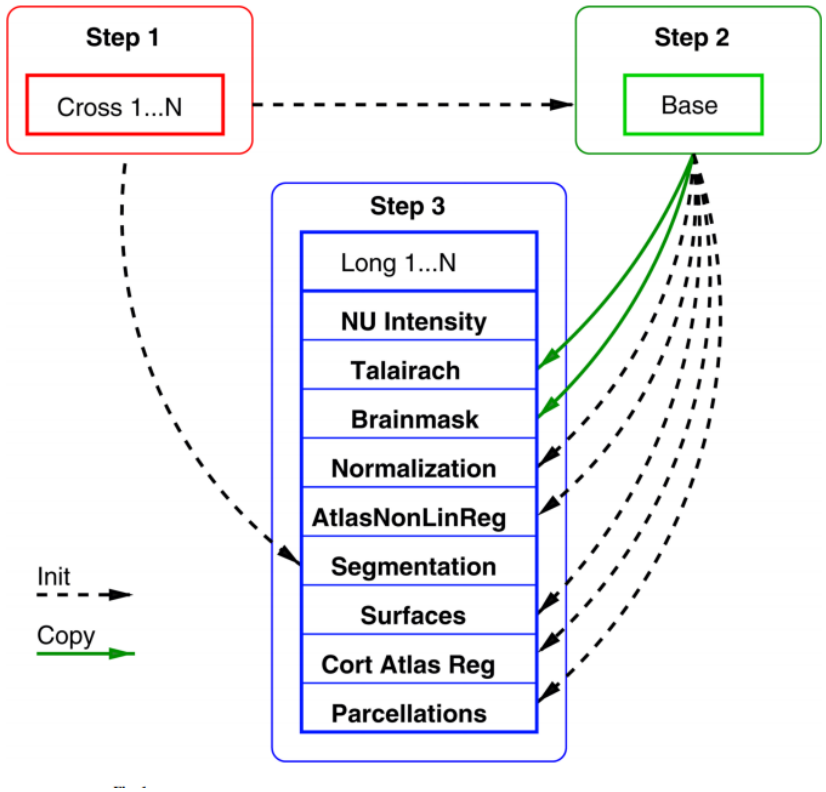

Figure 2.124 Simplified diagram of the three stages that make up longitudinal processing in FreeSurfer. Dotted line: Information used for initialization, Solid line: Information copied [8].

B. Generalized Linear Model (GLM)

The generalized linear model (GLM) encompasses the distribution of non-normal responses and function modeling based on the arithmetic mean of the data. GLMs refer to a set of model classes that McCullagh and Nelder [53] popularized. From those existing to date, they assumed that the response variable of the system *y* has an exponential family distribution with mean u_{yo} that is supposed to be a function of $X_{yo}{}_T\beta$. The GLM comprises three parts: the random component, the systematic component, and the link function.

The random component is the probability distribution of the response variable Y. These components follow a probability density function as shown in equation (2.1).

$$Y = f(y_i; \theta_i) = a(\theta_i)b(y_i)exp\big(y_i\ Q(\theta_i)\big) \quad \textbf{(2.1)}$$

In this case, $f(y_i; \theta_i)$ represents an exponential distribution. The value of y_i correspond to the independent observation of the response variable Y and the value of θ_i varies between 1 and N, where N is the total number of subjects to be analyzed. In addition, we have the parameter $Q\ (\theta)$, called the natural parameter. The *a, b, and the exponential* combine functions to create a specific distribution.

The systemic component is associated with the explanatory variables in the model, more specifically, their linear combination. Also, the systemic component is considered a linear predictor, as shown in equation (2.2). Here, the x_{ij} are the explanatory variables, and the β_j is the intercept term.

$$\eta_i = \sum_j \beta_j x_{ij} \tag{2.2}$$

Finally, we have the link function, which aims to unify the random and systemic components. It indicates how the expected response values relate to the linear combination of the explanatory variables. To define the link function, we have to first redefine the response variable Y according to equation (2.3). From here, the E represents the expected value of Y.

$$\mu = E(Y) \tag{2.3}$$

So after that, the link function $g(\ .\ )$ is the one that joins μ, with the systemic component, represented as η. This relation is defined according to equation (2.4).

$$\eta = g(\mu) \tag{2.4}$$

Since the GLM is a group of statistical models, the link function will determine the appropriate model to work. A summary of the most popular GLMs is in Table 2.22.

Table 2.2 Most popular GLM models for statistical analysis [53].

Model Name	Random Component	Link Function	Systemic Component
Linear Regression	Normal	Identity	Continuous
ANOVA	Normal	Identity	Categorical
ANCOVA	Normal	Identity	Mixed
Logit Mixed	Binomial	Logic	Mixed
Log-linear	Poisson	Logarithmic	Categorical
Poisson Regression	Poisson	Logarithmic	Mixed
Multinominal Response	Multinominal	Generalized Logic	Mixed

The use of the GLM model is popular among researchers. One of these is the work by Gracien et al. [54] which presents an approach that relates to the thickness cortical damage to T1 relaxation time and the increase in proton density using MRI images. The implementation of the GLM model was through FreeSurfer. The model used a t-test to calculate the metrics of all the time points for all the subjects. They use a FWHM equal to 5 [mm]. The FWHM is a measurement used to determine how smooth the image will be. The most common values are between 5 and 25 [mm]. In addition to the model, a test was applied to correct for multiple comparisons based on Monte Carlo simulation. They used a significance level of a p-value less than 0.05. Figure 2.15 indicates an increase in T1 and

proton density (PD), but those were unrelated to age, EDSS value, or disease duration. However, the researchers mention that these changes could be related to the MRI parameters.

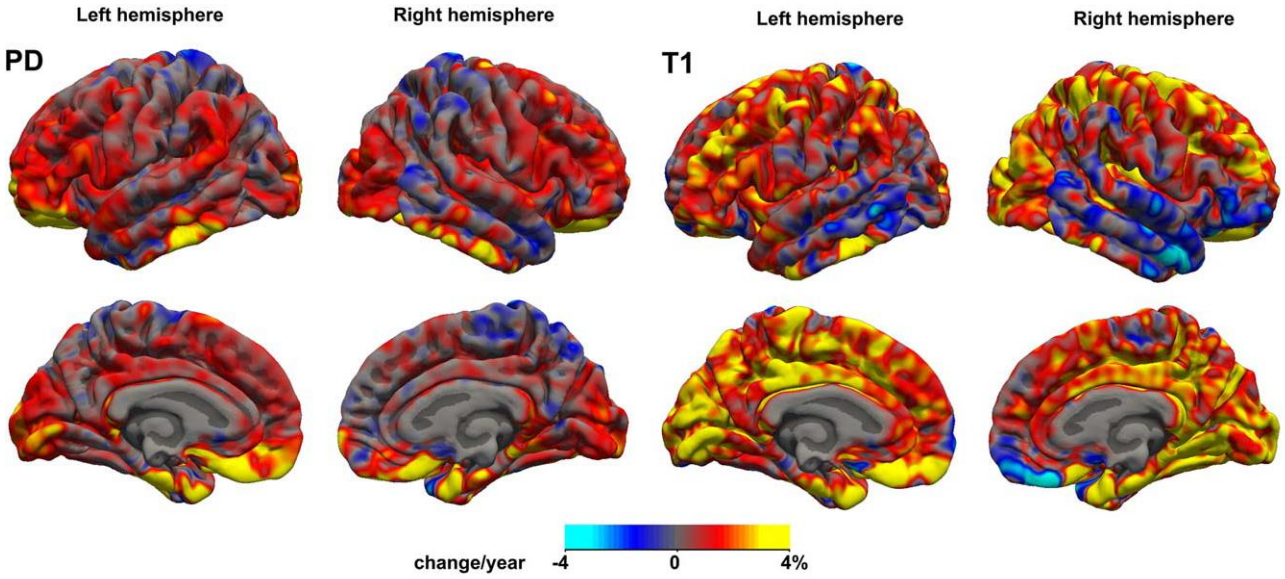

Figure 2.135 Map of percentage of change per year of PD and T1; red indicates a positive change, and blue indicates a negative change [54].

As we saw in the previous work, the correlation between the progress of the pathology and the parameters of an MRI image allows us to detect the effects of the MS on the brain and establish a relation with clinical and anatomical variables, which is highly relevant. Tillema et al. [55] described an approach to look for a pattern between cortical thickness change and cognitive impairment in RRMS subjects. Using the FreeSurfer software, they extracted the cortical thickness change for each image for every subject and used a GLM model to analyze the data. They used an FWHM equal to 10 [mm] and multiple comparisons based on the Monte Carlo method, with a significant threshold of less than 0.001. In Figure 2.16, there are some regions in the cortex where the cortical thickness presents some level of decrease, as shown in the blue areas. In patients with MS, the cortical regions that show more significant changes are the medial temporal and inferior parietal regions. Finally, the researchers said the relation between cortical thickness change and cognitive impairment was present but not at a high level. However, one point to consider is that in this study, most of the patients are old, which could affect the results.

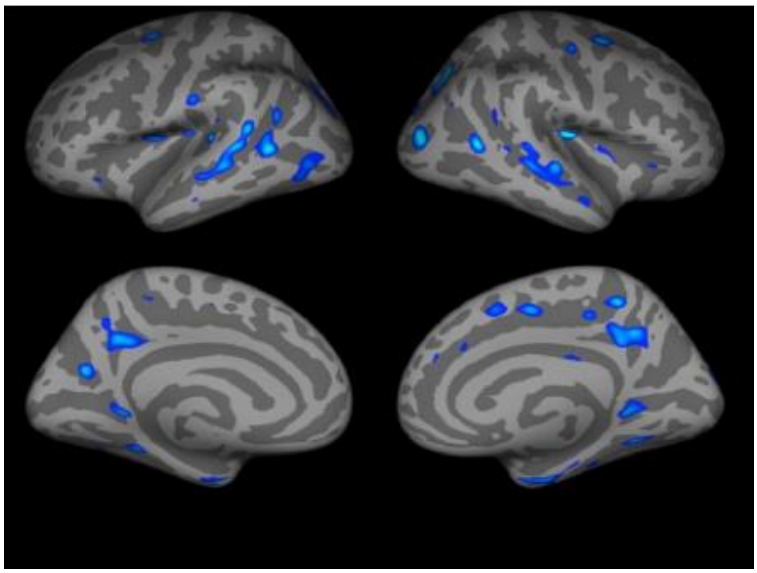

Figure 2.146 Comparison between healthy and MS patients shows limited but present thinning. The blue indicates the areas with the highest significance level with a negative correlation [55]**.**

C. Analysis of Brain Fibers Bundles

One of the analyses over the diffusion MRI images is the superficial white matter (SWM) analysis. SWM is characterized by short-association U-fibers [56]. The use of SWM analysis instead of the deep white matter (DWM) is because the myelin in the fibers in SWM wraps more sparsely than in the DWM [57]. Also, in the SWM, is the region with more amount of lesions in MS patients [58].

The use of SWM in studies associated with MS is not very frequent, highlighting the one done by Buyukturkoglu et al. [15]. In this work, the authors found non-random patterns in the early stages of MS before witnessing anatomical and functional changes. On the other hand, there are works associated with SWM but applied to other pathologies where the WM is also affected. One of these works is the one by Veale et al. [59] where SWM analysis was performed using DTI in patients with Alzheimer's. Their goal was to differentiate between changes caused by degeneration and organizational changes caused by illness. The researchers used FA, MD, neurite density index, scatter orientation index, and tissue fraction as metrics. They found that the changes in the microstructures of SWM and along the cortical surface suggest a change in the WM fibers by degeneration and at the organizational level, with low values of the neurite density index and a high value of the dispersion orientation index.

Another related work was done by Phillips et al. [60], aiming to establish the relevance of SWM for Huntington's disease, given the area's sensitivity to the effects of neurodegenerative diseases. The researchers used the DTI and T1 anatomical images of the subjects to achieve this goal. FA, MD, RD, AD, metrics were calculated from the DTI images. The researchers found an increase in AD and RD in pre-symptomatic subjects compared to control patients. In contrast, patients with the entire pathology present an increase in all diffusivity parameters, as shown in Figure 2.157. These results indicated that the SWM is where the pathology has a particular effect in previous stages or during the disease.

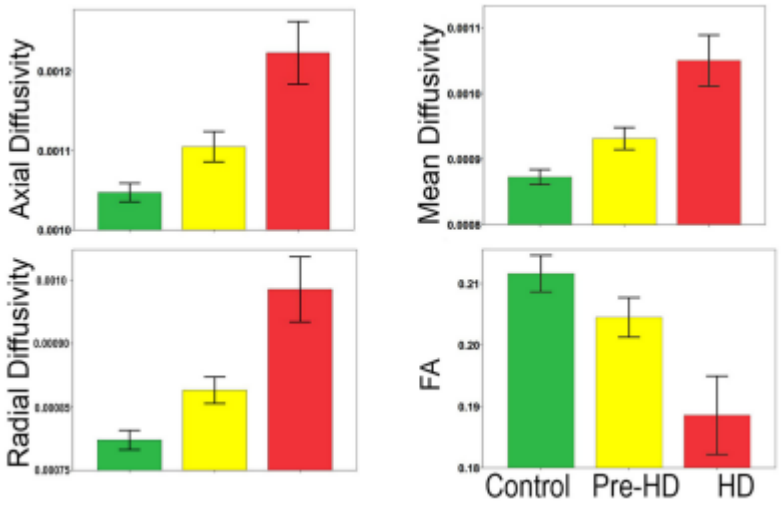

Figure 2.157 Whole-brain mean diffusion metrics for SWM and group comparison. Bar graphs show significant differences between SWM AD, RD, MD, FA. FA, Fractional Anisotropy; AD, Axial Diffusivity; RD, Radial Diffusivity; MD, Mean Diffusivity (Units: 10−3 mm2/s**)** [60]**.**

B..4 Superficial White Matter Analysis

The SWM analysis performed for this research is like that done by the co-supervising professor at [15]. The application of this analysis is divided into four stages: tractography calculation, image normalization and coregistration, SWM bundle segmentation, and the calculation of the SWM metrics. All this process was applied through Python codes. All this processing of obtaining the diffusion metrics was done by the engineer Christopher Vergara.

A ..4.1 Tractography calculation

This is an image preprocessing stage in which raw diffusion magnetic resonance images (dMRI) are used. For this stage, two software were used. First, the FSL tool, available in FMRIB's Diffusion Toolbox [12], was used to correct the distortions caused by the movement, the eddy currents, and the non-homogeneous field of the images. Also, the DSI Studio software was used to obtain the steamline deterministic tractography of the entire brain through the diffusion MRI images resulting from the previous stage [61]. For this research, the GQI images model was used [62].

The GQI model differs from the DTI model in that the isotropic diffusion and the anisotropic diffusion are separated in GQI, thus minimizing the partial volume of free water. Anisotropic diffusion is further quantified for each main diffusion direction, thus minimizing the partial volume of the crossed fibers [63]. In this step, all the diffusion metrics were calculated, such as FA, MD, RD, AD, and QA. Figure 2.168 shows a comparison between FA, obtained by DTI, and QA, obtained through GQI model.

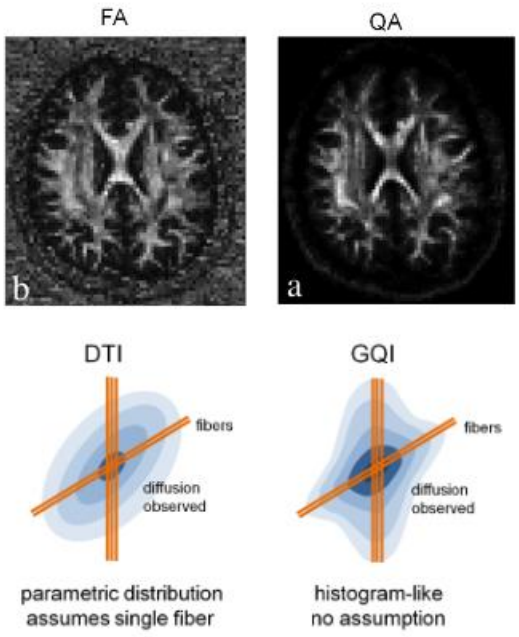

Figure 2.168 Difference between the FA and QA based on observed diffusion [62].

The use of the GQI model on data from patients with MS is rare, and there is not much literature in this area. Still, there is some work comparing the results between the DTI and the GQI models for other neurodegenerative diseases. For example, Guo et al. [64], to quantified how both models behaved by comparing their reference metrics, FA for the DTI model and QA for the GQI model. They used brain age to compare the models, which is a good predictor of neuroimaging. The

methodology for this study was based on machine learning models to predict the behavior of the metrics. The main results were that the predictions made using FA were more accurate and with a higher degree of sensitivity than those made with QA. However, the researchers mention that, according to previous studies [65], DTI images have a high degree of sensitivity to age and that the DTI model cannot detect differences between an intra- and extra-axonal compartment [66].

Another work related to the GQI model is by Li et al. [67], whose main objective was to establish an anatomical relationship between the trajectory of the medial longitudinal fasciculus (MLF) and the oculomotor nerve through tractography data. They reconstructed the fibers using the HCP-1065 protocol as a template [68]. The evaluation of the MLF is based on the Center for In Vivo Microscopy template at Duke University. They used the QA and FA metrics to compare the results of the GQI and the DTI model. One of the results the researchers highlighted was a decrease in all the metrics in the MLF regions that present lesions versus those without the WM lesions. The researchers interpreted these results as a decrease in the spin density of diffusion anisotropy when comparing the MLF of the areas with and without lesions. In addition, they highlight the relevance of the protocols used and the use of GQI-based tractography as a new evaluation and reconstruction tool.

A ..4.2 Image normalization and coregistration

During this research stage, we used two different kinds of images, T1 and DW images, to normalize them to the MNI space. The T1 and DW images were corrected using the SPM12 software. This process is the same as that used for the anatomical analysis, which will be described in greater detail later in section 3.3.1.C. Then, the T1 images were normalized to the MNI space. Also, the tractography was transformed into the MNI space. In this space, the WM bundles are identified and segmented directly from each subject's tractography dataset.

A ..4.3 Superficial White Matter Bundle Segmentation

In the segmentation stage of the SWM bundles, the fibers of each tractography dataset already in the MNI space must be resampled with 21 equidistant points, as described in the work by Guevara et al. [69]. The algorithms used for segmentation are based on the combination of two atlas of SWM bundles. One is described by Guevara et al. [61], and the second is defined by Roman et al. [70]. The algorithm calculates a pairwise distance between each fiber of the resampled tractography dataset and each fiber of the atlas. Then, each fiber is labeled with the closest bundle when the distance is less than the threshold given by the atlas. Then, the indices of previously labeled fibers are used to extract the segmented bundles from the original tractography dataset in the diffusion space of every subject.

A ..4.4 Calculation of different metrics for SWM bundles

A mask is created for each bundle to obtain the different diffusion metrics we use during this research. The bundle masks were then used to obtain diffusion metrics across the bundles, and the average of the obtained values are calculated. After this process, we got the mean diffusion metrics FA, QA, MD, AD, and RD for each bundle and each subject.

D. Discussion

Based on the literature on the different data modeling methods for longitudinal analysis, we choose FreeSurfer software for the anatomical study, the GLM model for the statistical anatomical research, and the SWM analysis for the diffusion MRI analysis.

Several works support the use of FreeSurfer to carry out longitudinal analysis. The most significant advantage of this software is the quality of the calculations performed, especially the creation of cortical and subcortical masks, enabling for a more detailed description of the studied regions. Due to the quality of the results, especially at the cortical level, many researchers rank it above other software that performs similar analyses. However, one of the disadvantages is the significant learning curve for using the software. Also, the high demand for technical resources, as the time it takes to complete the analysis is of approximately 10 hours per subject.

Regarding the statistical models available for carrying out longitudinal studies, the most used by several authors is the GLM model. This model's two most important advantages are its simplicity during its application and its good results. Although it is one of the most used, it has disadvantages. The first is that it only uses the arithmetic mean of the data to do its analysis. This could misrepresent the results because just one statistical variable could not represent all the effects of the disease on the subjects. The second disadvantage is the non-consideration of the covariates that change over time. The difficulties we experienced during this research focused on the learning curve for its application and the time consumed to learn how to interpret the results generated.

Finally, using SWM analysis over diffusion MRI data is fundamental for analyzing brain connectivity. Using the diffusion metrics from this analysis allows us to more precisely detect the WM fibers bundles altered in MS. These affected fiber bundles can be connected to changes at the cortical surface.

Understanding the effects of MS on brain connectivity and the cortical surface and the relationship between them may produce to a better understanding of the pathology.

Capítulo 3. Longitudinal Analysis in Multiple Sclerosis

3.1. Introduction

Figure 3.1 shows a graphical representation of all the analysis done during this research.

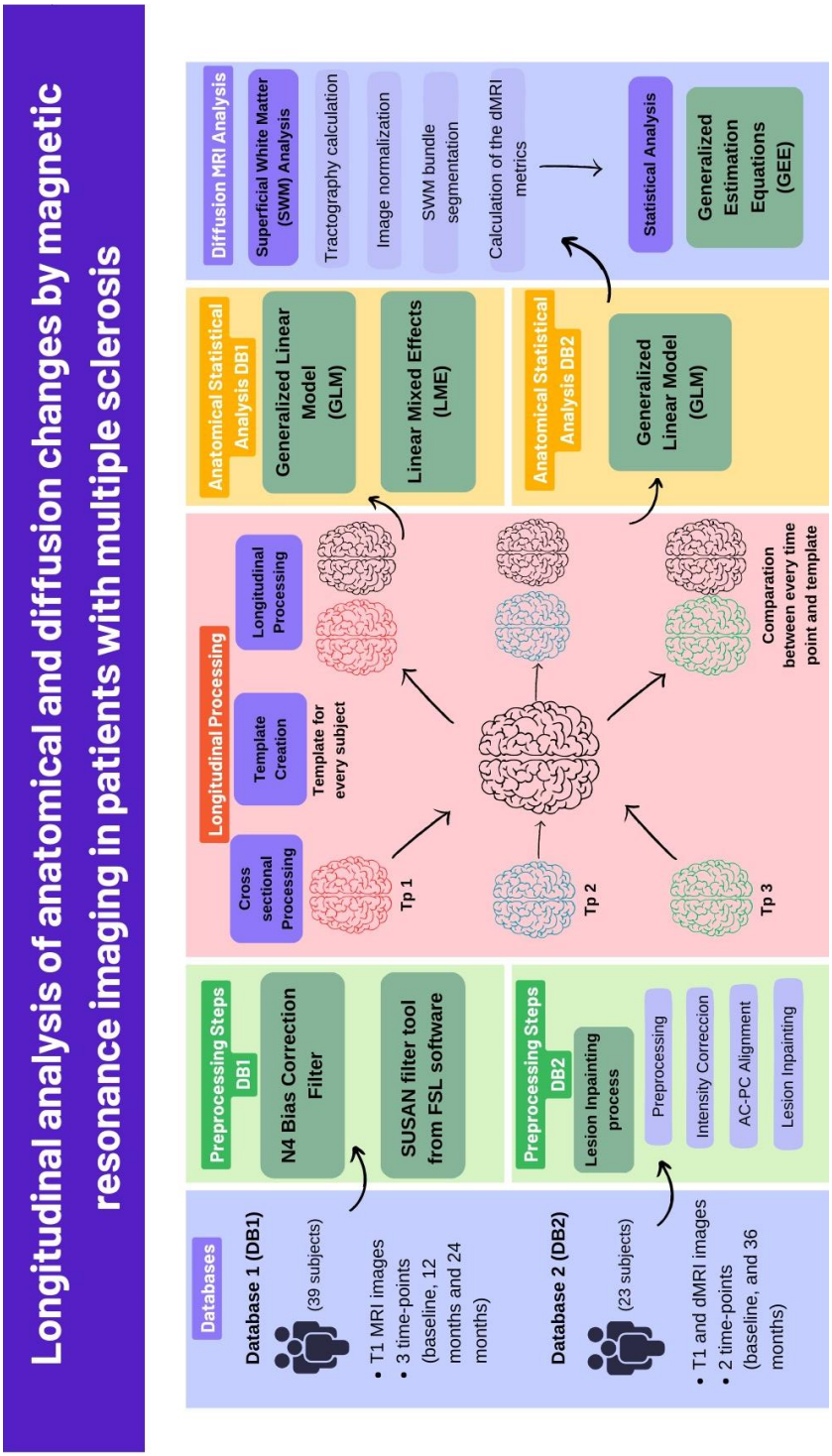

Figure 3.1 Graphical abstract of the longitudinal analysis in MS.

3.2. Longitudinal anatomical study on the DB1 database

In this first section, the objective will be to expose the different tests carried out on the DB1 database. This analysis of DB1 had two goals. The first was to generate anatomical results to compare with the results given by DB2. The second is using it as a test to determine the best metrics for future analysis and understand the software's functionality. All this analysis was done in the local cluster.

3.2.1 Image ordering and preprocessing stage

Figure 3.2 shows the schematic of each image's preprocessing steps. Here, a structural similarity index measurement (SSIM) was used to verify the performance of this stage. It is a metric for determining the similarity between two images, which is based on discarding those distortions that do not affect the structure of the image and do not affect the local intensity patterns. Finally, structural information considers the interdependence between each image pixel, carrying valuable information about its visual structure [71].

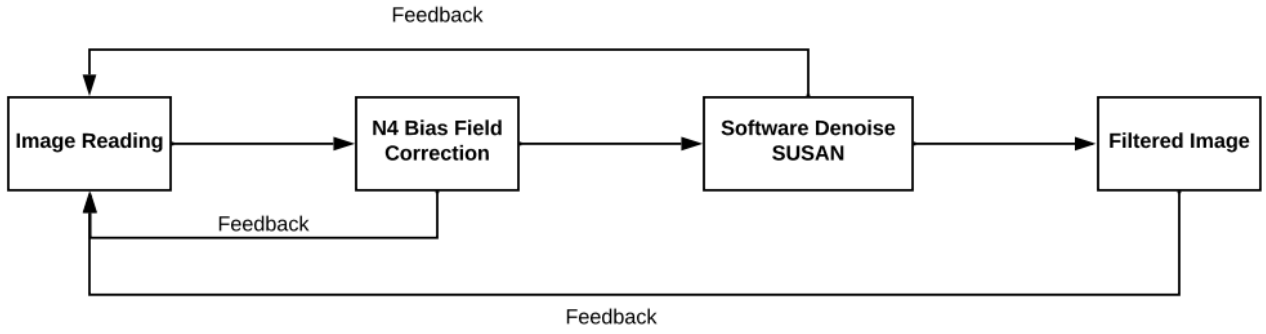

Figure 3.2 Flowchart of the preprocessing step. The feedback process corresponds to the application of the SSIM metric to compare the results of different step with the previous one of the pre-processing stage.

A. N4 Bias Correction Filter (N4ITK)

The first step of image filtering was using the N4 Bias Correction filter. In general terms, this filter is an iterative method that seeks to maximize the high-frequency content of the intensity distribution of the tissue in the image. In other words, the algorithm assumes that the deviation field is a type of statistical error corresponding to a low-frequency artifact that alters the intensity of the image, so this filter seeks to attenuate these frequencies, improving the image quality [72].

The initial variables required for its operation can be found in Table 3.1. The execution of this filter was through Python scripts. We used, the Simple ITK, with its

N4BiasFieldCorrectionImageFilter () function. The execution time of this filter is around 10 minutes for each image [73]. The SSIM coefficient was used to check this filtering step's performance.

Figure 3.3 shows an example of a comparison between the original image of a subject versus the same image already filtered. When applying the SSIM coefficient, the average result among all the images was 0.982, which can be interpreted as a small decrease in the noise of the image.

Table 3.1 Variables of N4 Bias Correction [73].

Parameters	Definition	Values
Image Mask	It is generated when executing the script	Not Applicable
Shrinkage Factor	Defined in image subsampling (reduces time)	0-1, 1 indicates the original resolution
Full with half maximum (fwhm)	The FWHM is a measurement used to determine how smooth the image will be. Defined by default	0
Convergence Threshold	Determined by the radius variation coefficient (defined by default).	High values decrease execution time.
Maximum Number of Iterations	Defined by default	High values increase execution time but improve results. In this case, 4

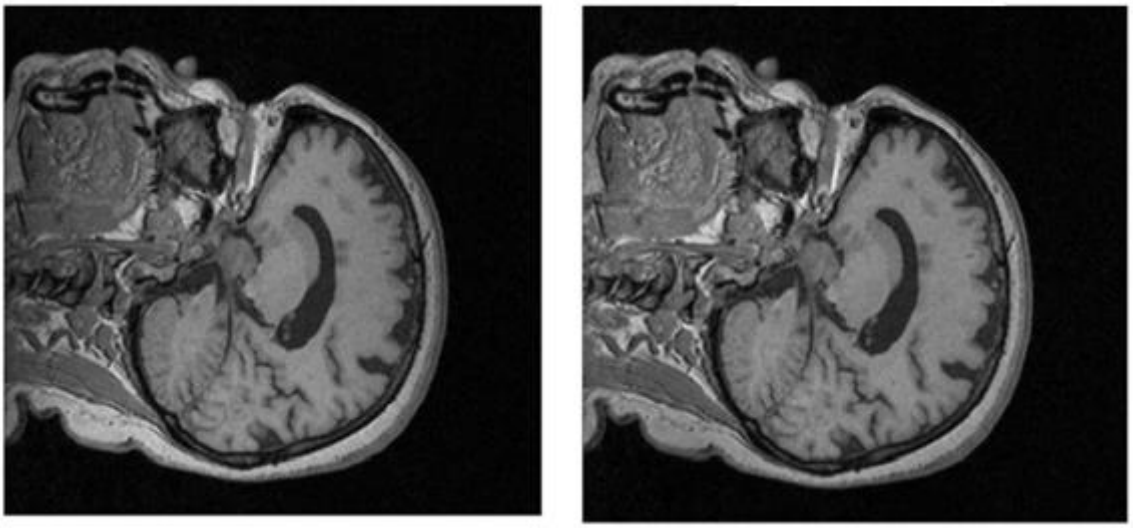

Figure 3.3 Example of an original image and its image filtered using the N4ITK filter. On the left is a section of the original image before applying the N4ITK filter on the right, the same section, but after applying the N4ITK filter. From a qualitative point of view, no significant differences are observed, this is reflected in the value obtained from the SSIM metrics (0.982) which indicates that the level of similarity is very high.

B. Filtering using the SUSAN tool available in FSL software

After using the N4ITK filter, it was possible to conclude that there was a noise reduction, but this was not very significant, so applying another filter was necessary. SUSAN is a tool available in the FSL software [9], whose primary function is reducing image noise. This tool is available for Linux operating system.

The general operation of the SUSAN filtering tool consists of applying a non-linear filter for noise reduction. This filter calculates the averages of each voxel using the nearest voxels with similar intensity. The software takes approximately five minutes to process each image. Also, through the processing of the filter the software defines certain variables that, due to the nature of the process, these variables change throughout the execution. The definition of each variable was detailed in work conducted by Smith et al. [11].

Figure 3.4 shows an example of the result of this filtering step. Qualitatively, there is a visible improvement regarding the enhancement in the high-frequency areas. Also, there is an average SSIM value of 0.90, which could be interpreted as a noise reduction and greater effectiveness of the process, improving the quality of the images.

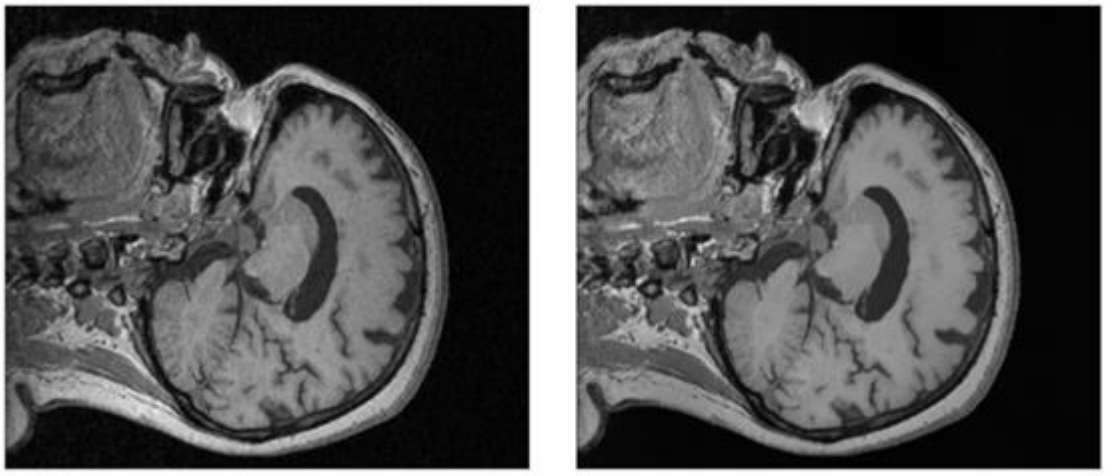

Figure 3.4 Example that compares the original and filtered images using the SUSAN tool. On the left is a section of the original image before application; on the right is the same cut but after the pre-processing stage**.**

3.2.2 Longitudinal Processing

Longitudinal processing was performed using FreeSurfer software [8]. This processing was applied to images after the pre-processing stage. Firstly, the CROSS stage was applied, whose main objective is the full cortical reconstruction of the images of each subject. This took a series of steps,

all detailed in Table A.1 of Annex A. The process took four to five hours for each image. At the end of this stage, a series of images and files were available, highlighting the ones that had measurements of cortical changes of white and gray matter.

Then, the BASE stage was applied. Here, a template was generated from the three images of each subject. This stage created a template image for every subject. Then, a whole segmentation and surface reconstruction was performed over this template. The execution time of this step was between four to six hours to create every template. Figure 3.5 shows an example of the template created for one of the subjects. The image shows its average anatomy over time, superimposed with the white matter and pial surfaces, highlighted in blue and red, respectively.

Finally, the LONG stage was applied. Here is where each time point was processed together with the template. This step performed the same processing and calculations described in Table A.1 of Annex A. An example of the results obtained is shown in Figure 3.6, where three time points are shown, one on top of the other, the third time being the most visible. The white matter and pial surfaces are drawn in different colors, one on top of the other. Red and blue were used for the first time point, pink and light blue for the second, and yellow and green for the third time-point. You can see if there are any anatomical changes between the three time points. This stage took two to three hours to perform all the processes and calculations per subject. The results from this final stage are used in the statistical analysis.

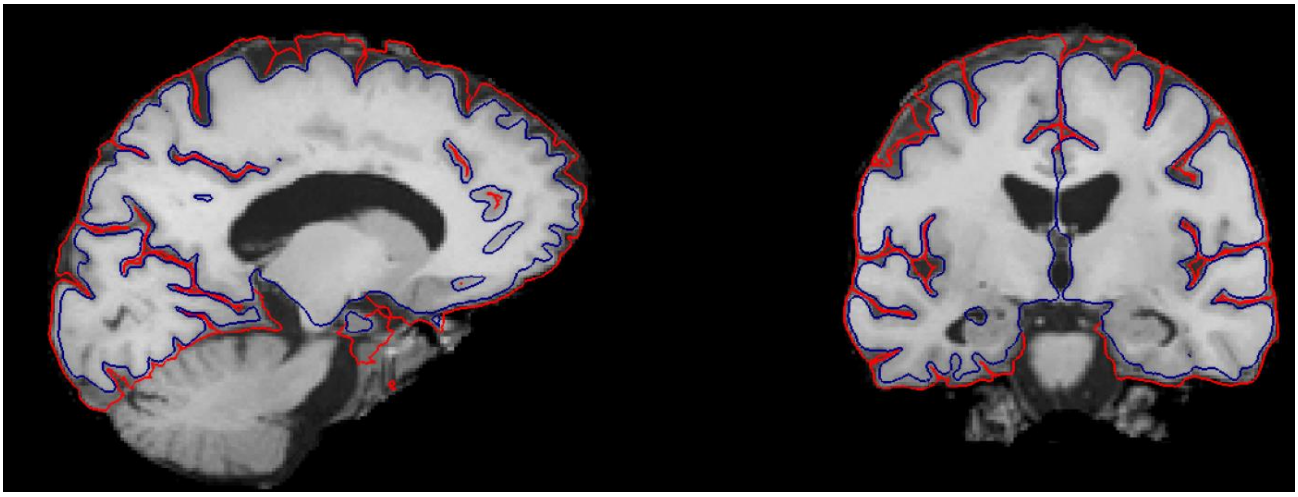

Figure 3.5 Example of a BASE stage results—template of images of a subject, sagittal section (left), coronal section (right). The red indicates the gray matter and the blue indicate the pial surface.

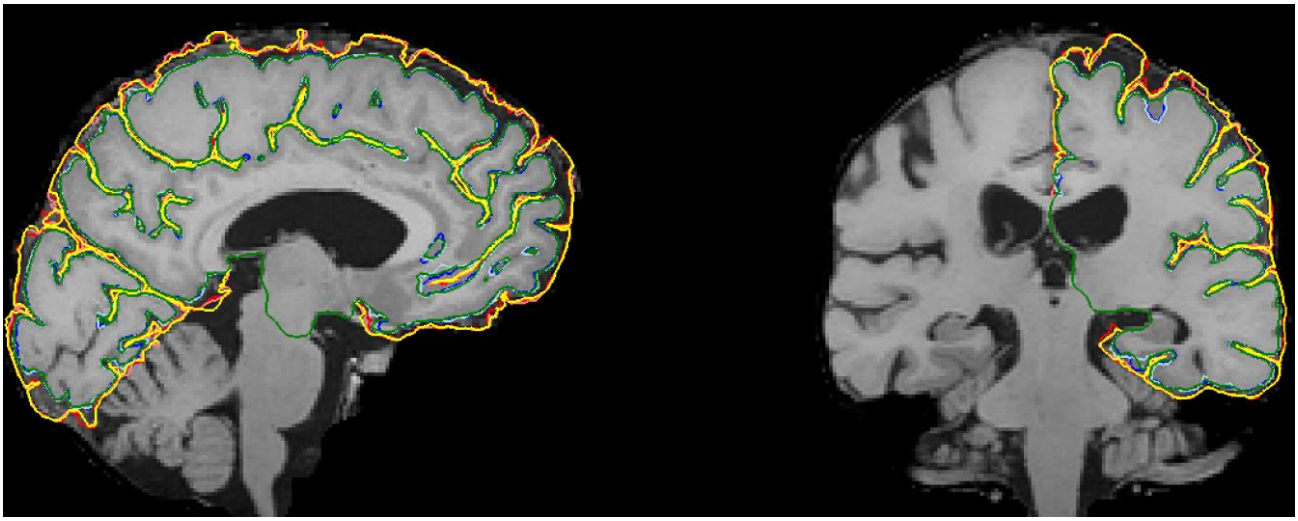

Figure 3.6 Example of LONG stage results, sagittal slice (left), coronal slice (right). Red and blue for the first time point, pink and light blue for the second time point, and yellow and green for the third time point**.**

3.2.3 Statistical analysis

The statistical analyses on the DB1 database were applied using the GLM and the LME models. The use of two different statistical models was intended to compare the results and then to be able to select the most appropriate model to be used during the analysis of the DB2 database.

A. Statistical analysis using GLM

The application of the GLM was through FreeSurfer software. Its application is divided into three steps:

1. Creation of the contrast matrix,
2. Creation of a group description file FSGD (FreeSurfer Group Descriptor),
3. Application of GLM commands.

The first step consists of creating contrast vectors to find a relation between the cortical thickness and the cortical volume with the EDSS and the SDMT variables.

So, the contrast vector was defined to find any difference between the cortical changes (thickness and volume) and both variables.

The second step was creating a text file called the FSGD. This text file was used to describe the data and its characteristics, by FreeSurfer t read and process the data [74].

Finally, we applied of the GLM model, consisting of two parts: preprocessing, and analysis. For the preprocessing stage, each subject is resampling to a common space and then all the subjects are concatenated in the same file. Some variables must be initialized to perform this processing which

are listed in Table 3.2. Then, a spatial smoothing was executed, where the variables described in Table 3.2 were initialized similarly to the preprocessing part.

Table 3.2 Parameters used in the preprocessing stages of the GLM model.

Part	Function	Description of the input
Initial Preprocessing	*fsgd*	Table with initial data.
	target	In this case, the space where the subjects will be analyzed is the space of average characteristics (fsaverage) from FreeSurfer.
	hemi	Specify the hemisphere.
	meas	Measure to be calculated, in this case, the cortical thickness and volume.
Smoothing Stage	*hemi*	Specify the hemisphere.
	s	Space to work (fsaverage).
	fwhm	Specify the fwhm, in this case, 10.
	cortex	Specifies the region of the brain where you work

After this step, the statistical analysis itself is applied. To do this, FreeSurfer used a specific command called *mri_glmfit*, which uses the result of the previous steps and the contrast vectors as inputs. At the end of this step, a directory was created in which a series of documents were found, highlighting the one that showed the regions that present the most significant changes, called *sig.mgh*. The data types in these documents highlight significance levels (p values) for cortical surface regions. The entire execution of this analysis took ten minutes for each measurement to be analyzed (cortical volume and cortical thickness).

For this model, a couple of definitions were made. One was the concept of correlation, which refers to the proportional between two variables. For this part of the study, the variables were the cortical thickness, cortical volume, and EDSS and SDMT variables. For visualization purposes, the positive correlation was shown in red, and the negative correlation was in blue. Another parameter to explain is the determination of the significance threshold. The software delivers all possible results, and limiting them to only those with a p-value of less than 0.05 is necessary. For this, FreeSurfer uses the equation $-log\,p$, so, a significance level of 1.30 was established since $0.05 = 10^{-1.30}$. In addition, to visualize better the affected regions, the Desikan-Killiany-Tourville (DKT) cortical region annotation map [75] was used, shown in Figure 3.7.

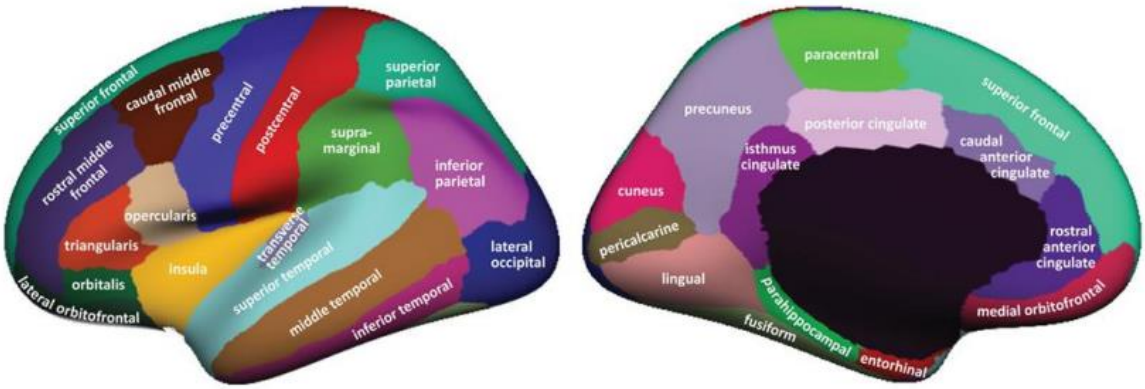

Figure 3.7 Regions in the DKT cortical labeling protocol [75].

B. Statistical analysis using LME

The second statistical analysis of the DB1 database was the LME model. This considers other statistical variables besides the arithmetic mean, such as variance and standard deviation, which allow a better understanding of the results. Also, this model can take covariates that change over time, which is a difference from the GLM.

Implementing the LME model using FreeSurfer gives the option to perform two types of analysis: univariate and massive univariate. In general terms, the univariate analysis will focus on the statistics of each region, that is, the differences in metrics such as cortical volume and thickness. In addition to the statistics, a massive univariate analysis will be done focus in the changes on the cortical surface regions. The massive univariate analysis was performed over the DB1 database. The application of this model is divided into four stages.

B..1 Ordering the data

The first thing to do in the data ordering stage was to create a table with all the subject's data. All this process was done in FreeSurfer. The table contains the disease duration, age, EDSS disability index value, and SDMT test result value.

To execute the model, we used two functions available on FreeSurfer: *mris_preproc* and *mri_surf2surf*. The first function receives the table with the data of the subjects. Then, the hemisphere to be analyzed on and the space where the analyses are carried out. In this case, we consider the *fsaverage* space. The second command was used to smooth the cortical maps, which received as input the hemisphere, the space and the output of the previous process. As an additional parameter, the

FWHM value was added, for which, according to the literature, the best value is in the range between 5 to 10 [mm]. For this study, we used a value of 10 [mm].

B..2 Reading the data and initializing the model

From this stage, all the process was executed using the MATLAB software (version R2020b).

For this stage, we must install a package of functions developed by J. Bernal et al. [76], [77] that were available in FreeSurfer. To be used, they must be added to the path in MATLAB. They can be added through the GUI of MATLAB by following the instructions in [78].

The first step was reading the file resulting from the previous stage. This file was read using a function that allows reading this type of file called *fs_read_Y*. The result of this function corresponds to a matrix where its columns contain all the information of each subject considering each time point.

Then, we used the functions *fs_read_surf* and *fs_read_label*, whose role was to read the locations of the cortical surface and labeling to be used in later processing steps.

Before the analysis, the linear model used must be defined. In this case, we used a simple model, as shown in equation (3.1).

$$Y_{ij} = \beta_1 + \beta_2 \cdot t_{ij} + \beta_3 \cdot t_{ij}^2 + b_{2i} \cdot t_{ij} + e_{ij} \quad \textbf{(3.1)}$$

First, the Y_{ij} represent the measurement j of subject i. The cortical variables (thickness and volume) were used in this case. Also, during the construction of the model, given the possibility of some non-linear variation of the vertices of the images, quadratic terms were added to the time t_{ij} to prepare the model for this eventuality.

In this case, we considered the age of the subjects as a random variable of the model, represented by b_{2i} in equation (3.1). In this model, this variable was used to construct the covariance matrix and contribute to the variability, which allows for inferring the impact of the fixed effects on cortical atrophy.

Then, a design matrix was created that incorporates all the fixed effects that, according to equation (3.1), correspond to the values represented by β. In this case, we used the variables of age, time, and the result of the SDMT neurological test and EDSS value were considered fixed effects of this model, used to estimate the levels of cortical atrophy. It should be noted that β corresponds to the regression coefficients of the fixed values. These values were taken as the population-averaged

interpretation, for example, the mean trajectories of the age of the subjects. Finally, e_{ij} correspond to the error generated when making the estimates.

B..3 Parameter Estimation

The first part of the longitudinal analysis using the LME model was the parameter estimation. This stage aims to provide parsimonious models for the trend in the mean response over time and for the covariance between repeated measurements in the same subject.

For this, a spatiotemporal model was used, which is more powerful for detecting effects in the data than traditional vertex models when two or more random effects were included in the longitudinal statistical model. Also, even when we used just one random variable, the developers suggested using this model because it generated better results. Its application is divided into three steps. The initial temporal covariance component estimates are calculated in the first step. For this, the *lme_mass_fit_EMinit* function was used, which receives as an argument the design matrix, the original data, the random variables, and some parameters defined by default. The result of this step was a covariance matrix for each of the locations. In the second step, the covariance results were grouped into a homogeneous region using the *lme_mass_RgGrow* function, receiving the covariance matrix, the cortical surface for the left or right hemisphere, and the cortical labeling. Then, this process gives a matrix of the average values of the estimation and covariance for each location and generates a segmentation vector containing the number of regions for each vertex. These first two steps took an average calculation of no more than five minutes.

Finally, the third step consists of adjusting the space-time model. This was performed using the *lme_mass_fit_Rgw* function, initialized using the covariance matrix and the segmentation vector, and the original data, the design matrix, and the random variable. At the end of this process, a matrix containing a list of variables for each voxel/vertex was delivered. The obtained variables were found in Table B.1, in Annex B. The total processing of this step took approximately 30 minutes.

B..4 Correction for multiple comparisons

In this last stage of processing, the results were generated. The first step was creating a contrast vector. In this case, the vector was designed to test if there is any difference in the cortical level (thickness and volume) due to the change in the SDMT and EDSS values.

Finally, the *lme_mass_F* function was used, which receives the matrix with the variables for each voxel/vertex and the contrast vector as an argument. A matrix with the significant level for each

voxel/vertex was generated based on the p-value. These results were not immediately viewable and must go through a multiple comparison correction step to “filter” those regions with a significant level higher than 0.05. After this, the regions with the highest significance were obtained, and a table of values that correspond to those changes.

3.3. Longitudinal anatomical study on the DB2 database

In this section we describe the analysis of DB2 database, that aimed to determine the anatomical changes of the cortical surface regions affected by MS. All this processing was executed in an external cluster provided by Professor Dr. Victoria M Leavitt.

3.3.1 Image preprocessing

The preprocessing stage of the DB2 database images was divided into four steps, whose goal was to prepare the structural images for their subsequent longitudinal analysis in FreeSurfer to obtain better results by inpainting the lesions in the WM. The execution of this stage was carried out through a bash master script. The entire process took approximately twenty minutes per image.

A. Preprocessing

In this first step, the inputs of the script were defined. The images used were the T1 and T2-FLAIR images. A kappa value was used as a threshold for highlighting lesions. In this case, a kappa of 0.07 was used.

This preprocessing step aims to prepare the images for later analysis in FreeSurfer, for which they went through a reorientation and extraction of regions of interest (ROIs). The *fslreorient2std* function [79] was used for the reorientation process, available in the FSL software, which seeks to reorient the image to match the standard image template (MNI152). This function receives the original image as argument and the name of the output image. Then, we used the function *fslroi* to extract the ROIs, also available in FSL. It receives as arguments the image resulting from the reorientation process and the name of the output image. It also gets the values of reference associated with the areas to be considered. In this case, we chose arguments that considered the full image [80].

B. Intensity Correction

The second step corresponds to an intensity correction of the T1 image. To do so, we used the *mri_nu_correct.mni* function that is available in FreeSurfer. The function used *nu_correct*, a Montreal Neurological Institute (MNI) algorithm, to correct the lack of intensity uniformity. During the

execution, this function used values of float type instead of char. It also rescales the output so that the global mean was the same as the input. Finally, it received as arguments the image resulting from the preprocessing step and the name of the output of this process [81].

C. AC-PC Alignment

In this third step, the objective was to reorient the T1 and FLAIR images. This step considers the anterior and posterior commissure reorientation, hence the ac-pc alignment. To carry out the co-registration, we used the DARTEL tool available in the SPM12 software [82]. The idea was to register images by calculating a "flux field", which was "exponentiated" to generate forward and backward deformations. There were two ways to do this: Single images could be matched or simultaneous registration of, e.g., GM with GM, WM with WM. This procedure began by creating an average of all the images used as the initial template. Then, the deformations of this template were calculated for each of the individual images, and then the template was regenerated by computing the inverses of the images and averaging them. This procedure was repeated several times. And finally, the reoriented images were generated. The reference image obtained from this process served as the input argument for the co-registration process.

Then to execute the co-registration process, we used the SPM co-registration module [83] that used as inputs: the reference image created from the previous process, the T1 or FLAIR image, depending on the alignment to be performed, and finally, associated parameters were defined: the objective function, the separation between sampling points, the accuracy of each variable and the smoothing of the histogram, the majority set to the default variables provided by the software.

D. Lesion Inpainting

Finally, there was the step of lesion inpainting. This was divided into two parts. The first part consists of generating the lesion map, for which the LST toolbox available in the SPM8 software was used [84]. It should be noted that although better versions of this toolbox are available in other versions of the SPM software, this version was chosen given the best results obtained by testing different thresholds and their subsequent comparison.

The algorithm for the masks was based on lesion growth [85]. For this research, the most general version of the algorithm was used, which received as input arguments: the T1 image, the FLAIR image, the threshold value (the *kappa* value) that was used for the creation of the lesion map, and a threshold for the calculation of the binary lesion map. In addition, other values could be selected,

such as the maximum number of iterations and the Markov Random Field (MRF) parameter. In this case, these values were chosen by default. The algorithm took five to ten minutes to process each pair of images, although the time could be longer depending on the resolution of the T1 image. The result that we used to generate the lesion inpainting was the binary lesion map [84].

For the generation of the lesion inpainting, we used the function *lesion_filling* available in the FSL software [86]. This function used the binary lesion map and the T1 image as input arguments to "fill" the areas in the structural image corresponding to the lesioned regions with similar intensities to the non-lesioned areas. Finally, the function receives as a final argument the name of the resulting image that has the lesion inpainted.

As a form of validation of the results obtained in this stage of lesion inpainting, a review was carried out by Dr. Korhan Buyukturkoglu, who has experience in detecting lesions in the cerebral white matter in subjects with MS.

The benefits of this stage are the determination of the percentage of the volume that these lesions occupy concerning the total volume of the brain. This value allows us to have an overview of the impact that MS has at this level on the brain, in particular on the volume of cerebral white matter.

3.3.2 Longitudinal Processing

The longitudinal processing applied to the images of the DB2 database was the same used for the images of the DB1 database, with the only difference being that the DB2 images were processed in the cluster provided Professor Victoria M Leavitt Ph.D. from Columbia University, New York, USA.

The DB2 images were processed using FreeSurfer, passing the three stages of longitudinal processing: CROSS, BASE, and LONG.

3.3.3 Statistical Analysis using GLM

The statistical analysis of the longitudinal data was based on a two-stage model. The first stage of this model allows for converting the longitudinal data to a statistical variable, for example, the rate of atrophy or the percentage of change at the cortical level. The second stage allows for comparison of the measurements between groups or some covariate, for example, age, gender, time, etc. In this second stage, we applied the GLM analysis. One of the advantages of using this model was the possibility of working with the statistics and the cortical maps simultaneously and avoiding modeling the correlation structure of repeated measures.

First, we ordered the longitudinal data. This was done by creating a table where the name of the subjects was specified with their respective time point and the name given to the directory that contains the template of the subject (the result of the BASE stage at the longitudinal processing). In the other columns other variables could be added such as time, duration of the disease, among others.

Then, the first stage consists of preparing the data. This stage was executed through FreeSurfer software, using the command *-qcache*. It prepares the data to be analyzed in the QDEC stage, an acronym for Query, Design, Estimate, and Contrast. The QDEC stage is the way that FreeSurfer applies the GLM model. The function *long_mris_slopes* was used, which has several input arguments. The first inputs corresponds to the data table, called longitudinal table *qdec*. Also, the type of measurement to be analyzed is specified, for example, cortical thickness, volume or curvature, then the hemisphere is selected. Finally, the column of the longitudinal table that represents the time, and the space where the study was performed are specified. In this case, we worked with the average space called *fsaverage*. All the measurements described in Table 3.3 were performed in this part of the analysis.

Table 3.3 Functions associated with calculations performed in the data preparation stage [87].

Function	Description
--do-avg	Compute the temporal average.
--do-rate	Compute the rate of change.
--do-pc1	Compute the percentage change.
--do-spc	Compute a symmetrized percent of change.
--do-stack	Output a stacked thickness file for every subject.
--do-label	Intersect the cortex label to ensure we do not include non-cortex regions.

After this preparation stage, the QDEC group analysis begins, for which a *qdec table* was built. The construction of this table was necessary because this analysis does not allow the direct application of a table with longitudinal data. To do so, the *long_qdec_table* function was used, whose role was to transform the previously used longitudinal table into a table based on cross-sectional analysis. The resulting table contains a line for each patient, which has the path to the directory where the *template* was located. We used this analysis because we did not use cofactors that change over time. The only variable that we used was the time.

In addition, a text file was created with the names of the new files created in the preparation stage. An example of this text file is shown in Table 3.4.

Table 3.4 Lines with the names of measures calculated on the preparation step.

Names of measures calculated on the preparation step
MEASURE1=long.thickness-avg
MEASURE2=long.thickness-rate
MEASURE3=long.thickness-pc1
MEASURE4=long.thickness-spc

After the previous steps, the group-based surface analysis platform was opened through the GUI.

Once the GUI was executed, the table created by *long_qdec_table* was loaded. In this process, values such as the mean and standard deviation of the data were obtained, which were used to calculate the different metrics. In addition, the lists of factors enumerated during the creation of the longitudinal data table were displayed, such as age, gender, and disease duration. Similarly, there was the option to generate new statistics, such as cortical thickness measurements or volume of the different cortex areas. Due to the purpose of this research, this last function was not used since they were calculated separately through FreeSurfer.

After this, we proceeded to the design stage, where the variables to be considered were established, such as discrete and continuous factors, as well as the type of measurement to use, such as volume or cortical thickness, and if the analysis was structural or functional, among others.

For this research, an analysis based on the surface and the morphological variations was considered. The cortical thickness for both hemispheres was considered a metric of interest, considering a smoothing (*FWHM*) of 10. Then, the variables to be evaluated must be selected. In this case, only time was considered as a continuous variable to determine the cortical thickness changes between the two time points of the DB2 database (3 years difference between each sample). Then, the design matrix type and the number of degrees of freedom for the calculations were left by default, which the platform developers recommend. The design matrix was based on the model *Different Onset, Different Slope* that estimated a separate intercept and slope for each covariate. The analysis process could take a few minutes depending on the number of subjects to be analyzed; in our case, the complete processing took around 30 minutes.

The last stage was the result visualization process where the changes of the cortical thickness over time was visualized. The premise with which it starts was that if there is any relation between the cortical thickness changes and the time between samples, a first approximation was obtained where all the differences between these two variables, significant and non-significant, are highlighted. Then, a new threshold was established to highlight the most significant regions based on a p-value less than 0.05 [88].

Finally, the statistics of the regions that present the most significant correlations were obtained for the change in cortical thickness over time, considering all the subjects.

For the extraction of the statistical values of the most significant regions, the *mri_glmfit-sim* function was used. This function took four arguments. The first entry was *–glmdir,* which received the directory on which the correction was made for multiple comparisons and statistics extraction. The following entry was the command *--2spaces,* which specifies that the analysis was performed on both hemispheres and thus has positive or negative effects on the cerebral cortex. The following entry was *–cwp,* where we specified the threshold for the cluster-wise analysis; set the default value of 0.05. Finally, the *--cache* entry receives two arguments. The first argument establishes the threshold value for the vertex-wise analysis, which defines the statistical significance for vertex selection. The program does not directly use the p-value as input, it must be specified employing the formula *-log (p)*. We used a value of 4.0, translated as a p-value less than 0.0001, generating important significance levels. This value was based on the recommendation established in [89] where it was shown that using values lower than 3.0 significantly increased the number of false positives. The second argument for *--cache* specifies the direction of the analysis to perform: positive, negative, or both. In the case of this research, the positive direction (for positive correlations) and the negative direction (for negative correlations) were considered [90]. For this research, the negative correlation was interpreted as a decrease of the cortical thickness with time and the positive correlation as an increase of the cortical thickness with time.

3.4. Longitudinal diffusion MRI study on the DB2 database

To analyze the diffusion MRI data longitudinally, we follow two steps. The first step involves processing and obtaining the diffusion indices for each SWM bundle described in the previous chapter. The second step consists of analyzing the data itself.

The analysis of the data was performed using spreadsheets. We created a spreadsheet with all the diffusion MRI metrics for each fiber bundle separated between the two time points, for all the

subjects. The spreadsheets were organized to consider the metrics for every fiber bundle; in this case, the FA, AD, RD, MD and QA.

We divided the analysis into two steps to determine the significance level between time points for each diffusion MRI metric. The first step involves a transversal approach, which acts as a “filter” for the metrics. The second step involves a longitudinal approach.

To start with the transversal approach, we used the t Student test. This test requires four arguments: two matrices containing the values of each subject for a specific bundle diffusion MRI metric, a value indicating the number of distribution tails (either one or two), and the type of test to perform on the data (paired, two-sample equal variance, or two-sample unequal variance). For this research, we chose a value of two for the number of distribution tails, corresponding to the probability of a higher absolute value of the t-statistic under the assumption of "same population means." Also, we selected the two-sample equal variance test, as it allows for a correlation between time points rather than just a correlation between the data from each time point.

After calculating the significant value for every fiber bundle, we set the threshold as a p-value less than 0.05. By doing that, we can select the diffusion MRI metrics more significant, reducing the number we can compare.

To compare the changes in the metrics, we calculated the arithmetic mean for each diffusion MRI metric for each time point. Then, we calculated the difference between these means and evaluated the result based on the guidelines established in [7].

Then, to determine the significance level of the mean difference, we corrected for multiple comparisons. For this, we performed the Tukey-Kramer Honest Significant Difference (HSD). We used this method because it is recommended when comparing groups of more than six subjects. To perform HSD, the first step was determining a critical value of studentized range distribution (q). That value was obtained from a table that related the degrees of freedom and the number of groups [91]. In this case, the q value was 2.858. The next step was determining the standard error for every diffusion MRI metric. To do so, we calculated the variance between the time points. We calculated the arithmetic mean of each time point's variance to divide by the number of subjects, in this case, 24 subjects, and finally got the square root of the value. Lastly, we determined the Tukey value for every diffusion MRI metric, which can be compared with our original q value. To do so, we divided the absolute mean difference by the standard error.

Finally, the Tukey value was compared with the q value, and if the Tukey value was bigger than the q value, we could interpret that the mean difference between the two time points was

significant. Then, we correlated the p-value from the t-test and the significant mean difference from HSD and made a relation. The fiber diffusion MRI metric was significant if the two values were considered significant.

After considering the limitations of the t-test for longitudinal analysis, we concluded that applying a longitudinal model was necessary. Upon review of the model presented in [92], we determined that the Generalized Estimation of Equations (GEE) model was the most fitting for our study. The GEE model establishes a regression relationship between covariates and changing variables over time. This effectiveness of the model lies in its ability to make correlations even when data is missing, particularly concerning variables that change over time. Additionally, it can provide dependable estimates even when the correlation structure contains errors. The GEE model has been widely utilized in other neurodegenerative pathologies studies, such as the work by R. Keogh et al. [93] and the work done by D. A. Maroof et al. [94].

In our case, GEE was applied through the SPSS software [10], allowing this model's most straightforward application through a GUI. Therefore, for its application, it is necessary to determine and establish specific parameters for use throughout the GEE.

The determination of the variables in this study was divided into four parts. The first part was to specify the repeated parameters, which included the subject variable. In this case, it only sets the subject ID and the time point. The other parameters, such as the covariance matrix, the correlation matrix, and the number of iterations, were set by default.

The second part was to specify the type of model, which involved selecting the distribution and the link function. SPSS provided two alternatives. The first was to choose from a list of possible responses, a combination of distribution and link functions. The second was to select the distribution and link functions manually. We determined that the first option was the best based on the data used in this research. We set the linear response with a normal distribution and an identity as a link function.

During the third part of our process, our main objective was to ascertain the model's response. To achieve this, we had to establish the dependent variable. This variable comprised all the diffusion MRI metrics identified as significant in the earlier analysis. We kept all other parameters at their default settings.

Next, we had to choose the predictors to include in our model carefully. For our particular study, we identified two types of predictors: factors and covariates. Factors are independent variables; in our case, we focused on the time difference between the two time points. Meanwhile, the covariates

were represented by the values of two variables - the EDSS and SDMT tests. It was essential to select these predictors thoughtfully to ensure accurate and meaningful results.

Then, we needed to choose the model effects. The default model only includes an intercept, so we had to specify additional effects to create new relationships. We selected the time, EDSS, and SDMT values as new effects based on our research goals to determine potential interactions with the diffusion MRI metrics. We opted for a primary effect on the factor and covariates as it provides the most comprehensive effects for each variable.

Our last part was determining the estimated marginal means for the factor, in this case, the time. We needed to specify a contrast to establish how hypothesis tests would compare the estimated means. We opted for pairwise contrast as it is computed for all-level combinations of the chosen factor, giving us an advantage over other possible differences. Additionally, we specified an adjustment for multiple comparisons. We decided on the Sequential Bonferroni method from the various possibilities SPSS offers. This procedure is a sequentially step-down rejective Bonferroni approach, which is less conservative when rejecting individual hypotheses than the original method.

Capítulo 4. Results

4.1. Introduction

This chapter will show the results of this work, including the anatomical analysis for both databases and the diffusion analysis of DB2. Also, at the end of this chapter will be a discussion section of the results.

4.2. Anatomical Results for DB1 Database

This section will show the results related to the cortical surface changes (thickness and volume) due to the shift in SDMT and EDSS metrics by applying the GLM and LME models.

4.2.1 Changes at cortical level over time

We conducted a study to analyze the changes in cortical surface over time by examining the correlation between the time and the cortical variables, thickness and volume. The results will be evaluated using statistical models, and we have set a significance threshold of $p < 0.05$.

In Figure 4.1 (top), a correlation is shown between cortical thickness and time. The yellow regions indicate a positive correlation, meaning there is a significant decrease in cortical thickness over time. Meanwhile, the red regions represent regions with a less significant reduction. The highlighted regions in this case are from the frontal and superior frontal regions of the brain and some from the parietal and anterior temporal regions.

In Figure 4.1 (bottom), we can observe the correlation between cortical volume and time. The color scheme used here is identical to the one used in the previous correlation. The highlighted regions in this correlation are similar to those for the cortical thickness correlation. However, the difference between these two correlations is that, in the case of cortical volume over time, the frontal regions present a higher coverage of changes than cortical thickness.

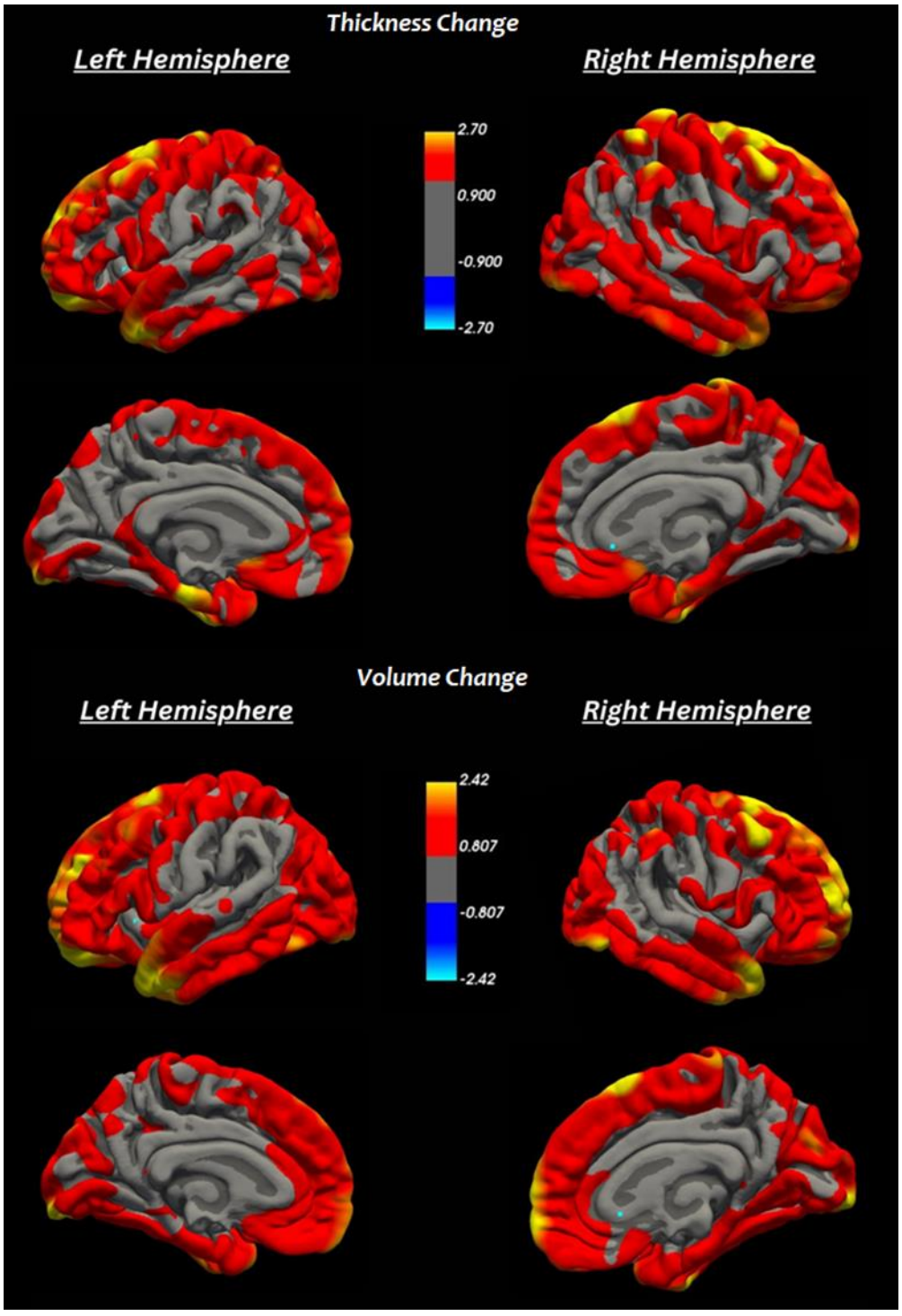

Figure 4.1 Cortical thickness and cortical volume change over time for left and right hemispheres. The regions in yellow have significant changes over time, and the red regions have a lower level of change over time. All the regions in the figure have a significance level of a p-value less than 0.05. The equation - log p = x is used to graph this measurement, so an x-value equal to 1.30 represents a p-value of 0.05.

4.2.2 GLM analysis

This analysis used the GLM model to determine a significant correlation between cortical volume change and EDSS/SDMT value.

Figure 4.2 (top) highlights the brain areas with the most significant changes in cortical volume related to EDSS. The pre-cuneus, rostral middle frontal, and superior frontal regions are most affected in the left hemisphere. Most affected areas show a negative correlation, represented by blue, indicating decreased cortical volume for increased EDSS values. Similarly, the superior parietal, rostral middle frontal, and superior frontal regions show the higher changes in the right hemisphere. While most regions show a negative correlation, some regions present a positive correlation.

Figure 4.3 (top) shows the cortical regions most affected by variations in cortical volume related to the SDMT value. The left hemisphere's pre-central and superior temporal regions are the most affected. Most of these areas show a negative correlation. However, some areas, particularly in the superior temporal region, show a positive correlation, indicating increased cortical volume for an increase in the SDMT value. For the right hemisphere, the post-central and medial orbitofrontal regions are the most affected, with most regions showing a negative correlation.

Furthermore, we have our second analysis using the GLM model to determine significant correlations between the changes in the cortical surface thickness and the EDSS and SDMT metrics.

In Figure 4.2 (bottom), we can see the cortical regions primarily affected by changes in cortical thickness correlated with the EDSS value. The left hemisphere is most involved in the precuneus, caudal middle frontal, and pars triangularis regions, with a negative correlation indicating decreased cortical thickness. Conversely, the right hemisphere is most affected in the superior parietal, superior frontal, and rostral middle frontal regions. The main difference between the two hemispheres is the extent of the affected region.

Figure 4.3 (bottom) shows the cortical regions with significant correlation of changes in cortical thickness and the SDMT value. The left hemisphere's pre-central and superior temporal regions have more affected surface areas. It is important to note that these regions are the same as those highlighted in the volume variation analysis. Similarly, the right hemisphere's pre-central and inferior parietal regions present related changes. Most of the affected regions in both hemispheres show a negative correlation.

All numerical variations for the analysis are listed in Table C.1 in Annex C.

Due to the lack of a control group for comparison, we conducted a separate analysis that considered the duration of the disease at the first MRI image acquisition as a co-factor. We used the

results of this analysis as a basis, which can be seen in Figure 4.4 for the correlation with the EDSS and Figure 4.5 for the correlation with the SDMT value. In all cases, the highlighted regions were almost the same as the analysis already described, with the main difference being the size of the affected areas. In this case, the affected regions were slightly smaller.

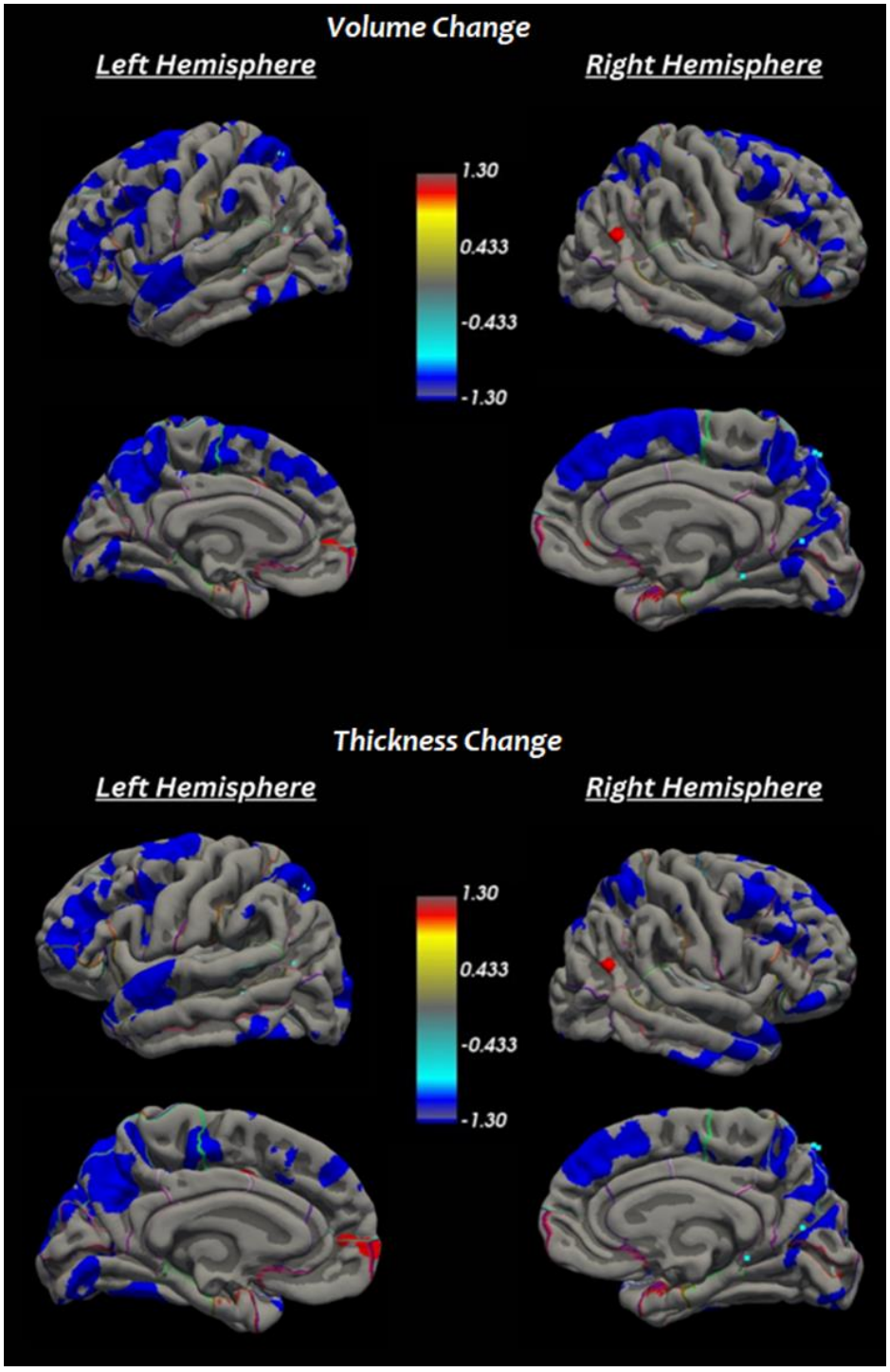

Figure 4.2 GLM analysis. Correlation between the volume and the thickness change with the EDSS value for the left and right hemispheres. The regions in blue have a negative correlation, which means a decrease in the volume change rate related to the EDSS. The red regions are those with a positive correlation. All the regions in the figure have a significance level of a p-value less than 0.05. The equation - log p = x is used to graph this measurement, so an x-value equal to 1.30 represents a p-value of 0.05.

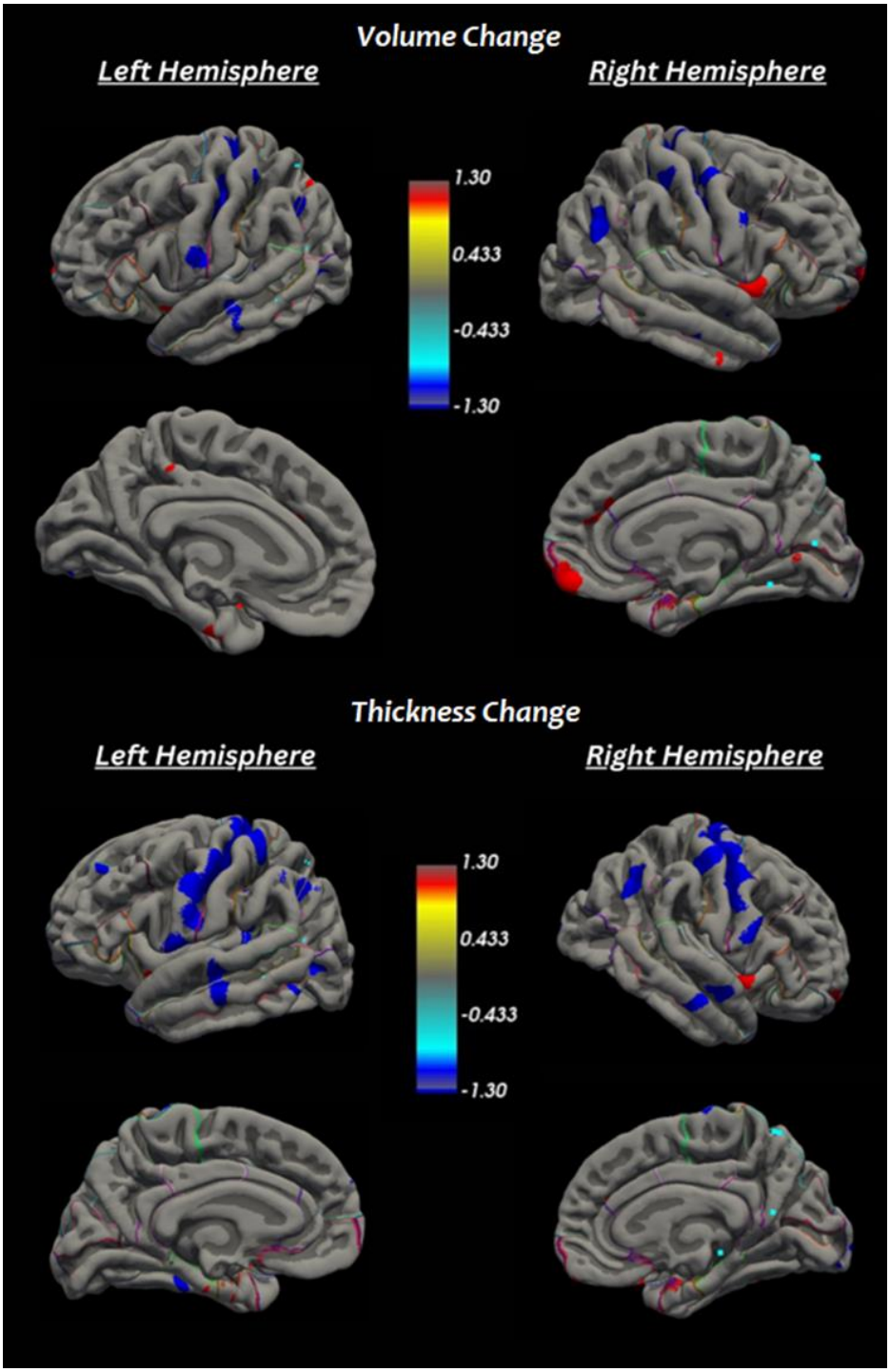

Figure 4.3 GLM analysis. Correlation between the volume and the thickness change with the SDMT value for left and right hemispheres. The regions in blue have a negative correlation, which means a decrease in the volume change rate related to the SDMT. The red regions are those with a positive correlation. All the regions in the figure have a significance level of a p-value less than 0.05. The equation - log p = x is used to graph this measurement, so an x-value equal to 1.30 represents a p-value of 0.05.

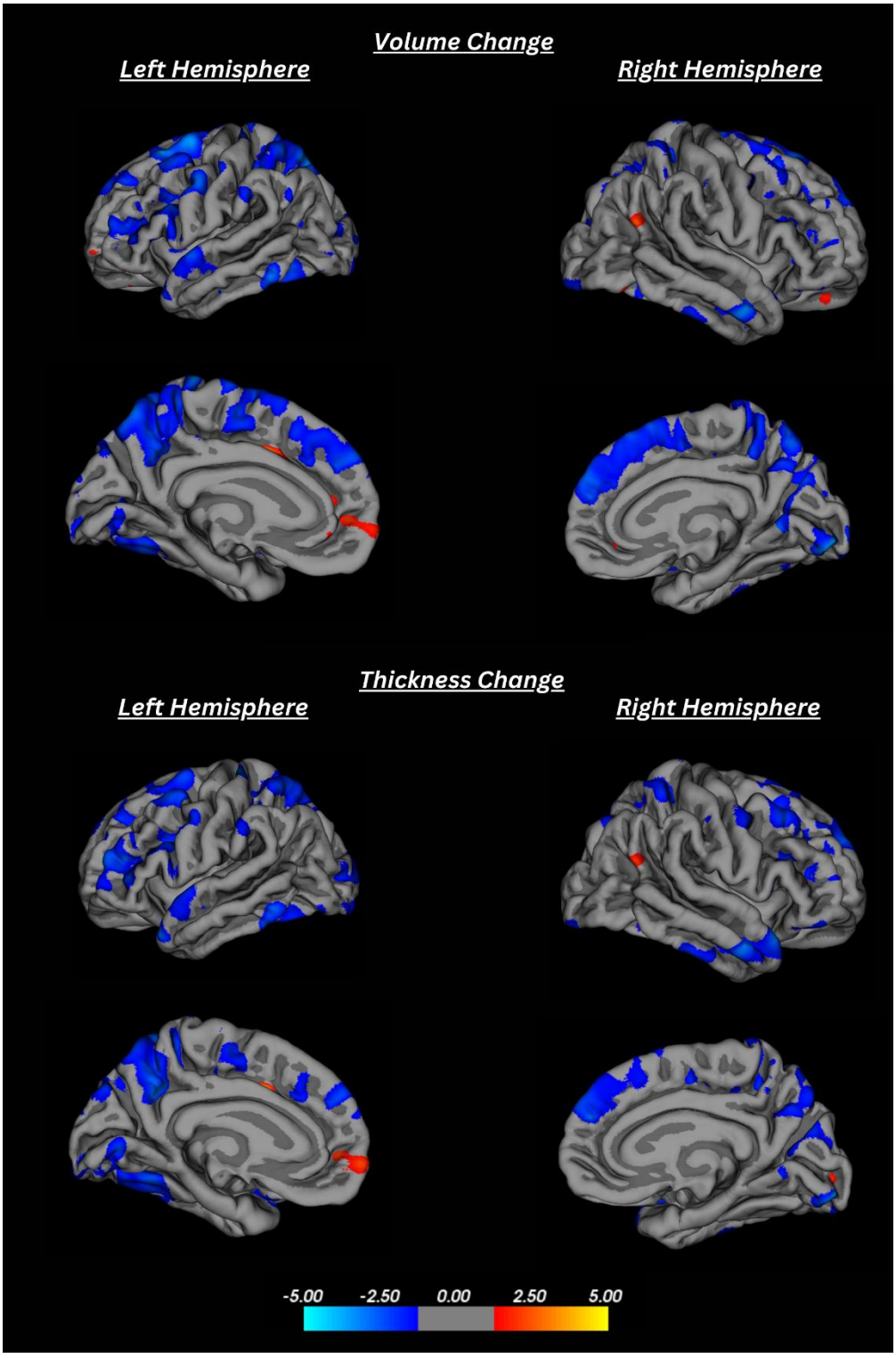

Figure 4.4 GLM analysis. Correlation between the volume and the thickness changes with the EDSS value for left and right hemispheres. This analysis considered the duration of the disease as a co-factor. The regions in blue have a negative correlation, which means a decrease in the volume change rate related to the EDSS. The red regions are those with a positive correlation. All the regions in the figure have a significance level of a p-value less than 0.05. The equation - log p = x is used to graph this measurement, so an x-value equal to 1.30 represents a p-value of 0.05.

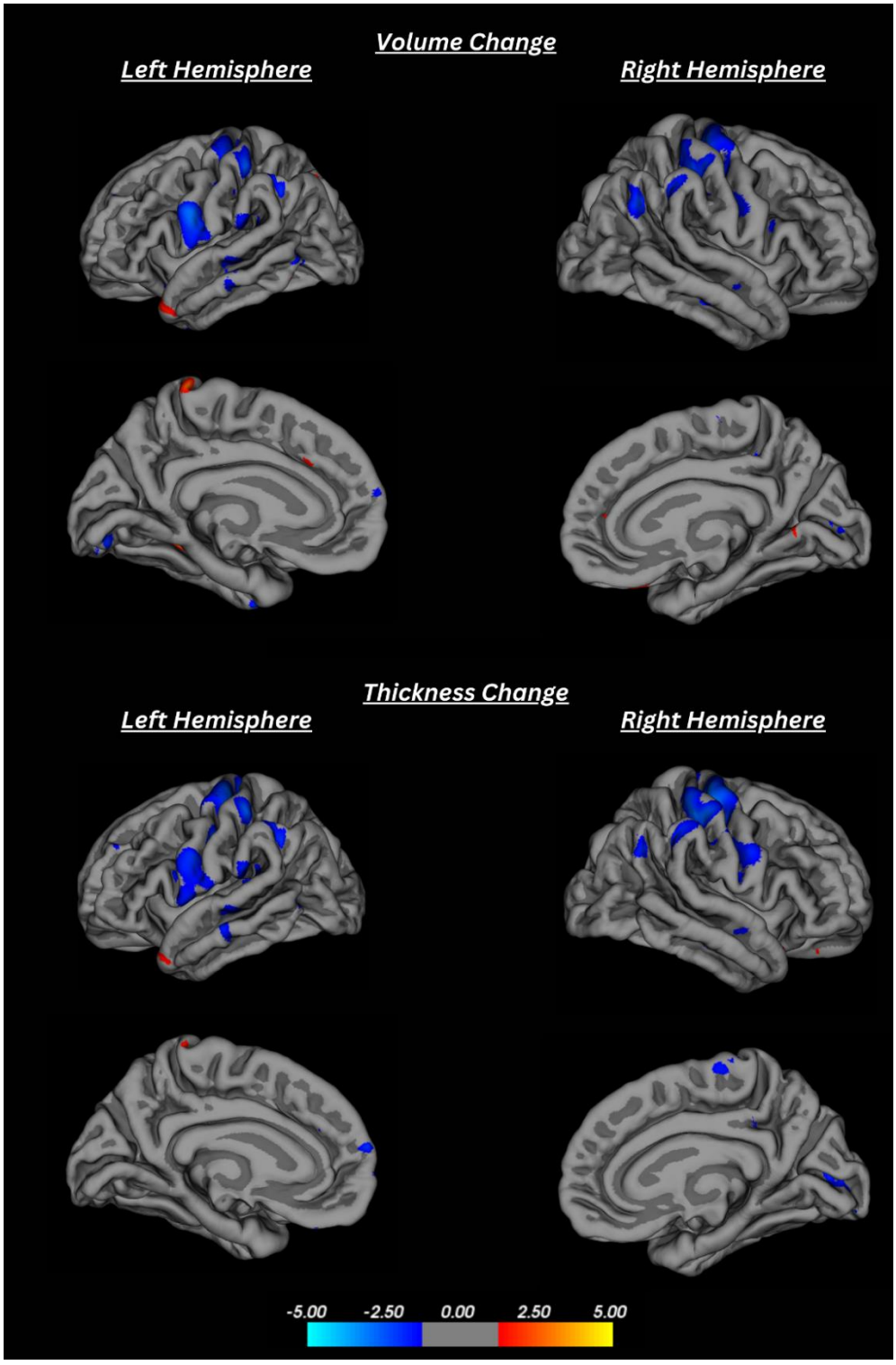

Figure 4.5 GLM analysis. Correlation between the volume and the thickness changes with the SDMT value for left and right hemispheres. This analysis considered the duration of the disease as a co-factor. The regions in blue have a negative correlation, which means a decrease in the volume change rate related to the SDMT. The red regions are those with a positive correlation. All the regions in the figure have a significance level of a p-value less than 0.05. The equation - log p = x is used to graph this measurement, so an x-value equal to 1.30 represents a p-value of 0.05.

4.2.3 LME analysis

In this section, we present the findings of the LME model analysis. The main objective of this analysis was to establish a correlation between the cortical thickness and volume, and the changes in the EDSS and SDMT metrics. The age of the subjects was used as a random variable in this model.

The correlation between the changes in cortical volume and the EDSS value was analyzed, and the results are presented in Figure 4.6 (top). The cortical regions in both hemispheres that present the significant changes in cortical volume correlated with the change in the EDSS value are in yellow. It is important to note that the subcortical region is entirely shown in yellow, but this does not represent any correlation because the analysis was performed only on the cortex surface. In the left hemisphere, the superior marginal and rostral middle frontal regions, among others, were the most affected. In the right hemisphere, the most affected regions were the supramarginal and superior temporal regions.

In Figure 4.7 (top), we can see the cortical regions that have undergone significant changes in cortical volume related to the SDMT value. The color map used in this analysis is the same as the one used for the EDSS analysis. In the left hemisphere, the supramarginal, pre-central, and superior frontal regions, among others, are the most affected. Similarly, the inferior parietal and rostral middle frontal regions have significantly changed in the right hemisphere.

The study also considered changes in cortical thickness and identified the most affected cortical regions related to the EDSS. Figure 4.6 (bottom) displays the color map used to illustrate these changes. The superior parietal and caudal anterior cingulate regions were among the most affected in the left hemisphere, while the inferior temporal and posterior cingulate regions were the most significantly changed in the right hemisphere.

In Figure 4.7 (bottom), we can see the cortical regions that exhibited significant variations in cortical thickness related to the SDMT value. The supramarginal and middle temporal regions are among the most affected areas of the left hemisphere. In contrast, the right hemisphere shows variations in the supramarginal and post-central regions.

All numerical changes for the analysis can be found in Table C.1 of Annex C.

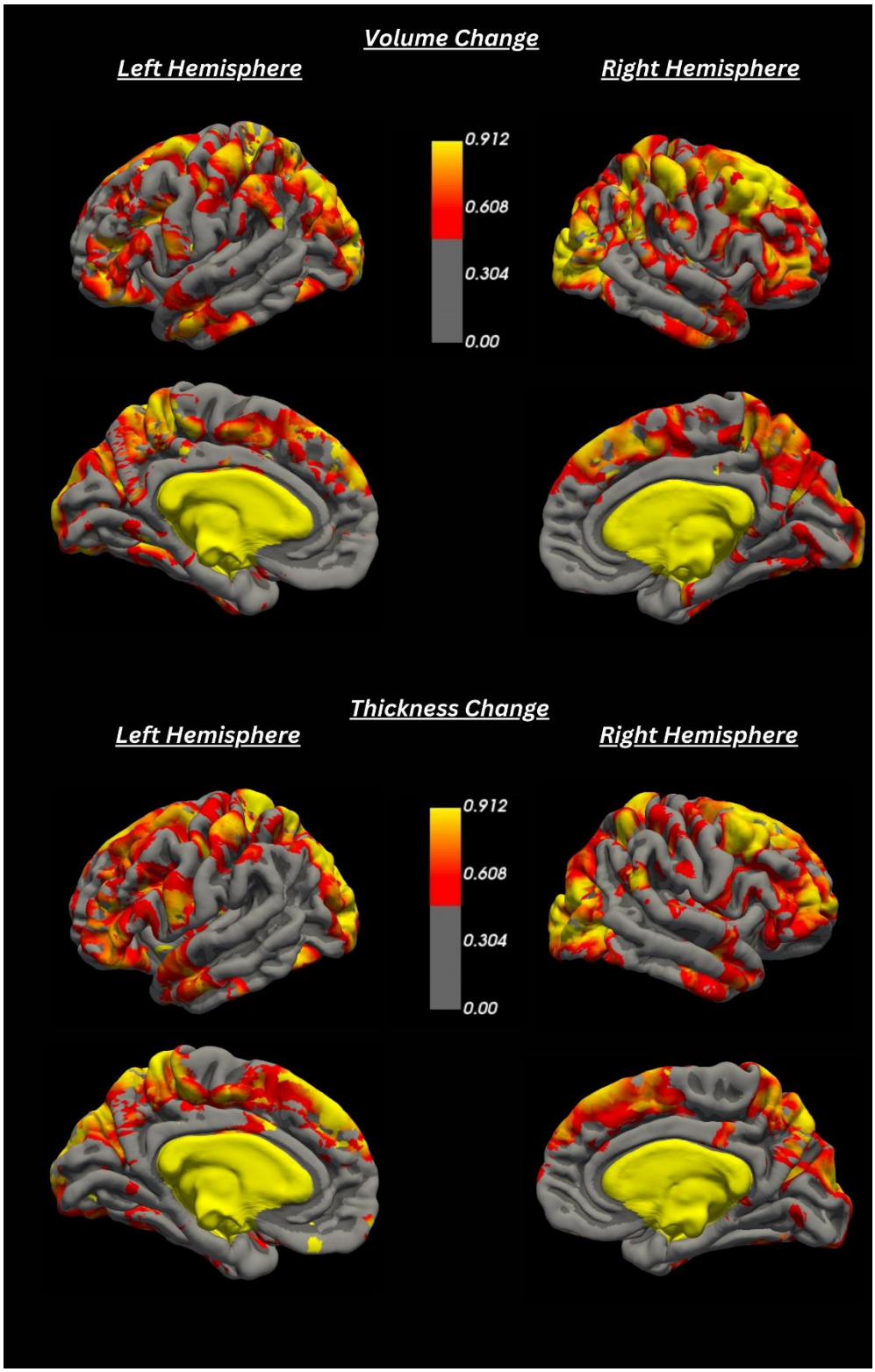

Figure 4.6 LME analysis. Regions that present the most significant changes in the cortical volume and cortical thickness related to the EDSS value. This analysis was done considering the age as a random variable. The yellow areas represent the regions with the highest change in the cortical thickness and volume correlation, while the red indicates that the rate of change tends to decrease. To graph this rate of change, the relation used is a normal distribution where the closest to 1 means a total change in that region.

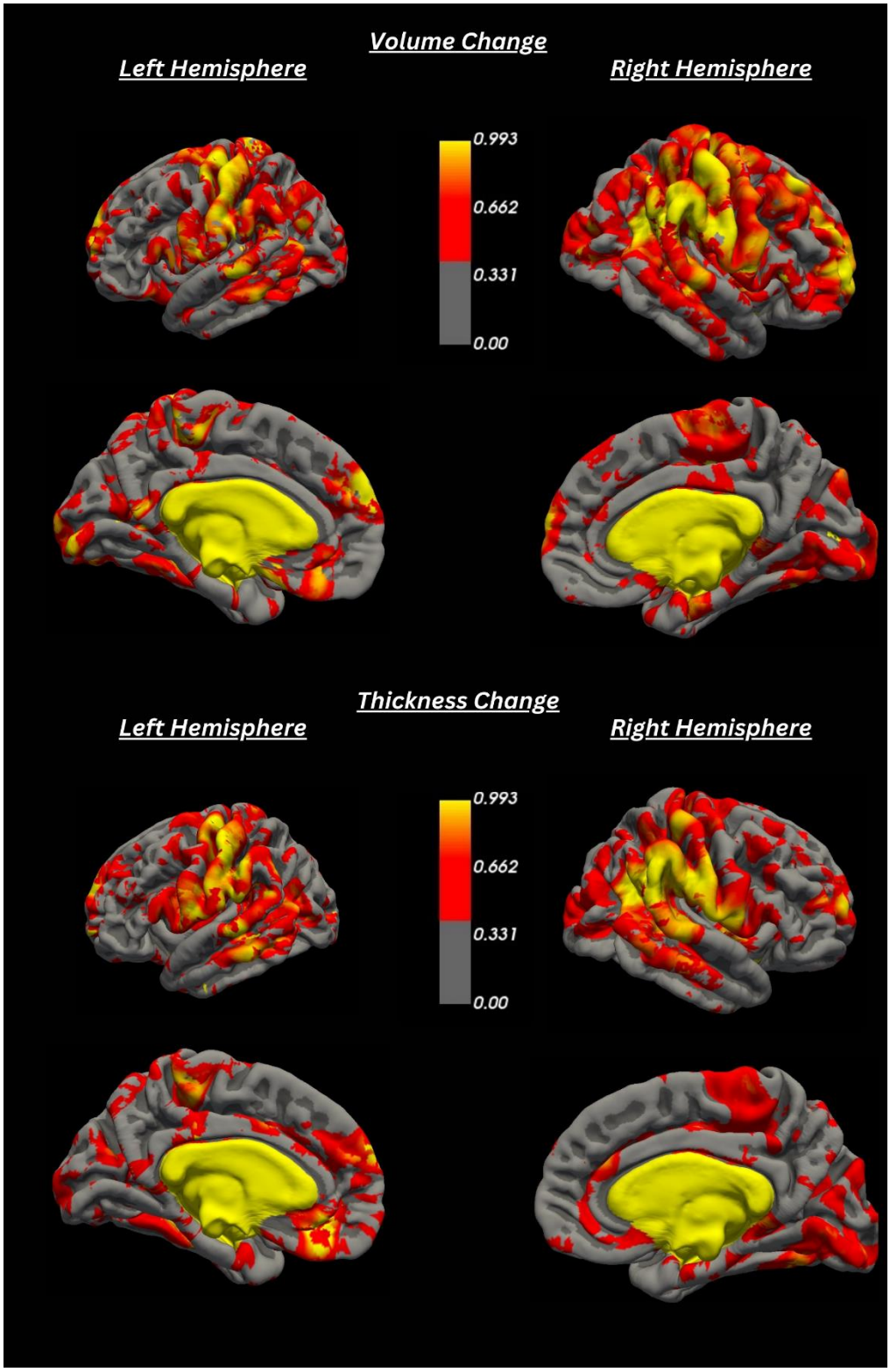

Figure 4.7 LME analysis. Regions that present the most significant changes in the cortical volume and cortical thickness related to the SDMT value. This analysis was done considering the age as a random variable. The yellow areas represent the regions with the highest correlation of the change in the cortical thickness and volume with SDMT value, while the red indicates that the rate of change tends to decrease. To graph this rate of change, the relation used is a normal distribution where the closest to 1 means a total change in that region.

4.3. Anatomical Results for DB2 database

This section presents the results of the GLM model applied to cortical thickness changes over time, as well as the preprocessing steps applied before the anatomical analysis to the DB2 database.

4.3.1 Lesion Inpainting and the change in the number of lesions

One of the preprocessing stages was the inpainting of the WM lesions. Table 4.1 shows the number of lesions and the percentage of volumetric change experienced between both time points for each subject. From here, we obtained positive and negative lesion variations. Thirteen subjects present positive variations in the volume of their lesions while ten subjects present negative variations in the volume of their lesions.

Table 4.1 Number of WM lesions and the percentage of WM lesion volume change of every subject for both time points. The negative values of the percentage of change refer that was a decrease in the number of the lesion detected. This decrease may be due to a lower detection of lesions or the increase in size of some lesions, which could have generated a decline in smaller lesions. The positive values of the percentage of change refer that was a increase in the number of the lesion detected.

Subjects	*N° of lesions on TP 1*	*N° of lesions on TP 2*	*Change of WM lesion volume (mm)*
1	52	52	-0.2
2	7	10	48.9
3	47	53	21.8
4	20	23	28.5
5	25	24	12.2
6	37	36	-0.8
7	56	46	-49.7
8	19	17	11.5
9	75	75	11.2
10	46	46	19.3
11	46	46	19.3
12	12	17	29.1
13	13	9	73.1
14	43	33	22.1
15	26	25	20.2

16	20	18	-18.0
17	28	25	-4.4
18	47	33	-22.3
19	46	47	-4.0
20	10	14	-8.7
21	27	50	10.6
22	51	47	-32.0
23	*63*	*57*	*-16.0*

4.3.2 Cortical thickness changes over time

For this part, the significance threshold was set to a p-value less than 0.05 to highlight the regions with significant changes.

First, for the left hemisphere, Table 4.2 shows the negative correlation between cortical thickness changes and the time between the acquired samples. The regions of the cortical surface that present the higher changes are the post-central, pre-cuneus, pars opercularis, lingual, and rostral anterior cingulate, among other regions with smaller affected surfaces. Also, Table 4.2 shows the positive correlation between the cortical thickness changes and the time between the samples. The regions of the cortical surface with the higher changes are the rostral medial frontal, insula, superior temporal, medial temporal, pars orbitalis, caudal medial frontal, superior frontal, lateral orbitofrontal, fusiform, and other regions with smaller affected surfaces. Figure 4.8 shows the affected areas with positive (in yellow) and negative (in blue) correlation with time.

Table 4.2 Surface of affected regions of the cortical surface in the left hemisphere with positive and negative correlations between the cortical thickness change and the time. The size of the regions is in mm^2. The regions in red are those that present both correlations. (*) indicate another vertex of a previously mentioned region.

Negative Correlation				Positive Correlation			
N°	Surface Cortical Region	Size (mm^2)	p-value	N°	Surface Cortical Region	Size (mm^2)	p-value
1	Post-central	11609.19	0.0002	**1**	Rostral Middle Frontal	795.23	0.0002
2	Pre-cuneus	7293.63	0.0002	**2**	Insula	712.38	0.0002
3	Pars Opercularis	2014.50	0.0002	**3**	Superior Temporal	565.92	0.0002
4	Lingual	1216.32	0.0002	**4**	Middle Temporal	313.90	0.0002
5	Rostral Anterior Cingulate	1058.52	0.0002	**5**	Pars Opercularis	275.34	0.0002
6	Rotral Middle Frontal	831.81	0.0002	**6**	Caudal Middle Frontal	177.78	0.0002
7	Inferior Temporal	577.72	0.0002	**7**	Superior Frontal	152.85	0.0002
8	Superior Temporal	384.39	0.0002	**8**	Lateral Orbitofrontal	133.50	0.0004
9	Caudal Anterior Cingulate	265.77	0.0002	**9**	Fusiform	119.38	0.001
10	Lateral Occipital	229.50	0.0002	**10**	Superior Temporal*	70.04	0.012
11	Superior Frontal	116.60	0.0006	**11**	Superior Frontal*	63.03	0.017
				12	Lateral Occipital	62.23	0.018
				13	Inferior Temporal	61.08	0.019
				14	Lateral Occipital*	*57.17*	0.023

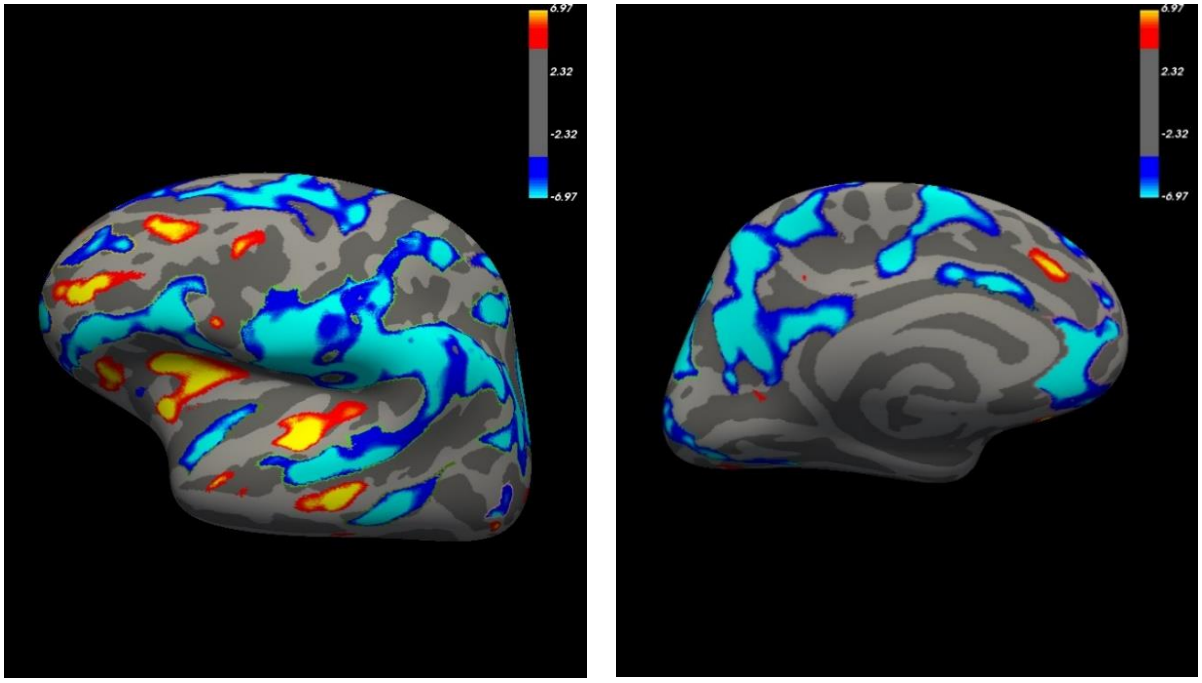

Figure 4.8 Regions of the cortical surface in the left hemisphere presenting correlation between cortical thickness changes and time. The blue regions show a negative, and the yellow regions show a positive correlation between cortical thickness change and time. The legend shows the level of significance based on the -log p equation.

In the same way, for the right hemisphere. Table 4.3 shows the correlations between cortical thickness changes and time. The regions of the cortical surface with the most negative correlations of significant changes are the superior parietal, medial orbitofrontal, superior temporal, precentral, postcentral, inferior temporal, and superior temporal. The regions with the most significant positive correlations of changes are the lateral orbitofrontal, superior temporal, middle temporal, insula, precentral, and superior parietal. Figure 4.9 shows the cortical regions with positive (in yellow) and negative (in blue) correlations.

Table 4.3 Surfaces affected regions of the cortical surface in the right hemisphere with positive and negative correlations between the cortical thickness change and the time. The size of the regions is in mm^2. The regions in red are those that present both correlations. (*) indicate another vertex of a previously mentioned region.

Negative Correlation			
N°	Surface Cortical Region	Size (mm^2)	p-value
1	Superior Parietal	11900.67	0.0002
2	Middle Orbito Frontal	10613.78	0.0002
3	Superior Temporal	801.04	0.0002
4	Pre-central	667.68	0.0002
5	Post-central	603.51	0.0002
6	Inferior Temporal	214.14	0.0002
7	Superior Temporal*	61.40	0.017

Positive Correlation			
N°	Surface Cortical Region	Size (mm^2)	p-value
1	Lateral Orbito Frontal	624.78	0.0002
2	Superior Temporal	623.34	0.0002
3	Middle Temporal	218.20	0.0002
4	Insula	189.36	0.0002
5	Pre-central	121.89	0.0002
6	Superior Parietal	121.07	0.0004
7	Banks of Superior Temporal Sulcus	86.30	0.0042
8	Superior Temporal*	50.29	0.034
9	Rostral Middle Frontal	48.81	0.039

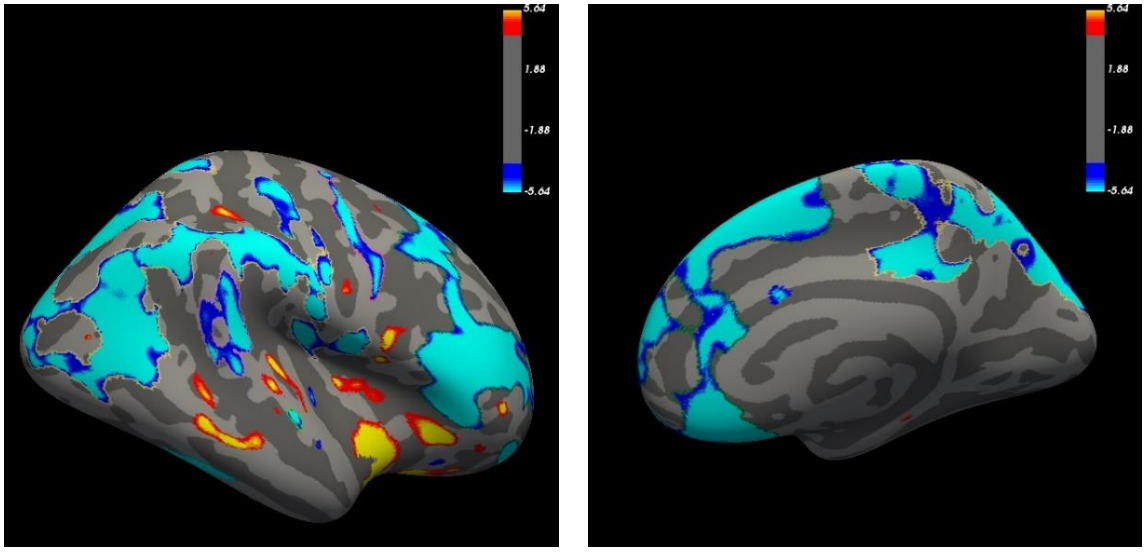

Figure 4.9 Regions of the cortical surface in the right hemisphere presenting correlation between cortical thickness changes and time. The blue regions show a negative, and the yellow regions show a positive correlation between cortical thickness change and time. The legend shows the level of significance based on the -log p equation.

4.4. Diffusion MRI Results for DB2 database

This section presents the changes in diffusion MRI metrics over time in the DB2 database.

4.4.1 Results from the transversal analysis over DB2

Here, we applied a transversal approach to the data to determine the most significant alterations of diffusion MRI metrics for every fiber bundle. We used the difference between the arithmetic means of the data for each fiber bundle to interpret each diffusion MRI metric. A t-test was performed on the data to determine the significance level. Then, a Tukey-Kramer Honest, Significant Difference test specified if the difference in the arithmetic means of each metric of each fiber bundle was considered significant.

Initially, there were 162 short fiber bundles, each with five diffusion MRI metric (AD, MD, RD, FA, and QA), leading to 810 short brain fiber bundles measures to analyze. After this analysis, the number was reduced to 68 short brain fiber bundles measures among all diffusion MRI metrics.

First, Table 4.4 shows the most significant fiber bundles measures separated by diffusion MRI metrics. As well as the previous analysis, the significant threshold was a p-value less than 0.05. There was no significant changes for the FA metrics. On the other hand, there are many brain fiber bundles where the QA metric was considered significant. This metric is also a measure of anisotropy but calculated for each fiber and is less sensitive to edema.

Table 4.4 Brain fiber bundles measures with a significant change in the arithmetic mean separated by diffusion MRI metrics. The presentation of the fibers is based on the abbreviations for each cortical region according to the Desikan - Killiany atlas; the list of abbreviations is shown in Table E in annex E. The fibers bundles in red have significant difference in more than one diffusion MRI metric. The brain fiber bundles in blue is the only one that show differences in all the diffusion MRI metrics.

Axial diffusivity (AD)	Left Hemisphere	CMF-SF_0	PoCi-PrCu_1	PrC-SF_0
		SF_SF_1r	ST-TT_0	
	Right Hemisphere	IC-PrCu_0	LOF-MOF_0	PoC-Ins_0
		PoCi-SF_0	ST-TT_0	
Mean diffusivity (MD)	Left Hemisphere	CMF-SF_0	CMF-SF_1	PrC-SF_0
	Right Hemisphere	PoC-Ins_0	SM-Ins_0	ST-TT_0
Radial diffusivity (RD)	Left Hemisphere	PrC-SF_0		
	Right Hemisphere	SM-Ins_0		
Quantitative anisotropy (QA)	Left Hemisphere	CAC-PrCu_0	CMF-Op_0	CMF-PrC_0
		CMF-PrC_1	CMF-RMF_0	CMF-SF_0
		CMF-SF_1	IC-PrCu_0	IP-SP_0
		IP-SP_1	Op-PrC_0	Op-SF_0
		PoC-PrC_1	PoC-SP_0	PoCi-PrCu_0
		PoCi-PrCu_1	PoCi-PrCu_2	PoCi-RAC_0
		PoCi-SF_0	PrC-SF_0	PreCu_PreCu_0r
		RMF-SF_1	RoMF_RoMF_0i	RoMF_RoMF_1i
		SF_SF_1r	SM-Ins_0	SP-SM_0
		Tr_RoMF_0i		
	Right Hemisphere	CAC-PrCu_0	CMF-PrC_0	CMF-SF_0
		IC-PrCu_0	IP-SM_0	IP-SP_1
		Op-SF_0	PoC-PrC_1	PoC-PrC_2
		PoC-SP_0	PoC-SP_1	PoCi-PrCu_0
		PoCi-PrCu_1	PoCi-PrCu_2	PoCi-RAC_0
		PoCi-SF_0	PrC-Ins_0	PrC-SF_0
		PrC-SM_0	PrC-SP_0	PreCu_PreCu_0r
		RMF-SF_1	SF_SF_1r	SM-Ins_0
		SP-SM_0		

4.4.2 Results from the longitudinal analysis over DB2

Due to the longitudinal nature of the data, also, we applied a longitudinal study, in this case, through the GEE model. This model was used for the same fiber bundles considered significant by the transversal analysis. Table 4.5 compares the significance level between the t-test and the GEE model of the mean difference for every fiber bundle considered significant by the t-test. Like the

transversal analysis, all the fiber bundles showed significant measures. Still, in the GEE model, the significance level has lower values, indicating a better significance level. Figure 4.10 shows all fiber bundles considered significant by the GEE model for both hemispheres.

The results for the diffusion MRI metrics we obtained were unlike what is normally expected, i.e, a decrease I anisotropy measures and an increase in diffusivity measures, differing from previous works related to the topic, as described in Chapter 2. We applied the GEE model again and, in this case, considering the EDSS value as a factor. The aim was to analyze the impact of the EDSS value on the fiber bundles metrics.

Table D from Annex D shows the significance level for every fiber bundle measure correlated with the change in the EDSS value. A high EDSS value, it indicates a bad performance in the disability of the MS. And a decrease in the EDSS value indicates an improvement in the disability of the subject. First, we highlight that the change in the EDSS value is not significant in all the fiber bundle measures. One interpretation is that the fiber bundles with significant changes in the EDSS value present an improvement, maybe related to the subject's treatment. When we look at all these changes in the EDSS value, these are mostly in the lower values of EDSS instead to the higher values of EDSS.

Table 4.6 shows the fiber bundles for both hemispheres where the EDSS value is significant and presents an improvement. Figure 4.11 shows these fiber bundles and the regions that these connect.

Table 4.5 Comparison of the significance level between the transversal analysis (t-test) and the longitudinal analysis (GEE model). The fibers' names are based on the abbreviations for each cortical region according to the Desikan - Killiany atlas; the list of abbreviations is shown in Table E in Annex E. The mean difference was calculated by subtraction between the diffusion MRI metric of the second and the first time point.

Left Hemisphere				Right Hemisphere			
Name	**Mean Dif.**	**p value t-test**	**p value GEE**	**Name**	**Mean Dif.**	**p value t-test**	**p value GEE**
CMF-SF_0_AD	-0.0579	0.011	0.007	IC-PrCu_0_AD	-0.0401	0.003	0.001
PoCi-PrCu_1_AD	-0.0468	0.004	0.002	LOF-MOF_0_AD	-0.0423	0.020	0.014
PrC-SF_0_AD	-0.0645	0.020	0.014	PoC-Ins_0_AD	-0.0409	0.033	0.025
SF_SF_1r_AD	-0.0539	0.038	0.029	PoCi-SF_0_AD	-0.0506	0.015	0.010
ST-TT_0_AD	-0.0582	0.045	0.035	ST-TT_0_AD	-0.0426	0.030	0.023
CMF-SF_0_MD	-0.0523	0.037	0.028	PoC-Ins_0_MD	-0.0403	0.032	0.024
CMF-SF_1_MD	-0.0419	0.045	0.035	SM-Ins_0_MD	-0.0421	0.001	0.001
PrC-SF_0_MD	-0.0700	0.017	0.011	ST-TT_0_MD	-0.0417	0.035	0.027
PrC-SF_0_RD	-0.0728	0.020	0.014	SM-Ins_0_RD	-0.0463	0.003	0.001
CAC-PrCu_0_QA	0.0108	0.003	0.001	CAC-PrCu_0_QA	0.0115	0.001	0.001
CMF-Op_0_QA	0.0084	0.022	0.016	CMF-PrC_0_QA	0.0099	0.033	0.025
CMF-PrC_0_QA	0.0097	0.037	0.029	CMF-SF_0_QA	0.0088	0.031	0.023
CMF-PrC_1_QA	0.0076	0.025	0.018	IC-PrCu_0_QA	0.0073	0.014	0.009
CMF-RMF_0_QA	0.0084	0.021	0.015	IP-SM_0_QA	0.0094	0.033	0.025
CMF-SF_0_QA	0.0098	0.018	0.012	IP-SP_1_QA	0.0098	0.025	0.018
CMF-SF_1_QA	0.0098	0.011	0.007	Op-SF_0_QA	0.0079	0.027	0.020
IC-PrCu_0_QA	0.0075	0.005	0.002	PoC-PrC_1_QA	0.0117	0.011	0.007
IP-SP_0_QA	0.0101	0.023	0.016	PoC-PrC_2_QA	0.0103	0.027	0.019
IP-SP_1_QA	0.0100	0.035	0.026	PoC-SP_0_QA	0.0096	0.020	0.014
Op-PrC_0_QA	0.0074	0.017	0.012	PoC-SP_1_QA	0.0107	0.013	0.008
Op-SF_0_QA	0.0093	0.013	0.008	PoCi-PrCu_0_QA	0.0088	0.006	0.003
PoC-PrC_1_QA	0.0112	0.015	0.010	PoCi-PrCu_1_QA	0.0104	0.002	0.001
PoC-SP_0_QA	0.0102	0.020	0.014	PoCi-PrCu_2_QA	0.0097	0.002	0.001
PoCi-PrCu_0_QA	0.0074	0.012	0.007	PoCi-RAC_0_QA	0.0106	0.001	0.001
PoCi-PrCu_1_QA	0.0097	0.004	0.002	PoCi-SF_0_QA	0.0100	0.007	0.004
PoCi-PrCu_2_QA	0.0084	0.004	0.002	PrC-Ins_0_QA	0.0075	0.013	0.008
PoCi-RAC_0_QA	0.0098	0.003	0.002	PrC-SF_0_QA	0.0096	0.022	0.016
PoCi-SF_0_QA	0.0081	0.004	0.002	PrC-SM_0_QA	0.0095	0.044	0.034
PrC-SF_0_QA	0.0122	0.006	0.003	PrC-SP_0_QA	0.0109	0.017	0.011
PreCu_PreCu_0r_Q	0.0075	0.042	0.032	PreCu_PreCu_0r_Q	0.0086	0.050	0.040
RMF-SF_1_QA	0.0081	0.027	0.020	RMF-SF_1_QA	0.0073	0.041	0.032
RoMF_RoMF_0i_Q	0.0082	0.007	0.004	SF_SF_1r_QA	0.0089	0.007	0.004
RoMF_RoMF_1i_Q	0.0073	0.019	0.013	SM-Ins_0_QA	0.0092	0.003	0.002
SF_SF_1r_QA	0.0098	0.001	0.001	SP-SM_0_QA	0.0086	0.019	0.013
SM-Ins_0_QA	0.0077	0.024	0.017				
SP-SM_0_QA	0.0069	0.029	0.038				
Tr_RoMF_0i_QA	0.0073	0.018	0.012				

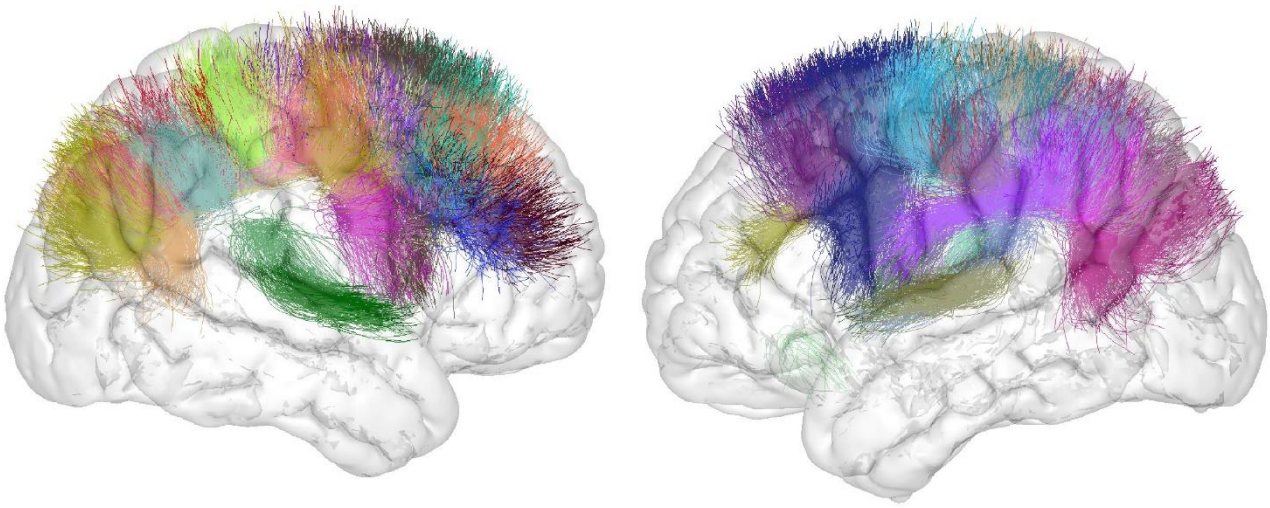

Figure 4.10 Short fiber bundles with significant difference in dMRI metrics for the left and right hemispheres. The significance was determined by a p-value less than 0.05, calculated using the GEE model.

Table 4.6 Brain fiber bundles with a significant change in the EDSS value, separated by diffusion MRI metrics. The presentation of the fibers is based on the abbreviations for each cortical region according to the Desikan - Killiany atlas; the list of abbreviations is shown in Table E in annex E. The fiber bundles in red have more than one significant diffusion MRI metric.

Axial diffusivity (AD)	Left Hemisphere	PrC-SF_0_AD		
	Right Hemisphere	PoCi-SF_0_AD		
Quantitative anisotropy (QA)	Left Hemisphere	CMF-PrC_1_QA	CMF-RMF_0_QA	CMF-SF_0_QA
		IP-SP_1_QA	Op-SF_0_QA	PrC-SF_0_QA
		RMF-SF_1_QA	RoMF_RoMF_0i_QA	RoMF_RoMF_1i_QA
		SP-SM_0_QA	Tr_RoMF_0i_QA	
	Right Hemisphere	CAC-PrCu_0_QA	IC-PrCu_0_QA	Op-SF_0_QA
		PoCi-PrCu_0_QA	PoCi-PrCu_1_QA	PoCi-PrCu_2_QA
		PrC-Ins_0_QA	PreCu_PreCu_0r_QA	

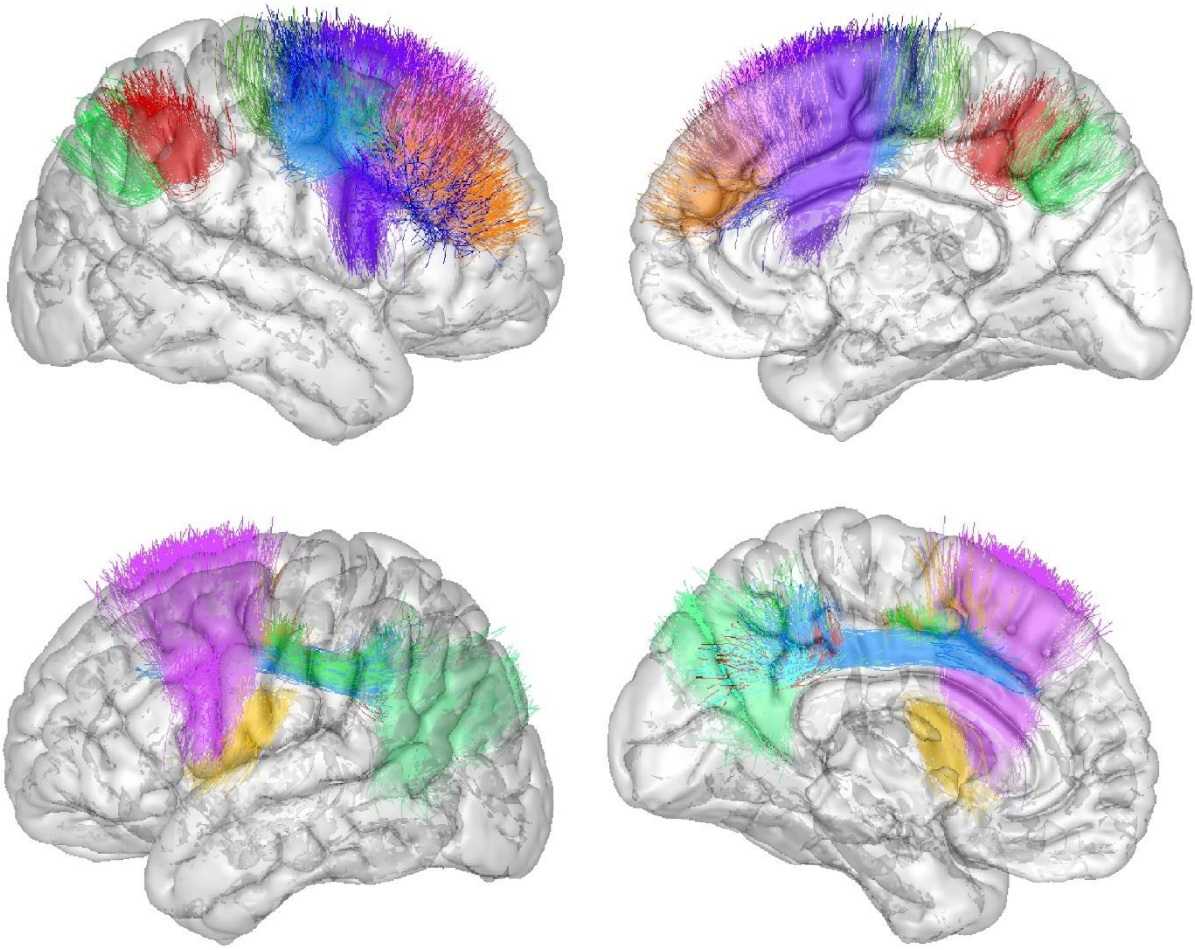

Figure 4.11 Short fiber bundles with significant difference in dMRI metrics for the left and right hemispheres considering the EDSS value as a cofactor. The significance was determined by a p-value less than 0.05, calculated using the GEE model.

Capítulo 5. Conclusion

5.1. Discussion

When analyzing the results obtained from the anatomical analysis of the DB1 database, the first thing to highlight is that regardless of the correlation that was carried out, the results obtained for the changes in cortical thickness and cortical volume were very similar.

Using the GLM model to determine the changes between cortical thickness and cortical volume related to the EDSS and SDMT variables allowed us to determine that the differences between cortical volume and thickness were similar and highlight mainly the same regions. In the case of the correlation between changes in cortical thickness and cortical volume related the EDSS value, the areas significant were mainly the precuneus, rostral middle frontal, caudal middle frontal, and superior frontal for the left hemisphere. While for the right hemisphere, we have the superior parietal, rostral middle frontal, and superior frontal regions. In these cases, the prevailing correlations were negative, indicating a decrease in cortical thickness related to the increase in the EDSS value. Additionally, it should be mentioned that although the predominant regions had negative correlations, there were also small regions with positive correlation, indicating an increase in cortical thickness. Our interpretation of this event can be explained as a kind of compensation by the brain in the initial stages of MS.

On the other hand, when correlating changes in cortical thickness and volume to the SDMT value, the most prominent regions were the precentral and superior temporal regions for the left hemisphere, and the precentral, inferior parietal, and medial orbitofrontal regions for the right hemisphere. These regions are associated with sensory processing and information processing speed, functions that are associated with the value measured by the SDMT test.

Something important to highlight about the GLM model was its simplicity of its application. This is partly due to the large amount of literature regarding its application since it is a model widely used in this type of research. However, it is not free from limitations, the main one being the use of only of the arithmetic mean of the data to determine the changes between the variables, limiting the interpretations that can be made of the results.

On the other hand, the use of the LME model for the analysis of the same correlations between cortical changes (thickness and volume) and the EDSS and SDMT variables allowed us to determine that the regions that presented the significant changes coincided mostly with those highlighted by the GLM model for both hemispheres. The main difference with the GLM model is that in the LME model, the interpretation of the results is based on the identification of the regions that present the

most significant changes rather than the types of changes (positive or negative). The advantage of this type of analysis is that we can have a more general view of the regions that present changes, given the changes in the EDSS and SDMT variables. Furthermore, another advantage of this model is that in addition to using the arithmetic mean to perform the calculations, it uses the variance and standard deviation of the data. Using these two additional metrics allows for a broader interpretation of the results. However, one of the main disadvantages of using this model was its complex implementation and slow learning curve, and less available information.

Given these results and the advantages and disadvantages of both models, it was decided to use the GLM model for the anatomical analysis of the DB2 database.

On the other hand, as shown in the results of the DB2 database, there are two types of changes: cortical changes and diffusion MRI metrics changes.

When we analyzed the anatomical changes in subjects with MS, we found negative and positive correlations. The negative correlations, which we interpret as decreased cortical thickness over time, cover a larger surface area and are much more predominant than the positive correlation. The regions most affected by this correlation were the left hemisphere's postcentral, precuneus, and lingual regions, and the right superior parietal, middle orbitofrontal, and superior temporal regions. In both cases, regions are associated with sensitive and sensory processing. Something to note about this correlation is that in the left hemisphere, there was a greater distribution in the size of the affected surface, while in the right hemisphere, two regions had the largest affected surface.

On the other hand, the positive correlations, interpreted as an increase in cortical thickness over time, were present in several brain regions but on a smaller scale, covering much less surface area than the negative correlations. Highlighting the left hemisphere's rostral middle frontal, insula, and superior temporal regions, and the right lateral orbitofrontal, superior temporal, and middle temporal regions. These affected regions focus on emotional functions, language processing, and space recognition. This correlation affected a much smaller surface area than the negative correlation, was not concentrated in a particular region. Given that there were regions of coincidence between correlations and between hemispheres, a possible interpretation of these results is that in the initial stages of MS, the brain seeks compensation between the regions to supply reduced functions, given the effect of MS.

In the case of the two anatomical studies, the results obtained, especially those associated with negative correlations with time, are related. This is because both databases highlight similar regions for both hemispheres in the same type of analysis. Also, the results of both studies are what was

expected according to the literature. Previous studies indicate that prominent regions in MS include the precentral, superior frontal, superior parietal, and superior temporal regions, which are motor and sensory regions.

Respecting the changes in the diffusion MRI metrics, we found several fiber bundles with significant difference, in their metrics means regardless of the analysis (transversal or longitudinal).

Given these results, we observed is the absence of significant change for FA in the fiber bundles. However, significant difference was found for QA, a more specific anisotropy metric. A main observation is the trend of the diffusion MRI metrics changes, which does not follow the expected sense according to the literature and previous works in the area. Our assumptions regarding these results are associated with a possible improvement of the subjects health given the treatments to which they are exposed. Using the EDSS value, we seek to verify if there was some degree of progress in the subjects' disability levels by correlating this value with the fiber bundles metrics. When performing this correlation, a favorable trend was obtained in the EDSS value related to the fiber bundles, showing a slight improvement in the subjects. Is important to highlight that these signs of improvement occur at the lowest levels of the EDSS value, which we interpret as the levels of progress that occur in subjects with initial stages of MS or who present a mild to moderate degree of disability. While the EDSS value trends show us somewhat positive trends, it is also essential to identify the regions that connect these fiber bundles with significant changes. The regions that connect these fibers for the left and right hemispheres are the superior temporal, superior frontal, and parietal regions, with the postcentral, posterior cingulate, and precentral regions. All of these regions are mainly associated with motor functions and sensory processing, which is in line with what is expected given the characteristics of the disease. Additionally, we can note that a brain fiber bundle presented significant changes in all diffusion MRI metrics, which is the fiber bundle that connects the precentral regions with the superior frontal region of the left hemisphere. This connection is also mainly associated with motor and working memory functions.

Finally, we can establish that there is a relationship between cortical anatomical changes and changes in diffusion metrics in subjects with MS. We can reach this conclusion given that the regions that presented the most significant changes at the cortical level for both hemispheres partly coincide with the regions connected by the fibers showing significant changes. In this case, the regions that stand out are the postcentral and superior temporal regions for the left hemisphere and the superior parietal and superior temporal regions for the right hemisphere. However, some regions were

identified in one type of analysis but not in the other. One explanation could be using statistical models and the small number of subjects in the database.

These finding are novel since there is no previous longitudinal study that analyzed anatomical and dMRI metrics in MS.

5.2. Conclusions

In conclusion, we could apply an anatomical longitudinal analysis on the T1 and FLAIR images on the subjects of the DB1 and DB2 databases using the FreeSurfer software. The results of this analysis were in line with what was expected since they highlighted regions of the cerebral cortex associated with the effects of MS. The regions that identified are motor and sensory processing areas, and regions related to processing speed.

In addition, the statistical models, GLM and LME, were correctly applied to the DB1 database. The main conclusion that we can obtain after using both statistical models is that the execution and subsequent interpretation of results of the GLM model were more straightforward than the execution of the LME model despite obtaining similar results concerning the highlighted regions. This is partly explained given that the application of the GLM model is widely exposed in the literature, while the application of the LME model is much less frequent.

Given these difficulties, applying the GLM model to the data from the DB2 database was decided. The results of the analysis of DB2 were in line with those expected from the literature. Regions very similar to those found for the DB1 database were identified. These regions have mainly motor and information processing speed functions.

On the other hand, a cross-sectional and longitudinal statistical analysis was carried out on the diffusion MRI metrics of the short WM bundles. The cross-sectional study, executed through a t-test, was an initial "filter" for the fiber bundles, identifying various fiber bundles with significant difference for different metrics. Furthermore, in the longitudinal analysis, executed using the GEE model, the results confirmed what was found in the transversal study, giving the same fiber bundles as significant. We observed in the opposite trend of the diffusion metrics considered significant, i.e., an increase in QA and a decrease in diffusivity metrics. The explanation for this may be due to the treatments the subjects underwent, which could positively affect the subjects.

Finally, when comparing the anatomical changes found with the changes in the diffusion MRI metrics, some coincidences could be found between the regions that presented a decrease in the

cortical thickness and the fiber bundle with significant changes. The most prevalent connection where between the precentral and the superior frontal regions. Also, these regions present significant anatomical changes. Based on these results and the highlighted regions, we can conclude that significant changes were found in cortical areas and associated with changes in brain fibers. This allows us to confirm our initial hypothesis.

5.3. Limitations and Future Works

This work was not free of limitations and difficulties. The first limitation of this work was the size of the databases used, being a small number of subjects, which generated difficulty in generalizing the results obtained. Another limitation was that the DB1 database had T1 images, and the DB2 database had T1 and FLAIR images. This difference made it difficult to compare the results since the two databases went through different preprocessing stages. Also, the absence of diffusion MRI data of DB1 made it impossible to compare results in that aspect of the research. On the other hand, there are difficulties with the learning curves of the statistical methods and software used during the study, which generated delays in their application. One of the reasons for those delays was the small amount of literature that have some of the statistical methods and some of the software used. Finally, there was a delay in data acquisition due to the sanitary conditions present during much of this research, delaying the application of the analyses and the later interpretation of the results.

On the other hand, a possible work is correlating anatomical and diffusion MRI changes concerning the EDSS and SDMT variables from the DB2 database. In addition, it uses information on the treatment to which the subjects are exposed to ratify or refute the observations found regarding the subjects' improvements when correlating with the EDSS variable and the fiber bundles changes.

5.4. Research Presentation

This section presents the national and international instances in which the work carried out during this research was presented.

5.4.1 Papers WoS

A paper was accepted in the Multiple Sclerosis and Related Disorders Journal (Q2). This paper aimed to compare the results of taking the Symbolic Digit Modalities Test (SDMT), the most reliable and sensitive cognitive measure in MS, measured in patients seen through telehealth versus in person.

- Title: **Brain volumetric correlates of remotely versus in-person administered symbol digit modalities test in multiple sclerosis**
- Authors: Korhan Buyukturkoglu, Jordan D Dworkin, Victor Leiva, Frank A Provenzano, Pamela Guevara, Philip L De Jager, Victoria M Leavitt, Claire S Riley
- Institutions: - Columbia University, New York, United States
  - Universidad de Concepción, Concepción, Chile

In addition, a paper will be sent to a specialized journal. This paper aims to show the results obtained using the DB1 database. The objective is to show the difference in outcomes between the GLM and LME statistical models and compare the regions that present the most significant changes at the cortical level.

- Title: **Longitudinal analysis of anatomical changes using magnetic resonance imaging in patients with Multiple Sclerosis**
- Authors: Víctor Leiva, Carlos Guevara, Pamela Guevara, Pablo Billeke, Alejandra Figueroa.
- Institutions: - Universidad de Concepción, Concepción, Chile
  - Universidad del Desarrollo, Santiago, Chile
  - Universidad de Chile, Santiago, Chile

Finally, another paper will be sent to a specialized journal. The content of this paper includes the results obtained throughout this research, both anatomical and diffusion MRI results, and the relation established between these two types of analysis.

- Title: **Longitudinal analysis of anatomical and diffusion changes by magnetic resonance imaging in patients with multiple sclerosis**
- Authors: Víctor Leiva, Korhan Buyukturkoglu, Christopher Vergara, Carlos Guevara, Pamela Guevara, Alexander Ratzan, Victoria M. Leavitt.
- Institutions: - Universidad de Concepción, Concepción, Chile
  - Columbia University, New York, United States
  - Universidad de La Frontera, Temuco, Chile
  - Universidad de Chile, Santiago, Chile

5.4.2 Conference Papers and Conference Abstracts

A paper was accepted to the 14th Biomedical Engineering Congress Universidad de Concepción in Concepción, Chile, held on October 6-9, 2021. This work was presented in the paper competition of the congress, obtaining third place. This paper showed the results associated with anatomical analysis based on the GLM and LME statistical models on the database DB1. In this case, the 39 subjects present in the database were used.

- Title: **Longitudinal study of anatomical changes in patients with multiple sclerosis using MRI**
- Authors: Víctor Leiva, Carlos Guevara, Pamela Guevara
- Institutions: - Universidad de Concepción, Concepción, Chile
  - Universidad de Chile, Santiago, Chile

A poster was presented at the Technical Conference of the Advanced Center for Electrical and Electronic Engineering, AC3E, of the Universidad Tecnica Federico Santa Maria, Valparaiso, Chile, held on August 19, 2022. This work showed the results associated with the complete analysis of the anatomical model based on GLM statistical models on subjects from the DB2 database. In this case, the 23 subjects present in the database were used.

- Title: **Longitudinal anatomical changes in patients with Multiple Sclerosis**
- Authors: Víctor Leiva, Korhan Buyukturkoglu, Carlos Guevara, Pamela Guevara
- Institutions: - Universidad de Concepción, Concepción, Chile
  - Columbia University, New York, United States
  - Universidad de Chile, Santiago, Chile

A poster was presented at the 15th IEEE EMBS-SPS International Summer School on Biomedical Imaging, Cartagena, Colombia, held on April 13-17, 2023. This work showed the results associated with the complete analysis of the anatomical model based on GLM statistical models on subjects from the DB2 database and the preliminary results of the study of the diffusion metrics. In this case, the 23 subjects present in the database were used.

- Title: **Longitudinal anatomical and diffusion changes in patients with Multiple Sclerosis.**
- Authors: Víctor Leiva, Korhan Buyukturkoglu, Carlos Guevara, Pamela Guevara

- Institutions: - Universidad de Concepción, Concepción, Chile
  - Columbia University, New York, United States
  - Universidad de Chile, Santiago, Chile

Finally, an abstract was accepted in the 9th Joint ECTRIMS-ACTRIMS Meeting, 11-13 October 2023, Milan, Italy. This abstract was presented as a poster. This poster is the presentation of a work that will later be sent as a paper for publication. This work aims to predict the cognitive performance of individuals with MS using radiomic features and volumetric measurements of the thalamus and its nuclei extracted from clinical MRI data. Radiomics is a quantitative approach that offers a solution to extract information from medical images.

- Title: **Thalamus-derived Radiomic Features to Predict Cognitive Performance in MS.**
- Authors: Korhan Buyukturkogu1, Lin Lu, Hao Yang, Renan E. Orellana, Alexander Ratzan, Victor Leiva, Sinem Ozcelik, Binsheng Zhao, Victoria M. Leavitt, Claire S. Riley, Phil De Jager.
- Institutions: - Columbia University Irving Medical Center, NY, USA.
  - Columbia University MS Center, NY, USA.
  - Universidad de Concepción, Department of Biomedical Engineering, Concepción, Chile
  - The Center for Translational and Computational Neuroimmunology, NY, USA.

Bibliography

[1] Wallin MT, Culpepper WJ, Nichols E, Bhutta ZA, Gebrehiwot TT, Hay SI, *et al.*, "Global, regional, and national burden of multiple sclerosis 1990–2016: a systematic analysis for the Global Burden of Disease Study 2016," *Lancet Neurol*, vol. 18, no. 3, Mar. 2019, doi: 10.1016/S1474-4422(18)30443-5.

[2] Haider L, Zrzavy T, Hametner S, Höftberger R, Bagnato F, Grabner G, *et al.*, "The topograpy of demyelination and neurodegeneration in the multiple sclerosis brain," *Brain*, vol. 139, no. 3, Mar. 2016, doi: 10.1093/brain/awv398.

[3] Multiple Sclerosis Association of America, "Types of Multiple Sclerosis." Accessed: Nov. 28, 2023. [Online]. Available: https://mymsaa.org/ms-information/overview/types/

[4] K. Cherry, "The Pros and Cons of Longitudinal Research." Accessed: Jun. 21, 2021. [Online]. Available: https://www.verywellmind.com/what-is-longitudinal-research-2795335

[5] Y. Baba and J. Jones, "T1 weighted image." Accessed: Jun. 21, 2021. [Online]. Available: https://radiopaedia.org/articles/t1-weighted-image

[6] Y. Baba and M. Niknejad, "Fluid attenuated inversion recovery," in *Radiopaedia.org*, Radiopaedia.org, 2013. doi: 10.53347/rID-21760.

[7] A. Fick, "On liquid diffusion," in *Philos. Mag. J. Sci*, vol. 10, 1855, pp. 31–39.

[8] M. Reuter, N. J. Schmansky, H. D. Rosas, and B. Fischl, "Within-subject template estimation for unbiased longitudinal image analysis," *Neuroimage*, vol. 61, no. 4, Jul. 2012, doi: 10.1016/j.neuroimage.2012.02.084.

[9] DSI Studio, "How to interpret dMRI metrics." Accessed: Jan. 04, 2023. [Online]. Available: https://dsi-studio.labsolver.org/doc/how_to_interpret_dmri.html

[10] IBM Corp., "IBM SPSS Statistics for Windows." Armonk, NY, 2021. Accessed: May 30, 2023. [Online]. Available: https://www.ibm.com/mx-es/products/spss-statistics

[11] S. M. Smith and J. M. Brady, "SUSAN—A New Approach to Low Level Image Processing.," *Int J Comput Vis*, vol. 23, no. 1, 1997, doi: 10.1023/A:1007963824710.

[12] M. Jenkinson, C. F. Beckmann, T. E. J. Behrens, M. W. Woolrich, and S. M. Smith, "FSL," *Neuroimage*, vol. 62, no. 2, Aug. 2012, doi: 10.1016/j.neuroimage.2011.09.015.

[13] P. Thevenaz, T. Blu, and M. Unser, "Interpolation revisited [medical images application]," *IEEE Trans Med Imaging*, vol. 19, no. 7, Jul. 2000, doi: 10.1109/42.875199.

[14] Schmidt P, Gaser C, Arsic M, Buck D, Förschler A, Berthele A, *et al.*, "An automated tool for detection of FLAIR-hyperintense white-matter lesions in Multiple Sclerosis," *Neuroimage*, vol. 59, no. 4, Feb. 2012, doi: 10.1016/j.neuroimage.2011.11.032.

[15] Buyukturkoglu K, Vergara C, Fuentealba V, Tozlu C, Dahan JB, Carroll BE, *et al.*, "Machine learning to investigate superficial white matter integrity in early multiple sclerosis," *Journal of Neuroimaging*, vol. 32, no. 1, pp. 36–47, Jan. 2022, doi: 10.1111/jon.12934.

[16] S. Ira Fox, *Human Physiology*, 14th ed. Mexico DF: McGraw-Hill Global Education, 2016.

[17] A. G. F. D. H. W. L. A. M. J. W. LE Purves D, *Neuroscience*, 4th ed. Sinauer Associates, 2008.

[18] S. Hitziger, " Modeling the variability of electrical activity in the brain. ," Ph.D. dissertation, Université Nice Sophia Antipolis, Niza, 2015.

[19] B. J. Jellison, A. S. Field, J. , L. Medow, M. S. Salamat, and A. L. Alexander, "Diffusion tensor imaging of cerebral white matter: a pictorial review of physics, fiber tract anatomy, and tumor imaging patterns.," *AJNR Am J Neuroradiol*, vol. 25, no. 3, pp. 356–369, 2004.

[20] B. J. Jellison, A. S. Field, J. , L. Medow, M. S. Salamat, and A. L. Alexander, "Diffusion tensor imaging of cerebral white matter: a pictorial review of physics, fiber tract anatomy, and tumor imaging patterns.," *AJNR Am J Neuroradiol*, vol. 25, no. 3, pp. 356–369, 2004.

[21] A. Goel and U. Bashir, “Diffusion-weighted imaging,” in *Radiopaedia.org*, Radiopaedia.org, 2012. doi: 10.53347/rID-16718.
[22] Caruana EJ, Roman M, Hernández-Sánchez J, and Solli P., “Longitudinal studies,” *J Thorac Dis*, vol. 7, no. 11, pp. 537–540, Nov. 2015, doi: 10.3978/j.issn.2072-1439.2015.10.63.
[23] Rocca MA, Amato MP, De Stefano N, Enzinger C, Geurts JJ, Penner IK, *et al.*, “Clinical and imaging assessment of cognitive dysfunction in multiple sclerosis,” *Lancet Neurol*, vol. 14, no. 3, Mar. 2015, doi: 10.1016/S1474-4422(14)70250-9.
[24] Camp SJ, Stevenson VL, Thompson AJ, Ingle GT, Miller DH, Borras C, *et al.*, “A longitudinal study of cognition in primary progressive multiple sclerosis,” *Brain*, vol. 128, no. 12, Dec. 2005, doi: 10.1093/brain/awh602.
[25] Hidalgo de la Cruz M, Valsasina P, Gobbi C, Gallo A, Zecca C, Bisecco A, *et al.*, “Longitudinal cortical thinning progression differs across multiple sclerosis phenotypes and is clinically relevant: A multicentre study,” *Multiple Sclerosis Journal*, vol. 27, no. 6, May 2021, doi: 10.1177/1352458520940548.
[26] J. F. Kurtzke, “Rating neurologic impairment in multiple sclerosis: An expanded disability status scale (EDSS),” *Neurology*, vol. 33, no. 11, pp. 1444–1444, Nov. 1983, doi: 10.1212/WNL.33.11.1444.
[27] Pravatà E, Rocca MA, Valsasina P, Riccitelli GC, Gobbi C, Comi G, *et al.*, “Gray matter trophism, cognitive impairment, and depression in patients with multiple sclerosis,” *Multiple Sclerosis Journal*, vol. 23, no. 14, Dec. 2017, doi: 10.1177/1352458517692886.
[28] A. Smith, *Symbol digit modalities test: Manual*. Los Angeles: Western Psychological Services, 1982.
[29] Fleischer V, Koirala N, Droby A, Gracien RM, Deichmann R, Ziemann U, *et al.*, “Longitudinal cortical network reorganization in early relapsing–remitting multiple sclerosis,” *Ther Adv Neurol Disord*, vol. 12, Jan. 2019, doi: 10.1177/1756286419838673.
[30] Mustafi S, Harezlak J, Kodiweera C, Randolph J, Ford J, Wishart H, *et al.*, “Detecting white matter alterations in multiple sclerosis using advanced diffusion magnetic resonance imaging,” *Neural Regen Res*, vol. 14, no. 1, p. 114, 2019, doi: 10.4103/1673-5374.243716.
[31] P. J. Basser, J. Mattiello, and D. LeBihan, “MR diffusion tensor spectroscopy and imaging,” *Biophys J*, vol. 66, no. 1, pp. 259–267, Jan. 1994, doi: 10.1016/S0006-3495(94)80775-1.
[32] Klistorner A, Wang C, Yiannikas C, Parratt J, Dwyer M, Barton J, *et al.*, “Evidence of progressive tissue loss in the core of chronic MS lesions: A longitudinal DTI study,” *Neuroimage Clin*, vol. 17, pp. 1028–1035, 2018, doi: 10.1016/j.nicl.2017.12.010.
[33] Kolasa M, Hakulinen U, Brander A, Hagman S, Dastidar P, Elovaara I, *et al.*, “Diffusion tensor imaging and disability progression in multiple sclerosis: A 4-year follow-up study,” *Brain Behav*, vol. 9, no. 1, p. e01194, Jan. 2019, doi: 10.1002/brb3.1194.
[34] Pokryszko-Dragan A, Banaszek A, Nowakowska-Kotas M, Jeżowska-Jurczyk K, Dziadkowiak E, Gruszka E, *et al.*, “Diffusion tensor imaging findings in the multiple sclerosis patients and their relationships to various aspects of disability,” *J Neurol Sci*, vol. 391, pp. 127–133, Aug. 2018, doi: 10.1016/j.jns.2018.06.007.
[35] Manca R, Stabile MR, Bevilacqua F, Cadorin C, Piccione F, Sharrack B, *et al.*, “Cognitive speed and white matter integrity in secondary progressive multiple sclerosis,” *Mult Scler Relat Disord*, vol. 30, pp. 198–207, May 2019, doi: 10.1016/j.msard.2019.02.021.
[36] J. Ashburner and K. J. Friston, “Voxel-Based Morphometry—The Methods,” *Neuroimage*, vol. 11, no. 6, pp. 805–821, Jun. 2000, doi: 10.1006/nimg.2000.0582.
[37] Smith SM, Jenkinson M, Johansen-Berg H, Rueckert D, Nichols TE, Mackay CE, *et al.*, “Tract-based spatial statistics: Voxelwise analysis of multi-subject diffusion data,” *Neuroimage*, vol. 31, no. 4, pp. 1487–1505, Jul. 2006, doi: 10.1016/j.neuroimage.2006.02.024.

[38] Zhao L, Ng A, Chen Q, Lam B, Abrigo J, Au C, *et al.*, "Impaired cognition is related to microstructural integrity in relapsing remitting multiple sclerosis," *Ann Clin Transl Neurol*, vol. 7, no. 7, pp. 1193–1203, Jul. 2020, doi: 10.1002/acn3.51100.

[39] L. Storelli, E. Pagani, P. Preziosa, M. Filippi, and M. A. Rocca, "Measurement of white matter fiber-bundle cross-section in multiple sclerosis using diffusion-weighted imaging," *Multiple Sclerosis Journal*, vol. 27, no. 6, pp. 818–826, May 2021, doi: 10.1177/1352458520938999.

[40] Preziosa P, Rocca MA, Pagani E, Stromillo ML, Enzinger C, Gallo A, *et al.*, "Structural MRI correlates of cognitive impairment in patients with multiple sclerosis," *Hum Brain Mapp*, vol. 37, no. 4, pp. 1627–1644, Apr. 2016, doi: 10.1002/hbm.23125.

[41] B. Jeurissen, J.-D. Tournier, T. Dhollander, A. Connelly, and J. Sijbers, "Multi-tissue constrained spherical deconvolution for improved analysis of multi-shell diffusion MRI data," *Neuroimage*, vol. 103, pp. 411–426, Dec. 2014, doi: 10.1016/j.neuroimage.2014.07.061.

[42] Cooper G, Chien C, Zimmermann H, Bellmann-Strobl J, Ruprecht K, Kuchling J, *et al.*, "Longitudinal analysis of T1w/T2w ratio in patients with multiple sclerosis from first clinical presentation," *Multiple Sclerosis Journal*, vol. 27, no. 14, pp. 2180–2190, Dec. 2021, doi: 10.1177/13524585211003479.

[43] Steenwijk MD, Daams M, Pouwels PJW, J. Balk L, Tewarie PK, Geurts JJG, *et al.*, "Unraveling the relationship between regional gray matter atrophy and pathology in connected white matter tracts in long-standing multiple sclerosis," *Hum Brain Mapp*, vol. 36, no. 5, pp. 1796–1807, May 2015, doi: 10.1002/hbm.22738.

[44] Dayan M, Hurtado Rúa SM, Monohan E, Fujimoto K, Pandya S, LoCastro EM, *et al.*, "MRI Analysis of White Matter Myelin Water Content in Multiple Sclerosis: A Novel Approach Applied to Finding Correlates of Cortical Thinning," *Front Neurosci*, vol. 11, May 2017, doi: 10.3389/fnins.2017.00284.

[45] Misaki M, Savitz J, Zotev V, Phillips R, Yuan H, Young KD, *et al.*, "Contrast enhancement by combining T1- and T2-weighted structural brain MR Images," *Magn Reson Med*, vol. 74, no. 6, pp. 1609–1620, Dec. 2015, doi: 10.1002/mrm.25560.

[46] Zhang J, Giorgio A, Vinciguerra C, Stromillo ML, Battaglini M, Mortilla M, *et al.*, "Gray matter atrophy cannot be fully explained by white matter damage in patients with MS," *Multiple Sclerosis Journal*, vol. 27, no. 1, pp. 39–51, Jan. 2021, doi: 10.1177/1352458519900972.

[47] L. Xu, K. M. Groth, G. Pearlson, D. J. Schretlen, and V. D. Calhoun, "Source-based morphometry: The use of independent component analysis to identify gray matter differences with application to schizophrenia," *Hum Brain Mapp*, vol. 30, no. 3, pp. 711–724, Mar. 2009, doi: 10.1002/hbm.20540.

[48] Pagani E, Rocca MA, De Meo E, Horsfield MA, Colombo B, Rodegher M, *et al.*, "Structural connectivity in multiple sclerosis and modeling of disconnection," *Multiple Sclerosis Journal*, vol. 26, no. 2, pp. 220–232, Feb. 2020, doi: 10.1177/1352458518820759.

[49] M. Rubinov and O. Sporns, "Complex network measures of brain connectivity: Uses and interpretations," *Neuroimage*, vol. 52, no. 3, pp. 1059–1069, Sep. 2010, doi: 10.1016/j.neuroimage.2009.10.003.

[50] Bussas M, Grahl S, Pongratz V, Berthele A, Gasperi C, Andlauer T, *et al.*, "Gray matter atrophy in relapsing-remitting multiple sclerosis is associated with white matter lesions in connecting fibers," *Multiple Sclerosis Journal*, vol. 28, no. 6, pp. 900–909, May 2022, doi: 10.1177/13524585211044957.

[51] D. S. Reich, C. F. Lucchinetti, and P. A. Calabresi, "Multiple Sclerosis," *New England Journal of Medicine*, vol. 378, no. 2, pp. 169–180, Jan. 2018, doi: 10.1056/NEJMra1401483.

[52] Van Essen DC, Ugurbil K, Auerbach E, Barch D, Behrens TEJ, Bucholz R,*et al.*, "The Human Connectome Project: A data acquisition perspective," *Neuroimage*, vol. 62, no. 4, pp. 2222–2231, Oct. 2012, doi: 10.1016/j.neuroimage.2012.02.018.

[53] P. McCullagh and J. A. Nelder, *Generalized Linear Models*, 2nd ed., vol. 37. London, 1989.

[54] Gracien RM, Reitz SC, Hof SM, Fleischer V, Droby A, Wahl M, *et al.*, "Longitudinal quantitative MRI assessment of cortical damage in multiple sclerosis: A pilot study," *Journal of Magnetic Resonance Imaging*, vol. 46, no. 5, Nov. 2017, doi: 10.1002/jmri.25685.

[55] Tillema J, Hulst H, Rocca M, Vrenken H, Steenwijk M, Damjanovic D, *et al.*, "Regional cortical thinning in multiple sclerosis and its relation with cognitive impairment: A multicenter study," *Multiple Sclerosis Journal*, vol. 22, no. 7, Jun. 2016, doi: 10.1177/1352458515607650.

[56] M. Guevara, P. Guevara, C. Román, and J.-F. Mangin, "Superficial white matter: A review on the dMRI analysis methods and applications," *Neuroimage*, vol. 212, p. 116673, May 2020, doi: 10.1016/j.neuroimage.2020.116673.

[57] Phillips OR, Clark KA, Luders E, Azhir R, Joshi SH, Woods RP, *et al.*, "Superficial White Matter: Effects of Age, Sex, and Hemisphere," *Brain Connect*, vol. 3, no. 2, pp. 146–159, Apr. 2013, doi: 10.1089/brain.2012.0111.

[58] Miki Y, Grossman RI, Udupa JK, Wei L, Kolson DL, Mannon LJ, *et al.*, "Isolated U-fiber involvement in MS: Preliminary observations," *Neurology*, vol. 50, no. 5, pp. 1301–1306, May 1998, doi: 10.1212/WNL.50.5.1301.

[59] Veale T, Malone IB, Poole T, Parker TD, Slattery CF, Paterson RW, *et al.*, "Loss and dispersion of superficial white matter in Alzheimer's disease: a diffusion MRI study," *Brain Commun*, vol. 3, no. 4, Oct. 2021, doi: 10.1093/braincomms/fcab272.

[60] Phillips OR, Joshi SH, Squitieri F, Sanchez-Castaneda C, Narr K, Shattuck DW, *et al.*, "Major Superficial White Matter Abnormalities in Huntington's Disease," *Front Neurosci*, vol. 10, May 2016, doi: 10.3389/fnins.2016.00197.

[61] F.-C. Yeh and W.-Y. I. Tseng, "NTU-90: A high angular resolution brain atlas constructed by q-space diffeomorphic reconstruction," *Neuroimage*, vol. 58, no. 1, pp. 91–99, Sep. 2011, doi: 10.1016/j.neuroimage.2011.06.021.

[62] Fang-Cheng Yeh, V. J. Wedeen, and W.-Y. I. Tseng, "Generalized ${ q}$-Sampling Imaging," *IEEE Trans Med Imaging*, vol. 29, no. 9, pp. 1626–1635, Sep. 2010, doi: 10.1109/TMI.2010.2045126.

[63] Zhang H, Wang Y, Lu T, Qiu B, Tang Y, Ou S, *et al.*, "Differences Between Generalized Q-Sampling Imaging and Diffusion Tensor Imaging in the Preoperative Visualization of the Nerve Fiber Tracts Within Peritumoral Edema in Brain," *Neurosurgery*, vol. 73, no. 6, pp. 1044–1053, Dec. 2013, doi: 10.1227/NEU.0000000000000146.

[64] Y. Guo, X. Yang, Z. Yuan, J. Qiu, and W. Lu, "A comparison between diffusion tensor imaging and generalized q-sampling imaging in the age prediction of healthy adults via machine learning approaches," *J Neural Eng*, vol. 19, no. 1, p. 016013, Feb. 2022, doi: 10.1088/1741-2552/ac4bfe.

[65] Beck D, de Lange AMG, Maximov II, Richard G, Andreassen OA, Nordvik JE, *et al.*, "White matter microstructure across the adult lifespan: A mixed longitudinal and cross-sectional study using advanced diffusion models and brain-age prediction," *Neuroimage*, vol. 224, p. 117441, Jan. 2021, doi: 10.1016/j.neuroimage.2020.117441.

[66] E. V. Sullivan, T. Rohlfing, and A. Pfefferbaum, "Longitudinal Study of Callosal Microstructure in the Normal Adult Aging Brain Using Quantitative DTI Fiber Tracking," *Dev Neuropsychol*, vol. 35, no. 3, pp. 233–256, May 2010, doi: 10.1080/87565641003689556.

[67] Li M, Yeh F, Zeng Q, Wu X, Wang X, Zhu Z, *et al.*, "The trajectory of the medial longitudinal fasciculus in the human brain: A diffusion imaging-based tractography study," *Hum Brain Mapp*, vol. 42, no. 18, pp. 6070–6086, Dec. 2021, doi: 10.1002/hbm.25670.

[68] Yeh FC, Panesar S, Fernandes D, Meola A, Yoshino M, Fernandez-Miranda JC, *et al.*, "Population-averaged atlas of the macroscale human structural connectome and its network topology," *Neuroimage*, vol. 178, pp. 57–68, Sep. 2018, doi: 10.1016/j.neuroimage.2018.05.027.

[69] Guevara P, Duclap D, Poupon C, Marrakchi-Kacem L, Fillard P, Le Bihan D, *et al.*, "Automatic fiber bundle segmentation in massive tractography datasets using a multi-subject bundle atlas," *Neuroimage*, vol. 61, no. 4, pp. 1083–1099, Jul. 2012, doi: 10.1016/j.neuroimage.2012.02.071.

[70] Román C, Guevara M, Valenzuela R, Figueroa M, Houenou J, Duclap D, *et al.*, "Clustering of Whole-Brain White Matter Short Association Bundles Using HARDI Data," *Front Neuroinform*, vol. 11, Dec. 2017, doi: 10.3389/fninf.2017.00073.

[71] Z. Wang, A. C. Bovik, H. R. Sheikh, and E. P. Simoncelli, "Image Quality Assessment: From Error Visibility to Structural Similarity," *IEEE Transactions on Image Processing*, vol. 13, no. 4, pp. 600–612, Apr. 2004, doi: 10.1109/TIP.2003.819861.

[72] U. Vovk, F. Pernus, and B. Likar, "A Review of Methods for Correction of Intensity Inhomogeneity in MRI," *IEEE Trans Med Imaging*, vol. 26, no. 3, pp. 405–421, Mar. 2007, doi: 10.1109/TMI.2006.891486.

[73] Slicer Wiki contributors, " Documentation/4.4/Modules/N4ITKBiasFieldCorrection," Slicer Wiki. Accessed: Jul. 26, 2022. [Online]. Available: https://www.slicer.org/w/index.php?title=Documentation/4.4/Modules/N4ITKBiasFieldCorrection&oldid=40124

[74] Athinoula A. Martinos Center for Biomedical Imaging, "Fsgd Format." Accessed: Jun. 24, 2021. [Online]. Available: https://surfer.nmr.mgh.harvard.edu/fswiki/FsgdFormat

[75] A. Klein and J. Tourville, "101 Labeled Brain Images and a Consistent Human Cortical Labeling Protocol," *Front Neurosci*, vol. 6, 2012, doi: 10.3389/fnins.2012.00171.

[76] J. L. Bernal-Rusiel, D. N. Greve, M. Reuter, B. Fischl, and M. R. Sabuncu, "Statistical analysis of longitudinal neuroimage data with Linear Mixed Effects models," *Neuroimage*, vol. 66, Feb. 2013, doi: 10.1016/j.neuroimage.2012.10.065.

[77] J. L. Bernal-Rusiel, M. Reuter, D. N. Greve, B. Fischl, and M. R. Sabuncu, "Spatiotemporal linear mixed effects modeling for the mass-univariate analysis of longitudinal neuroimage data," *Neuroimage*, vol. 81, Nov. 2013, doi: 10.1016/j.neuroimage.2013.05.049.

[78] MATLAB, "Change Folders on the Search Path." Accessed: Aug. 11, 2021. [Online]. Available: https://www.mathworks.com/help/matlab/matlab_env/add-remove-or-reorder-folders-on-the-search-path.html

[79] M. Jenkinson, "Orientation Explained," FSL. Accessed: Aug. 02, 2022. [Online]. Available: https://fsl.fmrib.ox.ac.uk/fsl/fslwiki/Orientation%20Explained

[80] M. Jenkinson, "Fslutils," FSL. Accessed: Aug. 02, 2022. [Online]. Available: https://fsl.fmrib.ox.ac.uk/fsl/fslwiki/Fslutils?highlight=%28fslroi%29

[81] Neuroimaging in Python, "interfaces.freesurfer.preprocess," Nipype: Neuroimaging in Python. Accessed: Aug. 02, 2022. [Online]. Available: https://nipype.readthedocs.io/en/0.12.1/interfaces/generated/nipype.interfaces.freesurfer.preprocess.html

[82] J. Ashburner, "A fast diffeomorphic image registration algorithm," *Neuroimage*, vol. 38, no. 1, pp. 95–113, Oct. 2007, doi: 10.1016/j.neuroimage.2007.07.007.

[83] A. Collignon, F. Maes, D. Delaere, D. Vandermeulen, P. Suetens, and G. Marchal, "Automated multi-modality image registration based on information theory," *Proc. Information Processing in Medical Imaging*, pp. 263–274, 1995.

[84] P. Schmidt, M. Mühlau, C. Gaser, and L. Wink, "LST: A Lesion Segmentation Tool For SPM, manual for version 1.2.3." Mar. 12, 2013. Accessed: Aug. 07, 2022. [Online]. Available: https://www.statistical-modeling.com/LST_manual.pdf

[85] Schmidt P, Gaser C, Arsic M, Buck D, Förschler A, Berthele A, *et al.*, "An automated tool for detection of FLAIR-hyperintense white-matter lesions in Multiple Sclerosis," *Neuroimage*, vol. 59, no. 4, pp. 3774–3783, Feb. 2012, doi: 10.1016/j.neuroimage.2011.11.032.

[86] M. Battaglini, M. Jenkinson, and N. De Stefano, "Evaluating and reducing the impact of white matter lesions on brain volume measurements," *Hum Brain Mapp*, vol. 33, no. 9, pp. 2062–2071, Sep. 2012, doi: 10.1002/hbm.21344.

[87] B. Ammon, "Longitudinal Two Stage Model," FreeSurfer. Accessed: Aug. 07, 2022. [Online]. Available: https://surfer.nmr.mgh.harvard.edu/fswiki/LongitudinalTwoStageModel

[88] M. Reuter, "FreeSurfer Tutorial: Surface Group Analysis with Qdec." Accessed: Sep. 25, 2022. [Online]. Available: https://freesurfer.net/fswiki/FsTutorial/QdecGroupAnalysis_freeview

[89] D. N. Greve and B. Fischl, "False positive rates in surface-based anatomical analysis," *Neuroimage*, vol. 171, pp. 6–14, May 2018, doi: 10.1016/j.neuroimage.2017.12.072.

[90] A. Jahn, "FreeSurfer Tutorial #9: Cluster Correction." Accessed: Oct. 11, 2022. [Online]. Available: https://andysbrainbook.readthedocs.io/en/latest/FreeSurfer/FS_ShortCourse/FS_09_ClusterCorrection.html

[91] C. Zaiontz, "Studentized Range q Table," REAL STATISTICS USING EXCEL. Accessed: May 25, 2023. [Online]. Available: https://real-statistics.com/statistics-tables/studentized-range-q-table/

[92] T. P. Garcia and K. Marder, "Statistical Approaches to Longitudinal Data Analysis in Neurodegenerative Diseases: Huntington's Disease as a Model," *Curr Neurol Neurosci Rep*, vol. 17, no. 2, p. 14, Feb. 2017, doi: 10.1007/s11910-017-0723-4.

[93] Keogh R, Frost C, Owen G, Daniel RM, Langbehn DR, Leavitt B, *et al.*, "Medication Use in Early-HD Participants in Track-HD: an Investigation of its Effects on Clinical Performance," *PLoS Curr*, 2016, doi: 10.1371/currents.hd.8060298fac1801b01ccea6acc00f97cb.

[94] D. A. Maroof, A. L. Gross, and J. Brandt, "Modeling longitudinal change in motor and cognitive processing speed in presymptomatic Huntington's disease," *J Clin Exp Neuropsychol*, vol. 33, no. 8, pp. 901–909, Oct. 2011, doi: 10.1080/13803395.2011.574606.

Anexo A. Stages that constitute the "recon-all" function.

Table A.1 Stages that constitute the "recon-all" function.

Stage Name	Definition
Motion Correction	When there are multiple source volumes, this step will correct small movements between them and then average them together.
NU intensity correction	Non-uniform intensity normalization (N3) non-parametric corrects non-uniformity of intensity in the MR data.
Talairach	This calculates the affine transformation from the original volume to the MNI305 atlas using the mritotal MINC program.
Normalization	Performs intensity normalization on the original volume and places the result in MRI/T1.mgz
Skull Strip	Delete the skull from MRI/T1.mgz.
Automatic Subcortical Segmentation	This is done in six stages. (1) CGA linear log. (2) Canonical Normalization, (3) Canonical Registration. (4) Neck removal, (5) Registration with skull, and (6) Subcortical labeling. The stages are listed below.
MS Registration (GCA)	Computes the transform to align the MRI/nu.mgz volume with the default GCA atlas
AC normalization	Greater standardization, based on the GCA model
AC Register	Computes a nonlinear transform to align with the GCA atlas
Neck removal	The neck region is removed from the volume corrected by NU MRI/nu.mgz
EM registration with the skull	Calculates the transformation to align the MRI / nu_noneck.mgz volume with the GCA volume that the skull has
AC Labels	Label subcortical structures based on the GCA mode.
ASeg Statistics	Calculate statistics on segmented subcortical structures.
Normalization 2	Make a second intensity correction.
WM segmentation	Attempts to separate white matter from everything else
Cut/Fill	This creates the subcortical mass from which the original surface is made.
Tessellation	This is the step where the original surface is created.
Original surface smoothing	After tessellation, the original surface is very irregular because each triangle is on the edge of a voxel face, and thus they are at right angles.
Inflation	Inflation attempts to minimize metric distortion so that distances and areas are preserved
QSphere	This is the initial step of automatic topology repair.
Automatic Topology Fixer	Finds topological defects (i.e., holes in a filled hemisphere)
Final Surface	Create the white and pial surfaces, as well as the thickness file and the curvature file
Cortical Ribbon Mask	Create binary volume masks of the cortical ribbon, i.e., each voxel is either a one or a 0
Spherical Inflation	Inflates the original surface into a sphere while minimizing metric distortion
Ipsilateral Surface Registration (Spherical Morph)	Records the original surface of the spherical atlas
Contralateral Surface Registration (Spherical	Same as ipsilateral, but recorded on the contralateral atlas

Morph)	
Average Curvature	Resample the mean curvature of the atlas to that of the subject.
Cortical Parcellation	Assign a neuroanatomical label to each location on the cortical surface. It incorporates both the geometric information derived from the cortical model and the neuroanatomical convention
Parcellation Statistics	Run mris_anatomical_stats to create a summary table of cortical parcellation statistics for each structure.

Anexo B. Variables resulting from the *lme_mass_fit_Rgw* function.

Table B.1 Variables resulting from the *lme_mass_fit_Rgw* function.

Variables Name	Definition
Stats. Bhat	Estimated vector of the population regression parameters
Stats.CovBhat	Estimated covariance matrix of the population regression parameters
Stats. phisqhat	Estimated intra-individual variability.
Stats.Dhat	Estimated random effects covariance matrix
Stats.invEI	Inverse of the expected information matrix of the constrained log-likelihood
Stats.Pth, Stats.Qthth	Matrices that are useful for inferences on fixed effects.
Stats.lreml	Values of the constrained maximum registration probability in the process of optimization.

Anexo C. Numerical variations from the GLM and LME analysis over DB1.

Table C Most affected regions by the cortical volume and thickness change due to the EDSS and SDMT parameters. All the areas shown are considered significant due to the threshold of a p-value less than 0.05. The surface size of the affected area is in mm^2. The numbers in blue indicate a negative correlation between the parameters, and the red ones show a positive correlation.

			Thickness				Volume			
			Model				Model			
			GLM		LME		GLM		LME	
Lobes	ROIs		Left	Right	Left	Right	Left	Right	Left	Right
Frontal	Superior Frontal	EDSS	1322.8	2903.9	368.1	-	2305.6	2150.4	-	95.4
		SDMT	6.6	13.7	413.2	28.3	23.9	107.3	1313.3	395.5
	Rostral Middle Frontal	EDSS	166.2	2541.2	31.5	36.3	3304.2	2422.0	17941.2	-
		SDMT	65.3	19.3	25.7	344.6	27.0	-	165.2	2431.8
	Caudal Middle Frontal	EDSS	1711.3	-	-	-	373.0	27.2	-	-
		SDMT	-	-	-	-	-	-	-	518.4
	Pars Opercularis	EDSS	-	155.4	-	-	-	101.2	-	10.9
		SDMT	-	-	-	49.8	-	-	128.5	27.8
	Pars Triangularis	EDSS	1616.6	-	-	-	155.0	-	-	-
		SDMT	-	-	-	242.9	-	-	8.0	296.9
	Pars Orbitalis	EDSS	-	-	-	-	-	-	-	-
		SDMT	-	-	-	-	-	-	104.7	-
	Lateral Orbitofrontal	EDSS	137.2	423.1	251.0	99.3	14.7	566.5	210.7	132.1
		SDMT	10.0	86.9	-	-	68.6	180.0	-	-
	Medial Orbitofrontal	EDSS	-	-	105.2	34.3	-	10.9	29.0	-
		SDMT	-	-	411.9	56.1	-	326.0	385.8	107.6
	Precentral	EDSS	114.3	98.5	-	249.3	65.5	251.0	83.9	1507.8
		SDMT	2253.2	2573.5	777.6	261.5	1267.9	250.8	1442.9	974.8
	Paracentral	EDSS	-	55.2	-	-	60.5	55.2	10.8	88.8
		SDMT	-	7.7	665.8	154.4	-	-	931.4	1207.0
	Frontal Pole	EDSS	145.3	-	90.1	-	-	-	-	-
		SDMT	-	92.3	-	-	-	-	-	-
	Rostal Anterior Cingulate	EDSS	-	-	29.0	-	-	-	-	-
		SDMT	-	-	26.5	-	-	-	-	-
	Caudal Anterior Cingulate	EDSS	-	-	769.8	276.6	-	-	21.3	-
		SDMT	-	-	140.8	267.0	-	-	-	168.4

Table C (continued)

			Thickness				Volume			
			Model				Model			
			GLM		LME		GLM		LME	
Lobes	ROIs		Left	Right	Left	Right	Left	Right	Left	Right
Parietal	Precuneus	EDSS	5891.8	213.0	70.9	-	4869.5	41.7	-	103.1
		SDMT	-	-	113.6	23.0	15.7	-	22.5	34.3
	Superior Parietal	EDSS	-	3156.0	53706.8	-	833.4	3641.8	-	62.3
		SDMT	-	4.3	22.7	429.0	38.1	-	-	1401.4
	Supramarginal	EDSS	36.1	471.2	-	375.0	164.6	434.4	26247.9	44624.3
		SDMT	162.6	30.9	4170.5	11096.5	183.3	23.5	3615.6	-
	Inferior Parietal	EDSS	49.9	196.6	-	-	-	298.4	8.3	9.6
		SDMT	110.6	269.4	470.2	58.3	-	274.2	748.1	12954.9
	Postcentral	EDSS	130.6	11.0	9.7	-	335.0	46.1	55.1	-
		SDMT	-	99.5	81.7	796.9	50.2	1559.5	249.0	1599.7
	Posterior Cingulate	EDSS	6.9	-	411.2	556.6	33.8	-	549.0	49.3
		SDMT	-	-	18.1	97.7	-	-	153.1	206.2
	Isthmus Cingulate	EDSS	-	-	-	213.4	-	-	8.4	111.9
		SDMT	-	-	12.1	135.6	-	-	73.0	121.2
Temporal	Superior Temporal	EDSS	927.5	5.0	-	9.8	1091.0	46.3	536.7	3622.2
		SDMT	1033.5	124.5	55.0	27.5	369.3	-	503.9	-
	Middle Temporal	EDSS	11.9	932.8	155.2	36.2	-	664.5	-	122.0
		SDMT	-	129.3	1238.4	542.3	142.7	66.9	446.1	108.8
	Inferior Temporal	EDSS	-	-	-	56155.3	157.0	-	32.4	-
		SDMT	51.7	-	9.7	-	18.7	15.8	134.9	-
	Banks of the Superior Temporal Sulcus3	EDSS	-	-	-	-	-	-	-	-
		SDMT	-	-	11.7	8.9	-	-	-	13.6
	Fusiform	EDSS	1222.9	53.2	-	-	1104.3	74.2	-	167.1
		SDMT	58.5	23.4	680.6	393.4		18.7	721.2	93.6

Table C (continued)

			Thickness				Volume			
			Model				Model			
			GLM		LME		GLM		LME	
Lobes	ROIs		Left	Right	Left	Right	Left	Right	Left	Right
Temporal	Transverse Temporal	EDSS	-	-	-	-	-	-	-	-
		SDMT	-	-	-	-	-	-	7.3	-
	Entorhinal	EDSS	-	-	19.3	-	-	-	32.9	125.2
		SDMT	5.6	-	-	-	86.1	-	56.7	198.3
	Temporal Pole	EDSS	22.7	-	-	-	-	-	-	-
		SDMT	-	-	-	-	-	-	-	-
	Para hippocampal	EDSS	-	-	102.8	16.8	-	-	40.2	75.2
		SDMT	6.6	-	-	234.1	-	-	-	199.2
Occipital	Lingual	EDSS	1214.0	308.2	150.6	-	-	585.1	413.1	263.4
		SDMT	-	6.2	134.2	90.9	-	13.8	550.0	915.8
	Lateral Occipital	EDSS	26.8	154.6	21.3	-	747.7	252.5	9.4	-
		SDMT	187.7	144.4	69.3	310.3	19.8	63.0	345.6	715.1
	Cuneus	EDSS	42.6	385.9	-	-	-	422.7	-	-
		SDMT	-	-	39.5	-	-	-	55.3	-
	Pericalcarine	EDSS	37.1	12.3	124.4	-	828.9	98.8	450.6	-
		SDMT	-	-	-	-	-	-	-	35.4
Insula		EDSS	233.8	-	76.6	9.9	20.9	41.2	39.7	97.8
		SDMT	21.2	67.0	-	387.3	-	101.4	161.6	179.1

Anexo D. Parameter Estimates tables for all the fiber bundles that the EDSS parameter's impact was considered significant in the general analysis.

Table D Parameter Estimates tables for all the fiber bundles that the EDSS parameter's impact was considered significant in the general analysis. The B column shows the rate of change between the fiber bundle and the time and the EDSS parameter. In the case of the EDSS, it shows the rate for all the possible values of EDSS. The Sig. column shows the level of significance for every correlation.

Parameter Estimates

Parameter	B	Std. Error	Interval Lower	Interval Upper	Hypothesis Test Wald Chi-Square	df	Sig.
(Intercept)	1.322	0.0248	1.273	1.370	2850.188	1	0.000
[Time=1]	0.056	0.0248	0.007	0.104	5.046	1	0.025
[Time=2]	0[a]						
[EDSS=.00]	-0.082	0.0275	-0.136	-0.028	8.926	1	0.003
[EDSS=1.00]	-0.097	0.0214	-0.140	-0.055	20.691	1	0.000
[EDSS=1.50]	-0.069	0.0350	-0.138	0.000	3.884	1	0.049
[EDSS=2.00]	-0.153	0.0238	-0.200	-0.106	41.340	1	0.000
[EDSS=2.50]	-0.060	0.0248	-0.109	-0.012	5.936	1	0.015
[EDSS=3.00]	-0.118	0.0248	-0.167	-0.070	22.776	1	0.000
[EDSS=3.50]	-0.203	0.0248	-0.252	-0.155	67.422	1	0.000
[EDSS=4.00]	-0.070	0.0248	-0.119	-0.022	8.065	1	0.005
[EDSS=5.00]	-0.010	0.0325	-0.074	0.054	0.094	1	0.760
[EDSS=6.00]	0.056	0.0535	-0.049	0.161	1.094	1	0.295
[EDSS=6.50]	-0.091	0.0248	-0.139	-0.042	13.432	1	0.000
[EDSS=7.50]	-0.046	0.0248	-0.094	0.003	3.416	1	0.065
[EDSS=8.00]	0[a]						
(Scale)	0.008						

Dependent Variable: lh_PrC-SF_0_AD
Model: (Intercept), Time, EDSS

a. Set to zero because this parameter is redundant.

Parameter Estimates

Parameter	B	Std. Error	Interval Lower	Interval Upper	Hypothesis Test Wald Chi-Square	df	Sig.
(Intercept)	1.184	0.0184	1.147	1.220	4124.824	1	0.000
[Time=1]	0.067	0.0184	0.031	0.103	13.217	1	0.000
[Time=2]	0[a]						
[EDSS=.00]	-0.055	0.0157	-0.085	-0.024	12.028	1	0.001
[EDSS=1.00]	-0.034	0.0222	-0.077	0.009	2.346	1	0.126
[EDSS=1.50]	-0.017	0.0214	-0.059	0.025	0.632	1	0.427
[EDSS=2.00]	0.001	0.0182	-0.035	0.036	0.002	1	0.969
[EDSS=2.50]	0.124	0.0184	0.088	0.160	45.024	1	0.000
[EDSS=3.00]	0.079	0.0184	0.043	0.115	18.218	1	0.000
[EDSS=3.50]	0.015	0.0184	-0.022	0.051	0.627	1	0.428
[EDSS=4.00]	0.002	0.0184	-0.034	0.038	0.011	1	0.916
[EDSS=5.00]	-0.014	0.0274	-0.068	0.040	0.263	1	0.608
[EDSS=6.00]	0.061	0.0531	-0.043	0.165	1.326	1	0.250
[EDSS=6.50]	0.033	0.0184	-0.004	0.069	3.112	1	0.078
[EDSS=7.50]	-0.029	0.0184	-0.065	0.007	2.429	1	0.119
[EDSS=8.00]	0[a]						
(Scale)	0.004						

Dependent Variable: rh_PoCi-SF_0_AD
Model: (Intercept), Time, EDSS

a. Set to zero because this parameter is redundant.

Table D (continued)

Parameter Estimates

Parameter	B	Std. Error	Interval		Hypothesis Test		
			Lower	Upper	Wald Chi-Square	df	Sig.
(Intercept)	0.080	0.0033	0.074	0.087	597.975	1	0.000
[Time=1]	-0.007	0.0033	-0.014	-0.001	5.186	1	0.023
[Time=2]	0[a]						
[EDSS=.00]	-0.014	0.0047	-0.023	-0.004	8.510	1	0.004
[EDSS=1.00]	-0.016	0.0044	-0.025	-0.008	13.594	1	0.000
[EDSS=1.50]	-0.013	0.0030	-0.019	-0.008	20.284	1	0.000
[EDSS=2.00]	-0.013	0.0070	-0.027	0.001	3.328	1	0.068
[EDSS=2.50]	-0.027	0.0033	-0.033	-0.020	65.716	1	0.000
[EDSS=3.00]	-0.033	0.0033	-0.039	-0.026	100.273	1	0.000
[EDSS=3.50]	-0.011	0.0033	-0.017	-0.004	10.276	1	0.001
[EDSS=4.00]	0.000	0.0033	-0.006	0.007	0.015	1	0.901
[EDSS=5.00]	-0.004	0.0019	-0.008	0.000	4.574	1	0.032
[EDSS=6.00]	-0.014	0.0024	-0.018	-0.009	31.896	1	0.000
[EDSS=6.50]	-0.008	0.0033	-0.014	-0.001	5.760	1	0.016
[EDSS=7.50]	0.002	0.0033	-0.004	0.009	0.411	1	0.522
[EDSS=8.00]	0[a]						
(Scale)	0.000						

Dependent Variable: lh_CMF-PrC_1_QA
Model: (Intercept), Time, EDSS

a. Set to zero because this parameter is redundant.

Parameter Estimates

Parameter	B	Std. Error	Interval		Hypothesis Test		
			Lower	Upper	Wald Chi-Square	df	Sig.
(Intercept)	0.080	0.0035	0.073	0.087	524.214	1	0.000
[Time=1]	-0.008	0.0035	-0.014	-0.001	4.761	1	0.029
[Time=2]	0[a]						
[EDSS=.00]	-0.016	0.0047	-0.025	-0.006	11.049	1	0.001
[EDSS=1.00]	-0.017	0.0047	-0.026	-0.008	13.118	1	0.000
[EDSS=1.50]	-0.014	0.0035	-0.021	-0.008	17.098	1	0.000
[EDSS=2.00]	-0.013	0.0073	-0.027	0.001	3.092	1	0.079
[EDSS=2.50]	-0.021	0.0035	-0.028	-0.014	37.320	1	0.000
[EDSS=3.00]	-0.036	0.0035	-0.043	-0.029	107.767	1	0.000
[EDSS=3.50]	-0.010	0.0035	-0.016	-0.003	7.577	1	0.006
[EDSS=4.00]	0.005	0.0035	-0.002	0.011	1.751	1	0.186
[EDSS=5.00]	-0.014	0.0027	-0.019	-0.009	26.745	1	0.000
[EDSS=6.00]	-0.010	0.0023	-0.015	-0.006	19.834	1	0.000
[EDSS=6.50]	-0.007	0.0035	-0.014	0.000	3.651	1	0.056
[EDSS=7.50]	0.004	0.0035	-0.003	0.011	1.213	1	0.271
[EDSS=8.00]	0[a]						
(Scale)	0.000						

Dependent Variable: lh_CMF-RMF_0_QA
Model: (Intercept), Time, EDSS

a. Set to zero because this parameter is redundant.

Table D (continued)

Parameter Estimates

Parameter	B	Std. Error	Interval Lower	Interval Upper	Hypothesis Test Wald Chi-Square	Hypothesis Test df	Hypothesis Test Sig.
(Intercept)	0.082	0.0041	0.074	0.090	395.873	1	0.000
[Time=1]	-0.010	0.0041	-0.018	-0.002	5.437	1	0.020
[Time=2]	0[a]						
[EDSS=.00]	-0.012	0.0064	-0.024	0.001	3.388	1	0.066
[EDSS=1.00]	-0.016	0.0049	-0.026	-0.007	11.146	1	0.001
[EDSS=1.50]	-0.012	0.0036	-0.019	-0.005	11.523	1	0.001
[EDSS=2.00]	-0.014	0.0044	-0.022	-0.005	9.793	1	0.002
[EDSS=2.50]	-0.024	0.0041	-0.032	-0.016	34.418	1	0.000
[EDSS=3.00]	-0.040	0.0041	-0.048	-0.032	94.422	1	0.000
[EDSS=3.50]	-0.008	0.0041	-0.016	-8.663E-05	3.924	1	0.048
[EDSS=4.00]	0.003	0.0041	-0.005	0.011	0.604	1	0.437
[EDSS=5.00]	-0.001	0.0021	-0.005	0.003	0.306	1	0.580
[EDSS=6.00]	-0.009	0.0027	-0.014	-0.003	9.972	1	0.002
[EDSS=6.50]	-0.005	0.0041	-0.013	0.003	1.262	1	0.261
[EDSS=7.50]	0.002	0.0041	-0.006	0.010	0.276	1	0.599
[EDSS=8.00]	0[a]						
(Scale)	0.000						

Dependent Variable: lh_CMF-SF_0_QA
Model: (Intercept), Time, EDSS

a. Set to zero because this parameter is redundant.

Parameter Estimates

Parameter	B	Std. Error	Interval Lower	Interval Upper	Hypothesis Test Wald Chi-Square	Hypothesis Test df	Hypothesis Test Sig.
(Intercept)	0.100	0.0047	0.091	0.109	457.996	1	0.000
[Time=1]	-0.012	0.0047	-0.021	-0.002	6.229	1	0.013
[Time=2]	0[a]						
[EDSS=.00]	-0.019	0.0054	-0.030	-0.009	12.724	1	0.000
[EDSS=1.00]	-0.015	0.0070	-0.029	-0.002	4.849	1	0.028
[EDSS=1.50]	-0.017	0.0047	-0.026	-0.008	13.483	1	0.000
[EDSS=2.00]	-0.022	0.0097	-0.041	-0.003	5.139	1	0.023
[EDSS=2.50]	-0.028	0.0047	-0.037	-0.018	35.019	1	0.000
[EDSS=3.00]	-0.039	0.0047	-0.048	-0.030	70.592	1	0.000
[EDSS=3.50]	-0.025	0.0047	-0.034	-0.016	29.159	1	0.000
[EDSS=4.00]	0.003	0.0047	-0.006	0.012	0.446	1	0.504
[EDSS=5.00]	-0.003	0.0056	-0.014	0.008	0.217	1	0.642
[EDSS=6.00]	-0.008	0.0041	-0.016	0.000	4.230	1	0.040
[EDSS=6.50]	-0.018	0.0047	-0.027	-0.009	15.040	1	0.000
[EDSS=7.50]	-0.005	0.0047	-0.014	0.004	1.279	1	0.258
[EDSS=8.00]	0[a]						
(Scale)	0.000						

Dependent Variable: lh_IP-SP_1_QA
Model: (Intercept), Time, EDSS

a. Set to zero because this parameter is redundant.

Table D (continued)

Parameter Estimates

Parameter	B	Std. Error	Interval		Hypothesis Test		
			Lower	Upper	Wald Chi-Square	df	Sig.
(Intercept)	0.083	0.0036	0.076	0.090	532.556	1	0.000
[Time=1]	-0.010	0.0036	-0.017	-0.002	6.949	1	0.008
[Time=2]	0[a]						
[EDSS=.00]	-0.014	0.0049	-0.023	-0.004	8.041	1	0.005
[EDSS=1.00]	-0.015	0.0049	-0.025	-0.006	9.860	1	0.002
[EDSS=1.50]	-0.014	0.0034	-0.021	-0.007	17.300	1	0.000
[EDSS=2.00]	-0.017	0.0074	-0.032	-0.003	5.498	1	0.019
[EDSS=2.50]	-0.025	0.0036	-0.032	-0.018	48.438	1	0.000
[EDSS=3.00]	-0.036	0.0036	-0.043	-0.029	99.346	1	0.000
[EDSS=3.50]	-0.009	0.0036	-0.016	-0.002	5.919	1	0.015
[EDSS=4.00]	0.001	0.0036	-0.006	0.008	0.037	1	0.847
[EDSS=5.00]	-0.004	0.0024	-0.009	0.001	2.550	1	0.110
[EDSS=6.00]	-0.010	0.0038	-0.018	-0.003	7.699	1	0.006
[EDSS=6.50]	-0.012	0.0036	-0.019	-0.005	11.097	1	0.001
[EDSS=7.50]	0.004	0.0036	-0.003	0.011	1.177	1	0.278
[EDSS=8.00]	0[a]						
(Scale)	0.000						

Dependent Variable: lh_Op-SF_0_QA
Model: (Intercept), Time, EDSS

a. Set to zero because this parameter is redundant.

Parameter Estimates

Parameter	B	Std. Error	Interval		Hypothesis Test		
			Lower	Upper	Wald Chi-Square	df	Sig.
(Intercept)	0.078	0.0043	0.069	0.086	321.718	1	0.000
[Time=1]	-0.012	0.0043	-0.020	-0.003	7.152	1	0.007
[Time=2]	0[a]						
[EDSS=.00]	-0.008	0.0060	-0.020	0.004	1.756	1	0.185
[EDSS=1.00]	-0.007	0.0057	-0.018	0.004	1.700	1	0.192
[EDSS=1.50]	-0.010	0.0033	-0.017	-0.004	9.158	1	0.002
[EDSS=2.00]	0.000	0.0099	-0.019	0.020	0.002	1	0.962
[EDSS=2.50]	-0.016	0.0043	-0.025	-0.008	13.802	1	0.000
[EDSS=3.00]	-0.023	0.0043	-0.031	-0.014	28.171	1	0.000
[EDSS=3.50]	-0.015	0.0043	-0.023	-0.006	11.331	1	0.001
[EDSS=4.00]	0.001	0.0043	-0.007	0.010	0.065	1	0.799
[EDSS=5.00]	0.009	0.0040	0.001	0.017	4.963	1	0.026
[EDSS=6.00]	0.001	0.0028	-0.005	0.006	0.032	1	0.857
[EDSS=6.50]	0.002	0.0043	-0.006	0.011	0.260	1	0.610
[EDSS=7.50]	0.015	0.0043	0.006	0.023	11.298	1	0.001
[EDSS=8.00]	0[a]						
(Scale)	0.000						

Dependent Variable: lh_PrC-SF_0_QA
Model: (Intercept), Time, EDSS

a. Set to zero because this parameter is redundant.

Table D (continued)

Parameter Estimates

Parameter	B	Std. Error	Interval		Hypothesis Test		
			Lower	Upper	Wald Chi-Square	df	Sig.
(Intercept)	0.079	0.0035	0.072	0.086	514.379	1	0.000
[Time=1]	-0.009	0.0035	-0.016	-0.002	6.365	1	0.012
[Time=2]	0[a]						
[EDSS=.00]	-0.014	0.0047	-0.023	-0.004	8.423	1	0.004
[EDSS=1.00]	-0.014	0.0051	-0.024	-0.004	7.306	1	0.007
[EDSS=1.50]	-0.013	0.0033	-0.020	-0.007	16.172	1	0.000
[EDSS=2.00]	-0.013	0.0084	-0.029	0.004	2.298	1	0.130
[EDSS=2.50]	-0.027	0.0035	-0.034	-0.020	61.328	1	0.000
[EDSS=3.00]	-0.034	0.0035	-0.041	-0.027	94.739	1	0.000
[EDSS=3.50]	-0.018	0.0035	-0.025	-0.012	27.925	1	0.000
[EDSS=4.00]	0.000	0.0035	-0.007	0.007	0.001	1	0.975
[EDSS=5.00]	-0.014	0.0018	-0.017	-0.010	60.478	1	0.000
[EDSS=6.00]	-0.007	0.0034	-0.014	0.000	4.182	1	0.041
[EDSS=6.50]	-0.012	0.0035	-0.018	-0.005	11.312	1	0.001
[EDSS=7.50]	0.005	0.0035	-0.002	0.012	2.134	1	0.144
[EDSS=8.00]	0[a]						
(Scale)	0.000						

Dependent Variable: lh_RMF-SF_1_QA
Model: (Intercept), Time, EDSS

a. Set to zero because this parameter is redundant.

Parameter Estimates

Parameter	B	Std. Error	Interval		Hypothesis Test		
			Lower	Upper	Wald Chi-Square	df	Sig.
(Intercept)	0.075	0.0027	0.070	0.081	761.963	1	0.000
[Time=1]	-0.009	0.0027	-0.014	-0.004	11.155	1	0.001
[Time=2]	0[a]						
[EDSS=.00]	-0.015	0.0035	-0.022	-0.008	18.396	1	0.000
[EDSS=1.00]	-0.015	0.0042	-0.023	-0.006	12.096	1	0.001
[EDSS=1.50]	-0.014	0.0027	-0.019	-0.008	25.078	1	0.000
[EDSS=2.00]	-0.016	0.0062	-0.028	-0.004	6.881	1	0.009
[EDSS=2.50]	-0.025	0.0027	-0.030	-0.020	83.213	1	0.000
[EDSS=3.00]	-0.033	0.0027	-0.038	-0.028	146.893	1	0.000
[EDSS=3.50]	-0.025	0.0027	-0.030	-0.019	80.648	1	0.000
[EDSS=4.00]	-0.005	0.0027	-0.010	0.001	2.774	1	0.096
[EDSS=5.00]	-0.012	0.0031	-0.018	-0.005	13.580	1	0.000
[EDSS=6.00]	-0.009	0.0022	-0.014	-0.005	17.298	1	0.000
[EDSS=6.50]	-0.008	0.0027	-0.014	-0.003	9.352	1	0.002
[EDSS=7.50]	0.005	0.0027	0.000	0.010	3.542	1	0.060
[EDSS=8.00]	0[a]						
(Scale)	9.740E-05						

Dependent Variable: lh_RoMF_RoMF_0i_QA
Model: (Intercept), Time, EDSS

a. Set to zero because this parameter is redundant.

Table D (continued)

Parameter Estimates

Parameter	B	Std. Error	Interval		Hypothesis Test		
			Lower	Upper	Wald Chi-Square	df	Sig.
(Intercept)	0.073	0.0032	0.066	0.079	519.199	1	0.000
[Time=1]	-0.007	0.0032	-0.013	-0.001	5.205	1	0.023
[Time=2]	0[a]						
[EDSS=.00]	-0.014	0.0039	-0.021	-0.006	12.555	1	0.000
[EDSS=1.00]	-0.015	0.0044	-0.024	-0.007	12.329	1	0.000
[EDSS=1.50]	-0.011	0.0030	-0.017	-0.005	13.447	1	0.000
[EDSS=2.00]	-0.015	0.0068	-0.028	-0.002	4.962	1	0.026
[EDSS=2.50]	-0.015	0.0032	-0.022	-0.009	23.587	1	0.000
[EDSS=3.00]	-0.029	0.0032	-0.035	-0.022	80.428	1	0.000
[EDSS=3.50]	-0.016	0.0032	-0.023	-0.010	26.848	1	0.000
[EDSS=4.00]	-0.006	0.0032	-0.012	0.000	3.376	1	0.066
[EDSS=5.00]	-0.010	0.0044	-0.018	-0.001	4.815	1	0.028
[EDSS=6.00]	-0.010	0.0021	-0.015	-0.006	24.282	1	0.000
[EDSS=6.50]	-0.003	0.0032	-0.009	0.004	0.624	1	0.430
[EDSS=7.50]	0.002	0.0032	-0.004	0.008	0.313	1	0.576
[EDSS=8.00]	0[a]						
(Scale)	0.000						

Dependent Variable: lh_RoMF_RoMF_1i_QA
Model: (Intercept), Time, EDSS

a. Set to zero because this parameter is redundant.

Parameter Estimates

Parameter	B	Std. Error	Interval		Hypothesis Test		
			Lower	Upper	Wald Chi-Square	df	Sig.
(Intercept)	0.088	0.0039	0.080	0.095	509.920	1	0.000
[Time=1]	-0.009	0.0039	-0.017	-0.002	5.979	1	0.014
[Time=2]	0[a]						
[EDSS=.00]	-0.015	0.0049	-0.025	-0.006	9.830	1	0.002
[EDSS=1.00]	-0.015	0.0054	-0.026	-0.005	7.929	1	0.005
[EDSS=1.50]	-0.016	0.0032	-0.022	-0.010	24.120	1	0.000
[EDSS=2.00]	-0.017	0.0083	-0.034	-0.001	4.227	1	0.040
[EDSS=2.50]	-0.020	0.0039	-0.027	-0.012	25.572	1	0.000
[EDSS=3.00]	-0.037	0.0039	-0.044	-0.029	88.842	1	0.000
[EDSS=3.50]	-0.022	0.0039	-0.030	-0.014	31.984	1	0.000
[EDSS=4.00]	0.003	0.0039	-0.005	0.010	0.415	1	0.519
[EDSS=5.00]	-0.001	0.0043	-0.010	0.007	0.079	1	0.779
[EDSS=6.00]	-0.010	0.0056	-0.021	0.001	3.022	1	0.082
[EDSS=6.50]	-0.012	0.0039	-0.020	-0.005	10.215	1	0.001
[EDSS=7.50]	-0.011	0.0039	-0.019	-0.003	7.868	1	0.005
[EDSS=8.00]	0[a]						
(Scale)	0.000						

Dependent Variable: lh_SP-SM_0_QA
Model: (Intercept), Time, EDSS

a. Set to zero because this parameter is redundant.

Table D (continued)

Parameter Estimates

Parameter	B	Std. Error	Interval Lower	Interval Upper	Hypothesis Test Wald Chi-Square	df	Sig.
(Intercept)	0.072	0.0029	0.066	0.078	616.768	1	0.000
[Time=1]	-0.008	0.0029	-0.013	-0.002	7.135	1	0.008
[Time=2]	0[a]						
[EDSS=.00]	-0.014	0.0037	-0.021	-0.006	13.195	1	0.000
[EDSS=1.00]	-0.016	0.0042	-0.024	-0.008	13.963	1	0.000
[EDSS=1.50]	-0.011	0.0029	-0.017	-0.005	13.954	1	0.000
[EDSS=2.00]	-0.017	0.0067	-0.030	-0.003	6.104	1	0.013
[EDSS=2.50]	-0.021	0.0029	-0.027	-0.015	52.285	1	0.000
[EDSS=3.00]	-0.033	0.0029	-0.038	-0.027	126.284	1	0.000
[EDSS=3.50]	-0.019	0.0029	-0.024	-0.013	40.634	1	0.000
[EDSS=4.00]	-0.006	0.0029	-0.012	-0.001	4.964	1	0.026
[EDSS=5.00]	-0.017	0.0018	-0.021	-0.014	88.458	1	0.000
[EDSS=6.00]	-0.009	0.0016	-0.013	-0.006	32.438	1	0.000
[EDSS=6.50]	-0.004	0.0029	-0.010	0.001	2.122	1	0.145
[EDSS=7.50]	0.004	0.0029	-0.001	0.010	2.161	1	0.142
[EDSS=8.00]	0[a]						
(Scale)	0.000						

Dependent Variable: lh_Tr_RoMF_0i_QA
Model: (Intercept), Time, EDSS

a. Set to zero because this parameter is redundant.

Parameter Estimates

Parameter	B	Std. Error	Interval Lower	Interval Upper	Hypothesis Test Wald Chi-Square	df	Sig.
(Intercept)	0.076	0.0035	0.069	0.083	478.312	1	0.000
[Time=1]	-0.013	0.0035	-0.020	-0.006	14.015	1	0.000
[Time=2]	0[a]						
[EDSS=.00]	-0.012	0.0040	-0.019	-0.004	8.473	1	0.004
[EDSS=1.00]	-0.012	0.0051	-0.022	-0.002	5.841	1	0.016
[EDSS=1.50]	-0.012	0.0027	-0.017	-0.007	19.083	1	0.000
[EDSS=2.00]	-0.013	0.0037	-0.020	-0.006	12.153	1	0.000
[EDSS=2.50]	-0.026	0.0035	-0.032	-0.019	54.881	1	0.000
[EDSS=3.00]	-0.033	0.0035	-0.040	-0.026	89.811	1	0.000
[EDSS=3.50]	-0.017	0.0035	-0.024	-0.010	23.872	1	0.000
[EDSS=4.00]	-0.007	0.0035	-0.014	-0.001	4.536	1	0.033
[EDSS=5.00]	-0.001	0.0017	-0.004	0.003	0.092	1	0.762
[EDSS=6.00]	-0.005	0.0055	-0.015	0.006	0.714	1	0.398
[EDSS=6.50]	-0.011	0.0035	-0.018	-0.004	10.451	1	0.001
[EDSS=7.50]	-0.002	0.0035	-0.009	0.005	0.402	1	0.526
[EDSS=8.00]	0[a]						
(Scale)	0.000						

Dependent Variable: rh_CAC-PrCu_0_QA
Model: (Intercept), Time, EDSS

a. Set to zero because this parameter is redundant.

Table D (continued)

Parameter Estimates

Parameter	B	Std. Error	Interval Lower	Interval Upper	Hypothesis Test Wald Chi-Square	df	Sig.
(Intercept)	0.063	0.0026	0.058	0.068	569.152	1	0.000
[Time=1]	-0.007	0.0026	-0.013	-0.002	7.747	1	0.005
[Time=2]	0[a]						
[EDSS=.00]	-0.011	0.0029	-0.017	-0.006	15.291	1	0.000
[EDSS=1.00]	-0.009	0.0044	-0.017	9.336E-05	3.759	1	0.053
[EDSS=1.50]	-0.011	0.0023	-0.015	-0.006	22.313	1	0.000
[EDSS=2.00]	-0.011	0.0043	-0.020	-0.003	6.884	1	0.009
[EDSS=2.50]	-0.014	0.0026	-0.020	-0.009	29.731	1	0.000
[EDSS=3.00]	-0.027	0.0026	-0.033	-0.022	106.712	1	0.000
[EDSS=3.50]	-0.011	0.0026	-0.016	-0.006	17.167	1	0.000
[EDSS=4.00]	0.012	0.0026	0.007	0.017	21.099	1	0.000
[EDSS=5.00]	0.004	0.0019	5.012E-05	0.008	3.944	1	0.047
[EDSS=6.00]	-0.007	0.0036	-0.014	0.001	3.267	1	0.071
[EDSS=6.50]	-0.012	0.0026	-0.017	-0.007	20.006	1	0.000
[EDSS=7.50]	0.005	0.0026	0.000	0.011	4.305	1	0.038
[EDSS=8.00]	0[a]						
(Scale)	8.446E-05						

Dependent Variable: rh_IC-PrCu_0_QA
Model: (Intercept), Time, EDSS

a. Set to zero because this parameter is redundant.

Parameter Estimates

Parameter	B	Std. Error	Interval Lower	Interval Upper	Hypothesis Test Wald Chi-Square	df	Sig.
(Intercept)	0.073	0.0035	0.066	0.080	424.370	1	0.000
[Time=1]	-0.008	0.0035	-0.015	-0.001	5.378	1	0.020
[Time=2]	0[a]						
[EDSS=.00]	-0.007	0.0047	-0.016	0.003	1.997	1	0.158
[EDSS=1.00]	-0.007	0.0053	-0.018	0.003	1.961	1	0.161
[EDSS=1.50]	-0.007	0.0033	-0.014	-0.001	4.648	1	0.031
[EDSS=2.00]	-0.004	0.0062	-0.016	0.008	0.468	1	0.494
[EDSS=2.50]	-0.017	0.0035	-0.024	-0.010	23.816	1	0.000
[EDSS=3.00]	-0.029	0.0035	-0.036	-0.022	69.030	1	0.000
[EDSS=3.50]	-0.008	0.0035	-0.015	-0.001	5.330	1	0.021
[EDSS=4.00]	0.011	0.0035	0.005	0.018	10.529	1	0.001
[EDSS=5.00]	0.004	0.0027	-0.001	0.010	2.431	1	0.119
[EDSS=6.00]	-0.001	0.0040	-0.009	0.007	0.082	1	0.775
[EDSS=6.50]	-0.001	0.0035	-0.008	0.006	0.138	1	0.710
[EDSS=7.50]	-0.001	0.0035	-0.008	0.006	0.138	1	0.710
[EDSS=8.00]	0[a]						
(Scale)	0.000						

Dependent Variable: rh_Op-SF_0_QA
Model: (Intercept), Time, EDSS

a. Set to zero because this parameter is redundant.

Table D (continued)

Parameter Estimates

Parameter	B	Std. Error	Interval		Hypothesis Test		
			Lower	Upper	Wald Chi-Square	df	Sig.
(Intercept)	0.070	0.0032	0.064	0.077	481.752	1	0.000
[Time=1]	-0.010	0.0032	-0.016	-0.003	8.883	1	0.003
[Time=2]	0[a]						
[EDSS=.00]	-0.014	0.0032	-0.020	-0.007	18.605	1	0.000
[EDSS=1.00]	-0.011	0.0051	-0.021	-0.001	5.067	1	0.024
[EDSS=1.50]	-0.013	0.0025	-0.018	-0.008	26.830	1	0.000
[EDSS=2.00]	-0.018	0.0035	-0.025	-0.011	26.493	1	0.000
[EDSS=2.50]	-0.018	0.0032	-0.024	-0.011	30.765	1	0.000
[EDSS=3.00]	-0.036	0.0032	-0.042	-0.030	126.549	1	0.000
[EDSS=3.50]	-0.011	0.0032	-0.018	-0.005	12.576	1	0.000
[EDSS=4.00]	0.004	0.0032	-0.003	0.010	1.243	1	0.265
[EDSS=5.00]	-0.003	0.0034	-0.010	0.003	0.954	1	0.329
[EDSS=6.00]	-0.012	0.0035	-0.019	-0.005	12.473	1	0.000
[EDSS=6.50]	-0.014	0.0032	-0.020	-0.007	18.456	1	0.000
[EDSS=7.50]	0.005	0.0032	-0.001	0.011	2.277	1	0.131
[EDSS=8.00]	0[a]						
(Scale)	0.000						

Dependent Variable: rh_PoCi-PrCu_0_QA
Model: (Intercept), Time, EDSS

a. Set to zero because this parameter is redundant.

Parameter Estimates

Parameter	B	Std. Error	Interval		Hypothesis Test		
			Lower	Upper	Wald Chi-Square	df	Sig.
(Intercept)	0.068	0.0032	0.062	0.075	467.424	1	0.000
[Time=1]	-0.012	0.0032	-0.018	-0.006	15.076	1	0.000
[Time=2]	0[a]						
[EDSS=.00]	-0.008	0.0029	-0.014	-0.003	8.104	1	0.004
[EDSS=1.00]	-0.007	0.0049	-0.016	0.003	1.806	1	0.179
[EDSS=1.50]	-0.006	0.0028	-0.012	-0.001	4.707	1	0.030
[EDSS=2.00]	-0.010	0.0047	-0.019	-0.001	4.414	1	0.036
[EDSS=2.50]	-0.018	0.0032	-0.024	-0.012	33.048	1	0.000
[EDSS=3.00]	-0.023	0.0032	-0.029	-0.017	51.729	1	0.000
[EDSS=3.50]	-0.021	0.0032	-0.027	-0.014	42.346	1	0.000
[EDSS=4.00]	-0.006	0.0032	-0.012	0.000	3.979	1	0.046
[EDSS=5.00]	0.007	0.0016	0.004	0.010	21.468	1	0.000
[EDSS=6.00]	0.002	0.0054	-0.008	0.013	0.178	1	0.673
[EDSS=6.50]	-0.007	0.0032	-0.013	0.000	4.266	1	0.039
[EDSS=7.50]	0.002	0.0032	-0.004	0.008	0.410	1	0.522
[EDSS=8.00]	0[a]						
(Scale)	0.000						

Dependent Variable: rh_PoCi-PrCu_1_QA
Model: (Intercept), Time, EDSS

a. Set to zero because this parameter is redundant.

Table D (continued)

Parameter Estimates

Parameter	B	Std. Error	Interval Lower	Interval Upper	Hypothesis Test Wald Chi-Square	Hypothesis Test df	Hypothesis Test Sig.
(Intercept)	0.068	0.0033	0.061	0.074	432.365	1	0.000
[Time=1]	-0.011	0.0033	-0.017	-0.004	10.970	1	0.001
[Time=2]	0[a]						
[EDSS=.00]	-0.008	0.0035	-0.015	-0.001	5.185	1	0.023
[EDSS=1.00]	-0.004	0.0052	-0.014	0.006	0.614	1	0.433
[EDSS=1.50]	-0.007	0.0026	-0.012	-0.002	7.508	1	0.006
[EDSS=2.00]	-0.011	0.0041	-0.019	-0.003	6.670	1	0.010
[EDSS=2.50]	-0.015	0.0033	-0.021	-0.009	21.412	1	0.000
[EDSS=3.00]	-0.025	0.0033	-0.031	-0.018	57.590	1	0.000
[EDSS=3.50]	-0.007	0.0033	-0.013	-0.001	4.471	1	0.034
[EDSS=4.00]	0.002	0.0033	-0.004	0.009	0.504	1	0.478
[EDSS=5.00]	0.003	0.0016	-0.001	0.006	2.627	1	0.105
[EDSS=6.00]	-0.002	0.0040	-0.010	0.006	0.304	1	0.581
[EDSS=6.50]	-0.004	0.0033	-0.010	0.002	1.530	1	0.216
[EDSS=7.50]	0.003	0.0033	-0.003	0.009	0.877	1	0.349
[EDSS=8.00]	0[a]						
(Scale)	0.000						

Dependent Variable: rh_PoCi-PrCu_2_QA
Model: (Intercept), Time, EDSS

a. Set to zero because this parameter is redundant.

Parameter Estimates

Parameter	B	Std. Error	Interval Lower	Interval Upper	Hypothesis Test Wald Chi-Square	Hypothesis Test df	Hypothesis Test Sig.
(Intercept)	0.064	0.0029	0.059	0.070	484.984	1	0.000
[Time=1]	-0.008	0.0029	-0.014	-0.002	7.654	1	0.006
[Time=2]	0[a]						
[EDSS=.00]	-0.007	0.0032	-0.013	-0.001	4.839	1	0.028
[EDSS=1.00]	-0.008	0.0049	-0.017	0.002	2.421	1	0.120
[EDSS=1.50]	-0.006	0.0028	-0.011	-7.080E-05	3.942	1	0.047
[EDSS=2.00]	-0.009	0.0031	-0.016	-0.003	9.164	1	0.002
[EDSS=2.50]	-0.012	0.0029	-0.018	-0.006	16.194	1	0.000
[EDSS=3.00]	-0.027	0.0029	-0.033	-0.021	84.168	1	0.000
[EDSS=3.50]	-0.009	0.0029	-0.015	-0.004	10.380	1	0.001
[EDSS=4.00]	0.005	0.0029	-0.001	0.011	3.000	1	0.083
[EDSS=5.00]	0.002	0.0016	-0.001	0.006	1.956	1	0.162
[EDSS=6.00]	0.000	0.0040	-0.008	0.007	0.011	1	0.917
[EDSS=6.50]	-0.004	0.0029	-0.010	0.001	2.356	1	0.125
[EDSS=7.50]	0.001	0.0029	-0.005	0.006	0.038	1	0.846
[EDSS=8.00]	0[a]						
(Scale)	0.000						

Dependent Variable: rh_PrC-Ins_0_QA
Model: (Intercept), Time, EDSS

a. Set to zero because this parameter is redundant.

Table D (continued)

Parameter Estimates							
			Interval		Hypothesis Test		
Parameter	B	Std. Error	Lower	Upper	Wald Chi-Square	df	Sig.
(Intercept)	0.084	0.0048	0.075	0.094	314.049	1	0.000
[Time=1]	-0.009	0.0048	-0.018	0.000	3.557	1	0.059
[Time=2]	0[a]						
[EDSS=.00]	-0.010	0.0049	-0.020	-0.001	4.440	1	0.035
[EDSS=1.00]	-0.009	0.0066	-0.022	0.004	1.892	1	0.169
[EDSS=1.50]	-0.009	0.0041	-0.017	-0.001	5.199	1	0.023
[EDSS=2.00]	-0.014	0.0076	-0.029	0.001	3.286	1	0.070
[EDSS=2.50]	-0.010	0.0048	-0.019	-0.001	4.442	1	0.035
[EDSS=3.00]	-0.028	0.0048	-0.037	-0.018	33.789	1	0.000
[EDSS=3.50]	-0.008	0.0048	-0.017	0.001	2.848	1	0.091
[EDSS=4.00]	0.010	0.0048	0.000	0.019	3.996	1	0.046
[EDSS=5.00]	0.006	0.0036	-0.001	0.013	2.977	1	0.084
[EDSS=6.00]	-0.003	0.0050	-0.013	0.006	0.490	1	0.484
[EDSS=6.50]	-0.016	0.0048	-0.025	-0.006	10.852	1	0.001
[EDSS=7.50]	0.002	0.0048	-0.007	0.011	0.181	1	0.671
[EDSS=8.00]	0[a]						
(Scale)	0.000						

Dependent Variable: rh_PreCu_PreCu_0r_QA
Model: (Intercept), Time, EDSS

a. Set to zero because this parameter is redundant.

Anexo E. Abbreviations for every region in the cortical parcellation, according to the Desikan-Killiany atlas.

Table E. Abbreviations for every region in the cortical parcellation, according to the Desikan-Killiany atlas.

Region	Abbreviation		Region	Abbreviation
Bankss	B		Pars tringularis	Tr
Caudal anterior cingulate	CAC		Pericalcarine	PeCa
Caudal middle frontal	CMF		Postcentral	PoC
Cuneus	Cu		Posterior cingulate	PoCi
Entorhinal	En		Precentral	PrC
Fusiform	Fu		Precuneus	PrCu
Inferior parietal	IP		Rostral anterior cingulate	RAC
Inferior temporal	IT		Rostral middle frontal	RMF
Isthmus cingulate	IC		Superior frontal	SF
Lateral occipital	LO		Superior parietal	SP
Lateral orbitofrontal	LOF		Superior temporal	ST
Lingula	Li		Supramarginal	SM
Medial orbitofrontal	MOF		Transverse temporal	TT
Middle temporal	MT		Insula	In
Parahippocampal	PH		Frontalpole	FPol
Paracentral	PC		Temporalpole	TPol
Pars opercularis	Op			
Pars orbitalis	Or			